Assessing the Influence of Mineralogy and Texture on the Ore Breakage Characteristics of Drill Core and Crushed Ore using the JKRBT

Herbert Edward Hill

A dissertation submitted to the Faculty of Engineering and the Built Environment, University of Cape Town in fulfilment of the requirements for the degree of Master of Science in Chemical Engineering

February 2020

ABSTRACT

Textural variability is a key component in addressing process challenges resulting from variability in the ore being mined. Textural variability arises from differences in the types of mineral grains present, their relative abundance and the type of interactions they have with one another. Increased textural variability is one of the largest challenges to mineral processing challenges in terms of maintaining mill throughput, flotation recovery and flotation concentrate grades. Geometallurgy provides a powerful tool to manage ore variability by using geological, mineralogical and metallurgical information to inform plant design and operation. The geometallurgical approach contributes towards minimizing and controlling operational and technical risk arising from ore variability.

Ore breakage characterisation, a pivotal part of geometallurgy, aims to quantify the relationship between the energy supplied for breakage and the size of the resultant progeny. The Julius Kruttschnitt Rotary Breakage Tester® (JKRBT) is an ore breakage characterisation device designed as a geometallurgical tool which can use both crushed ore and drill core samples. Drill core is especially important as it is the material used for geometallurgical testing during exploration and resource definition. The aim of this work is to further understand the relationship between mineral texture and the ore breakage characteristics by conducting controlled single impact breakage using the JKRBT on different ore types of both drill core and crushed ore - sample types typically used at the exploration and operational levels respectively. An additional objective of the work is to develop an ore breakage characterisation test protocol using minimal samples to extract relative hardness indices given that the availability of sufficient drill core for the breakage characterisation tests is often a challenge.

In order to assess the influence of mineral texture on the ore breakage characteristics, five different ore types were used representing a homogenous shale (Ore S) and four different heterogenous polymetallic sulfide ores (Ores A, B, C and P). The ore was prepared by coring different size drill core and crushing using a jaw crusher. Mineralogical and textural classification of the ores was done using Quantitative Evaluation of Minerals by Scanning Electron Microscopy (QEMSCAN) and X-Ray Diffraction (XRD). The samples were subjected to controlled single impact breakage tests using the JKRBT. A standard test consisted of 3 energy levels (low, medium and high) tested on 3-4 particle size fractions (small, medium, large and very large). In developing the least particles protocol, all the steps of the standard procedure were followed except the number of particles per test was progressively reduced from 30 particles to a threshold of 5 particles.

A comparison of the results showed that drill core particles consistently produced a coarser progeny than crushed particles at the same conditions (energy, particle size class). The same observations were made for all ore types tested. The observed trend was attributed to differences in the particle shape between the crushed particles (angular) and drill core particles (cylindrical). Angular particles have a larger surface area exposed for energy absorption and therefore break more easily than drill cores.

From ore breakage characterisation tests performed, the ore competence parameter (Axb) for drill core samples of ore S, ore A, ore B, ore C and ore P was 14.8, 67.4, 70.7, 84.4 and 136 respectively. These values show that ore P is the least competent (highest Axb) while ore S is the most competent (lowest Axb). The differences in the ore breakage characteristics were attributed to the grain size distribution of the constituent minerals for each sample. For example, the d_{50} for chalcopyrite in ores A, B, C and P was 38, 60, 75, 375 microns respectively. It was observed that as the grain sizes increased, so did the ore competence parameter i.e. the ore resistance to breakage decreased. The findings were attributed to an increase in the surface area available for contact due to the decrease in grain size which results in less stress per unit area and thus more resistance to breakage.

In terms of mineralogy, the differences observed in the ore breakage characteristics were also attributed to the relative mineral abundance and individual mineral Moh's hardness. Quartz – the hardest mineral of the ores investigated– is present in larger amounts in ore S than in the polymetallic sulfide ores which renders ore S more resistant to breakage. The three most dominant minerals in ore P are magnetite (hardness 7), pyrrhotite (hardness of 4) and chalcopyrite (hardness of 3.5). This would make Ore P the least resistant to breakage as it contains substantial amounts of the softer minerals (chalcopyrite and pyrrhotite) when compared to the other ores. The results showed that the more abundant the harder minerals, the more competent the ore type. Relating these two properties results in the conclusion that ore S is the hardest and ore P the softest ore.

Thereafter, the least particles protocol (LPP) was developed as an abridged ore breakage characterisation test protocol that can be applied to both crushed ore and drill core particles and considers the effects of textural variability. The LPP was developed using ore S which was homogenous and fine grained and then applied in a case study to a mineralogically different, heterogeneous and coarser grained ore (Ore P). The results proved that the proposed abridged ore breakage characterisation test that uses the minimal number of crushed or drill core particles to extract ore breakage indices can be applied for both homogenous and heterogenous ore types with mineral grains sizes between 10-1700 microns. The number of particles could be reduced to as

little as 10 particles per test while still obtaining the similar ore breakage indices as those obtained from the standard procedure.

This study showed the importance of mineralogy and texture on ore breakage characteristics. In order for mining companies to better manage the challenges (mill throughput, flotation recovery and grades) associated with ore variability, mineralogical and textural data should be considered during the design and optimization of mineral processing circuits. Understanding the core variations and interrelations among minerals/metals in heterogeneous ores is also imperative to developing efficient mine planning and scheduling methodologies for purposes of minimizing and controlling operational and technical risk of ore variability while maximising the overall net present value (NPV) of the operation. The least particles protocol developed in this study will be especially useful in situations where the amount of ore available for metallurgical testing is limited.

PLAGIARISM DECLARATION

I declare that this dissertation, submitted for the degree of Master of Science in Chemical Engineering at the University of Cape Town is my own work, and has not been submitted prior to this for any degree at this university or any other institution.

I know the meaning of plagiarism and declare that all the work in the document, save for that which is properly acknowledged, is my own.

This thesis/dissertation has been submitted to the Turnitin module (or equivalent similarity and originality checking software) and I confirm that my supervisor has seen my report and any concerns revealed by such have been resolved with my supervisor.

Signed by candidate

Signature: _____

01 October 2020

Date: _____

EBENEZER

Thus far the Lord has brought us.

Trust in the LORD with all thine heart; and lean not unto thine own understanding. In all thy ways acknowledge him, and he shall direct thy paths. (Proverbs 3 vs 5-6)

ACKNOWLEDGEMENTS

I would like to express my sincere gratitude to the following people and organisations for their assistance in this study:

- To the best primary supervisor anyone could wish for, Associate Prof Megan Becker, thank you for being supportive, patient, encouraging and always on the ball with excellent feedback that made this study possible.
- Prof Aubrey Mainza, thank you for your unparalleled support, excellent advice and encouragement both for this study and beyond.
- Dr Bbosa for all your help and advice throughout this thesis.
- A special thank you to my parents (Mr Eric Hill and Mrs Angella Hill) for always believing in me and for the sacrifices they made to enable me to reach this point. To my siblings (Natalie and Megan) and extended family members as well, thank you for your unwavering support and encouragement. I am privileged to have you by my side.
- To Ms Lungile Zwane, thank you for your unceasing support, patience and for always being so wonderful throughout this journey.
- A special mention to all my friends especially Lisa October, Simba Nyakunhuwa, Henry Gordon and Marcelene Voigt for helping in one way or another. You all made this journey bearable.
- The teams at Vedanta and Lafarge for their assistance with material for this work.
- I would like to thank the University of Cape Town and the Chemical Engineering Department for their academic and financial assistance and for providing world class facilities.
- A special mention to the CMR Lab 2B staff (Kenneth, Monde and Shireen), Keshree (XRD) and QEMSCAN Lab staff (Gaynor, Lorraine and Sandile) for always assisting me throughout this study.
- My sincere gratitude also goes to Mr Brian Chaponda and the team at the Sibanye Concentrator technical centre for providing the equipment and facilities that enabled me to carry out this study.
- Hardcore Drilling for assistance with coring process.
- Thank you for the financial support in part from the National Research Foundation of South Africa (Grant Numbers 86054, 99005). Any opinions, findings and conclusions or recommendations expressed in any publication generated by the NRF supported research is that of the author(s), and that the NRF accepts no liability whatsoever in this regard.

TABLE OF CONTENTS

LIST OF FIGURES

LIST OF TABLES

NOMENCLATURE AND SYMBOLS

A and b	Impact breakage parameters
C	Velocity constant
D_n	Damage accumulated at the nth impact
d	Feed particle size (mm)
E	Energy input (KJ)
E_{min}	Threshold energy (J/kg)
E_{sv}	Volumetric specific energy (kWh/m)
E_{cs}	Specific input energy (kWh/t)
E_k	Kinetic energy (kJ)

E_t	Energy transferred from the input pendulum (J)
P_{80}	Product 80% passing size (μm)
F_{80}	Feed 80% passing size (μm)
h_i	Initial drop weight height (cm)
h_f	Final drop weight height (cm)
h_d	Drop weight mass (kg)
K	Constant
k	Number of repetitive impacts
L	Pendulum length (m)
M	Particle mass (kg)
M_r	Mass of the rebound pendulum (kg)
M	Maximum t_{10} for the material (%)
N	Rotor speed (rpm)
p	Material characteristic parameter
q	Describes size effects on breakage
r	Rotor radius (m)
s	Breakage probability
t_{10}	Cumulative percentage passing 1/10 of the initial size (%)
V_i	Velocity just prior to impact (m/s)
W	Work input (kWh/t)
WI	Work index (kWh/t)
W_{min}	Theoretical minimum energy
W_{crit}	Critical energy value
x	Initial particle size (m)
X_f	Feed particle size (m)

X_p	Product particle size (m)
γ	Damage accumulation constant
θ	the angle through which the pendulum is displaced
$\alpha\infty$, $\beta\infty$, n	Parameters to be fitted to the test data

ACRONYMS AND ABBREVIATIONS

2D	two-dimensional
3D	three-dimensional
AG	Autogenous Grinding
AM	Amphibole Magnetite
BMS	Base Metal Sulfides
CP	Crushed ore particles
DC	Drill core particles
DWT	Simple Drop Weight Tests
GLCM	Grey-Level Co-occurrence Matrix
GSD	Grain Size Distribution
HPGR	High Pressure Grinding Roller
ILC	Impact Load Cell
JKMRC	Julius Kruttschnitt Mineral Research Centre
JKRBT	Julius Kruttschnitt Rotary Breakage Tester®
LPP	Least Particles Protocol
MLA	Mineral Liberation Analyser
NPV	net present value
PSD	product particle size distribution

QEMSCAN	Quantitative Evaluation of Minerals by Scanning Electron Microscopy
QM	Quartz Magnetite
RBT	Rotary Breakage Tester
SAG	Semi-Autogenous Grinding
SDM	size dependent model
SEM	Scanning Electron Microscopy
SHPB	Split Hopkinson Pressure Bar Test
SILC	Short Impact Load Cell
UCS	Unconfined Compressive Strength
UCT	University of Cape Town
UG2	Upper Group 2
XCT	X-ray Computed Tomography
XRD	X-Ray Diffraction

1. INTRODUCTION

Overview

The purpose of this thesis is to assess the influence of mineralogy and texture on the ore breakage characteristics of drill core and crushed ore performed using the JKRBT (Julius Kruttschnitt Rotary Breakage Tester®). This thesis also proposes an abridged ore breakage test protocol that requires minimal sample quantity to obtain the required ore breakage indices.

1.1 Background of the Research

Numerous ore deposits are found in different geological environments occurring in many parts of the world. Many of these deposits result from the mobilization of metals in solution that then precipitate out as minerals and are deposited throughout the earth's crust. Minerals and metals are currently the principal element in all services and infrastructure required for the growth of societies in countries worldwide (Kesler, 2007). As the world population grows and the standard of living increases, so does the consumption and demand for minerals and metals (Figure 1-1). In addition, the entrance of more consumers into the markets of minerals and metals, and the expansion of these is one of the drivers for the increasing demand.

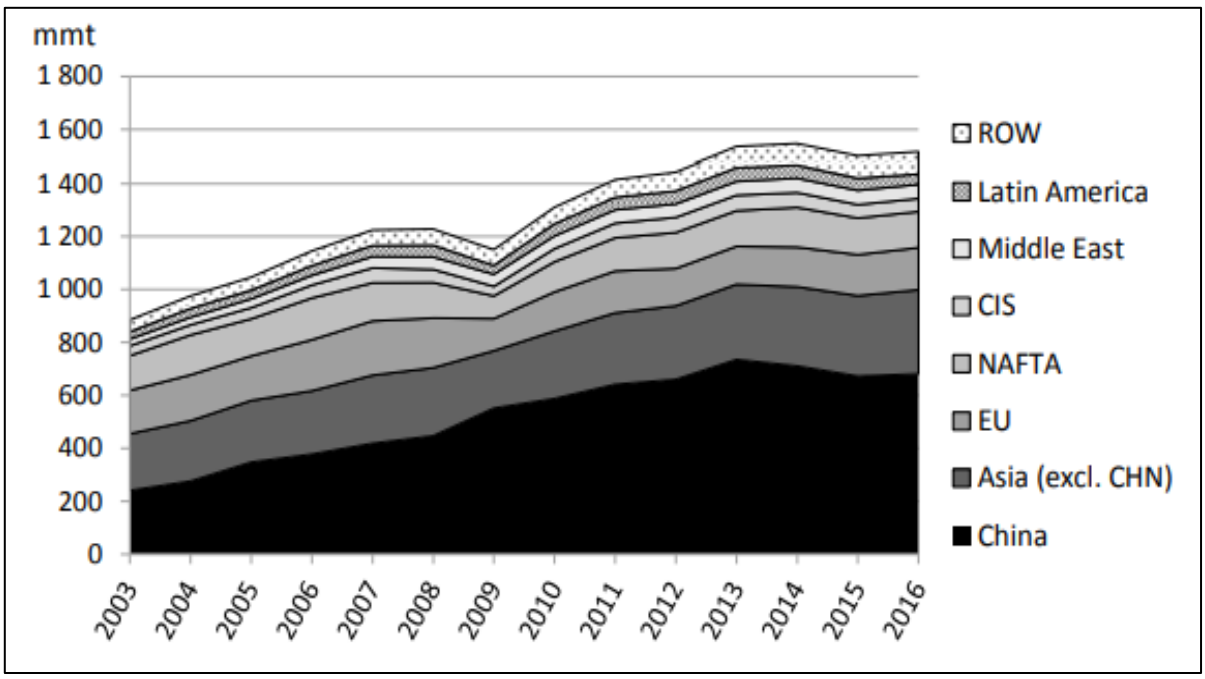

Figure 1-1: Apparent steel consumption by region in millions of metric tons (OECD, 2018).

Despite the continuous increase in metal demand, mining companies are currently facing challenges associated with declining ore grades (Figure 1-2), increasing ore heterogeneity and rising production costs (Tavares, 2007). Most of the remaining ore deposits contain complex ores resulting from the depletion of the high grade, 'simple' to process ore deposits. A complex ore refers to an ore which includes attributes such as more than one mineral in varying compositions, the presence of deleterious minerals and/or elements, complex metal deportment and inter-grained textures. The concept of ore heterogeneity defines the degree of variability of a mineral or metal within a given ore, where the mineral/metal content is irregular. Increased ore heterogeneity creates challenges in mineral processing, since traditional circuit designs are not necessarily equipped to manage these differences within the ore (King, 2001b). Processing of heterogeneous ores often results in the recovery of lower grade product, provided that no amount of low grade material is eliminated prior to a concentrator. Additionally, there are higher operating costs associated with extra waste disposal, material handling (Figure 1-2) and increased energy and water consumption per ton of product (Mudd, 2004). Therefore, understanding the core variations and interrelations among minerals/metals in heterogeneous ores is imperative to improving plant efficiency, grade and recovery, and operational economics (Cropp & Goodall, 2013).

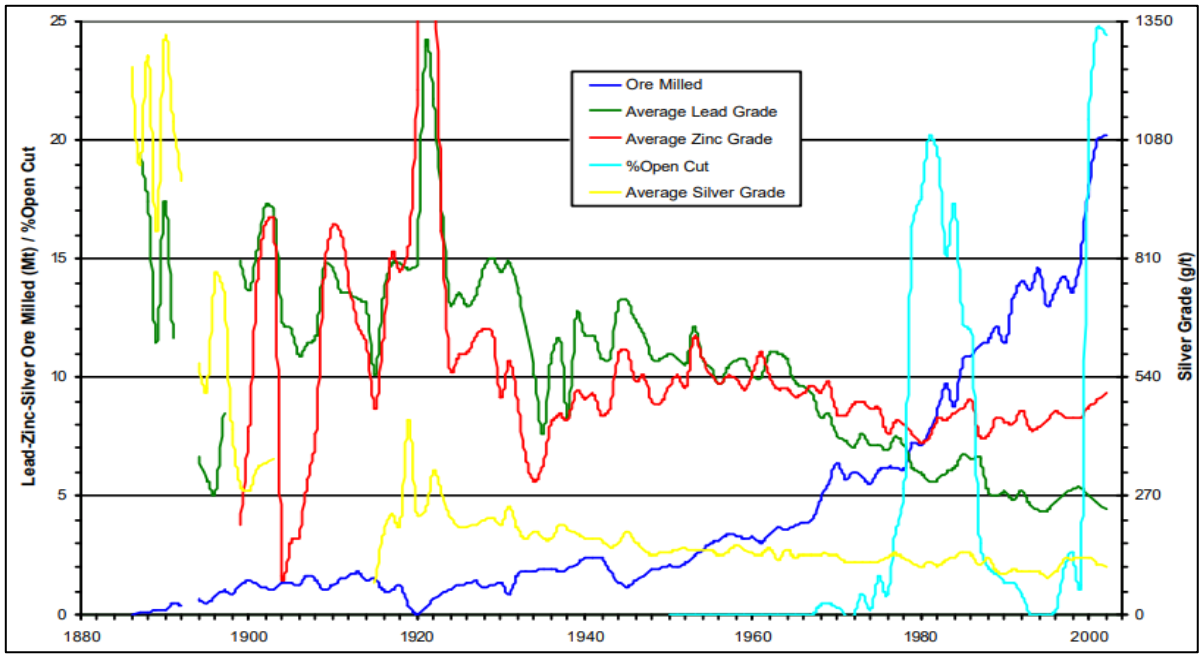

Figure 1-2: General trend illustrating declining ore grades for a Lead-Zinc-Silver ore (Mudd, 2004).

Ore heterogeneity often manifests itself as variations in the textural properties of the ore deposit. The definition of texture, in the mineral processing context, refers to the spatial interrelations exhibited by minerals in a rock sample. Textural variability arises from differences in the types of

mineral grains present, their relative abundance and the type of interactions they have with one another. Increased textural variability is the largest contributor to mineral processing challenges as there is a strong relationship between the textural characteristics of an ore body and the downstream processing of the ore in terms of mill throughput, flotation recovery and flotation concentrate grades. Developments in Automated Scanning Electron Microscopy (Auto-SEM) technology such as Quantitative Evaluation of Minerals by Scanning Electron Microscopy (QEMSCAN) have led to more studies that demonstrate the importance of texture on processing behaviour being published (Becker et al., 2016; McClung & Viljoen, 2011; Tungpalan, Wightman & Manlapig, 2015). Though various textural characteristics affect the mineral processing of an ore, Petruk (2000) reported that the mineral grain size distribution and mineral bonds are the most influential textural characteristics affecting ore breakage and mineral liberation. Similar findings on the influence of mineral grain size on processing behaviour were also reported by King (2001) and Napier-Munn et al. (2006).

The importance of process mineralogy on the mineral processing circuit has been well documented by the large body of literature currently available. It has been established that mineralogical characterisation is essential in interpreting the metallurgical response of an ore (Tungpalan, Wightman & Manlapig, 2015) . Characteristics like minerals present and mineral abundance have been reported to influence the ore properties and thus the metallurgical response of the ore. Being able to measure and use the mineralogical and textural information of an ore body is vital to mineral beneficiation processes such as breakage and comminution as these parameters affect the hardness of the ore, processing throughput, mineral liberation and mineral classification (Becker et al., 2016).

The introduction of Auto-SEM technology like QEMSCAN has made it easier to obtain more reliable approximations of mineralogical and textural characteristics. QEMSCAN can be used to obtain reliable parameters such as mineral grain size distributions, minerals present, mineral abundance and mineral liberation. Data validation for tests conducted using QEMSCAN can be achieved using X-Ray Diffraction (XRD). This study will make use of both QEMSCAN and XRD to obtain the most reliable mineralogical and textural characteristics for ores used.

Geometallurgy provides a powerful tool to better manage ore variability by using both geological and metallurgical information applied to plant design and operation. This approach involves the understanding of the mineralogy, geochemistry, metallurgical behaviour and grade variability within an ore deposit (Harbort, 2013; Mwanga et al, 2015). With this approach, samples are obtained from sample points that are spatially distributed throughout the ore body for adequate

representation of the entire ore deposit (Mwanga et al, 2015). The advantage of mapping out the textural variability of an ore body is that it can ultimately serve as a prediction tool that can save time and resources required to performed full set of metallurgical tests.

Drill core is especially important in geometallurgy as it the most reliable material available for geometallurgical testing during exploration and resource definition. Metallurgical tests conducted using drill core can therefore be used to inform mine planning and exploration where crushed ore is rarely available. The Geometallurgy approach contributes towards developing efficient mine planning and scheduling methodologies for purposes of minimizing and controlling operational and technical risk of ore variability while maximising the overall net present value (NPV) of the operation (Cloete et al, 2018).

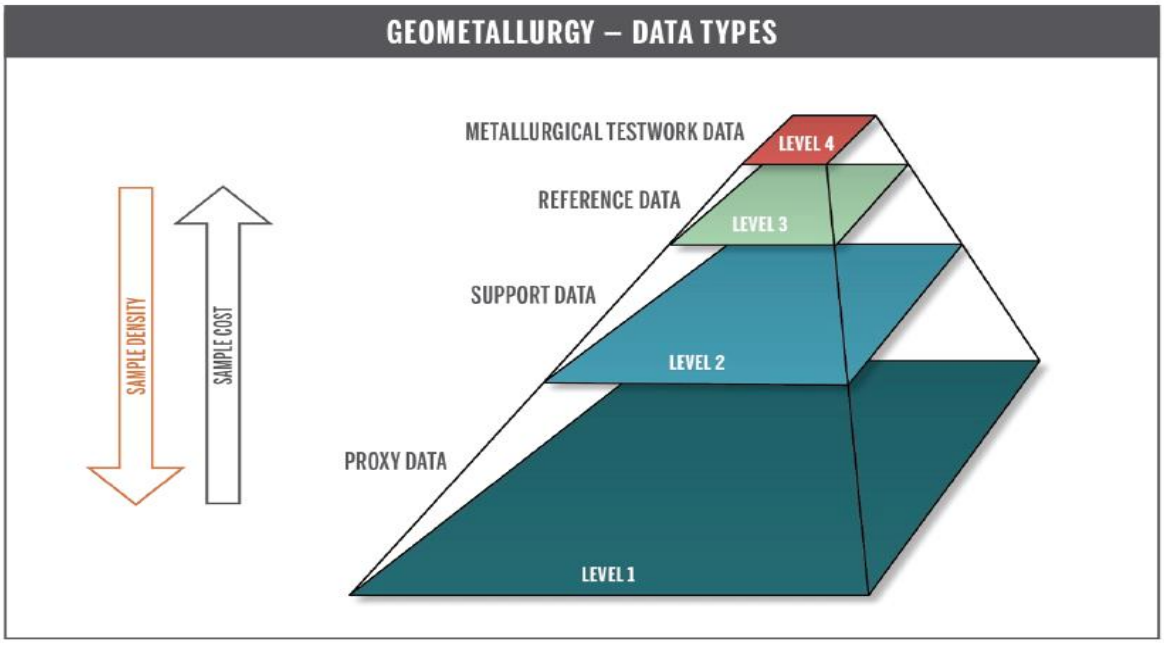

Figure 1-3: Geometallurgical data types (Cloete et al, 2018).

Figure 1-3 shows the different data types that form the basis of the geometallurgical approach to plant design and operation. Level 1 represents proxy data collected routinely which is used via correlation with other proxy data to indirectly measure the metallurgical response of a given ore type. Level 1 proxy data like textural data forms the basis of geometallurgical models and captures the variability of the ore body (Cloete et al, 2018). Level 2 represents support data which is extracted from small scale tests. Level 3 reference data provides a direct measure of the mineral processing characteristics that influence plant response. Level 4 data is obtained from full scale metallurgical tests like ore breakage characterisation tests that is essential in the design and operation for plants although it is expensive to obtain.

Comminution circuits have commonly been reported as being the largest energy consumers in mineral processing circuits (Napier-Munn, 2015). Cleary (1998) reported that the inefficiency of comminution circuits is a result of less than 5% of the supplied energy being utilized for breakage, with the majority being expended as heat and noise. With steadily declining fossil fuel supplies and a looming global energy crisis, the mineral processing industry has increased its focus on energy reduction measures.

Ore breakage characterisation plays a critical role is the design and optimization of comminution circuits. The main objective of ore breakage characterisation is to quantify the relationship between the energy supplied for breakage and the size of the resultant progeny through laboratory particle breakage tests (Napier-Munn et al., 1996). Impact breakage tests are commonly used in ore breakage characterisation as they represent the most elementary process in comminution (Tavares, 2007). Several single impact ore breakage devices have been developed of which the JK Rotary Breakage Tester (JKRBT) developed at the Julius Kruttschnitt Mineral Research Centre (JKMRC) is the focus of this study.

The JKRBT is a rapid characterisation device that was designed as a geometallurgical tool which can use both crushed ore and drill core particles to obtain the ore breakage characteristics required. The JKRBT is more accurate and the test work less time consuming than its predecessors (Kojovic & Shi, 2002). Practically speaking, sample availability is a major concern when performing metallurgical testing as numerous tests need to be performed to get a complete view of the metallurgical response of the ore type. This means that very little of the sample is available for ore breakage characterisation. This is the reason that this study will aim to develop an ore breakage characterisation test protocol that uses minimal samples to extract indices that can be used in design and optimisation studies.

1.2 Problem Statement

Increased mineralogical and textural variability leads to differences in rock strength and breakage characteristics. Breakage characteristics affect mineral processing by influencing mineral liberation, mill throughput and ore recovery in desliming and flotation processes. Ore breakage characterisation is an important part geometallurgy. Mapping of mineralogical and textural variations using drill core and crushed ore acts as a prediction tool to be manage ore variability. Understanding these relationships will also assist in the long-term development of models and expert control strategies.

1.3 Research Aims and Objectives

The aim of this work is to further understand the relationship between mineral texture and the ore breakage characteristics of both drill core and crushed ore by conducting controlled single impact breakage using the JKRBT. Additionally, the work is aimed at developing an ore breakage characterisation test protocol using minimal samples to extract relative hardness indices. The core objectives of this study are therefore to:

1. Determine the relationship between crushed ore and drill core particles.
2. Determine the relationship between ore mineral texture and the ore breakage characteristics in geometallurgy.
3. Develop an abridged ore breakage characterisation test protocol that can be applied to both crushed ore and drill core particles and considers the effects of textural variability.

1.4 Key Questions

The objectives of this study are addressed by the following key questions:

- Is there a difference in the ore breakage characteristics and liberation profiles of drill core and crushed ore?
- What is the effect of mineral texture variability on the ore breakage characteristics?
- Is there a relationship between the mineral texture, number of particles per test and the relative hardness indices for crushed ore and drill core?

1.5 Scope and Limitations

The influence of mineralogy and texture on the ore breakage characteristics of drill cores and crushed ore will be assessed by this study. QEMSCAN will be used to investigate mineralogical (mineral type and abundance) and textural (grain size) characteristics of the test ores selected for this thesis. The test ores that will be used in this study are extracted directly from the mining shafts. Ore hardness parameters will be established by fitting the experimental data to the JK breakage model and the JK size dependent model. This study will only consider the energy-size relationship. The work is also aimed at developing an ore breakage characterisation test protocol that uses minimal samples to extract indices that can be used in design and optimisation studies from drill core samples.

This project is limited to breakage characterisation caused by impact breakage only. This is because single impact breakage represents primary breakage and is usually linked to Geometallurgy. Despite many single impact breakage devices being commercially available, this study only considers impact breakage using the JKRBT which is a high impact velocity device. This is because of the numerous advantages associated with the JKRBT which will be shown in the following chapter. And even though other breakage models are available in literature, only the two mentioned models will be used in the data analysis as recommended by the developers of the device and they also provide the quantitative information desired for this type of work. This study will consider texture based on grain size only as this is quantifiable using the QEMSCAN device used in this study.

1.6 Thesis Structure

This thesis has been structured into six chapters as illustrated in Figure 1-4. The introduction sets the scene for problem definition. This is followed by a review of the literature relevant to the study, a summary of key literature and hypotheses formulation. The experimental methodology is followed by the presentation of the results from which the effect of mineralogy and texture on the ore breakage characteristics of drill core and crushed ore can be assessed. The development and testing of the least particles protocol is then presented. Conclusions are drawn from the results presented and recommendations for future work are made.

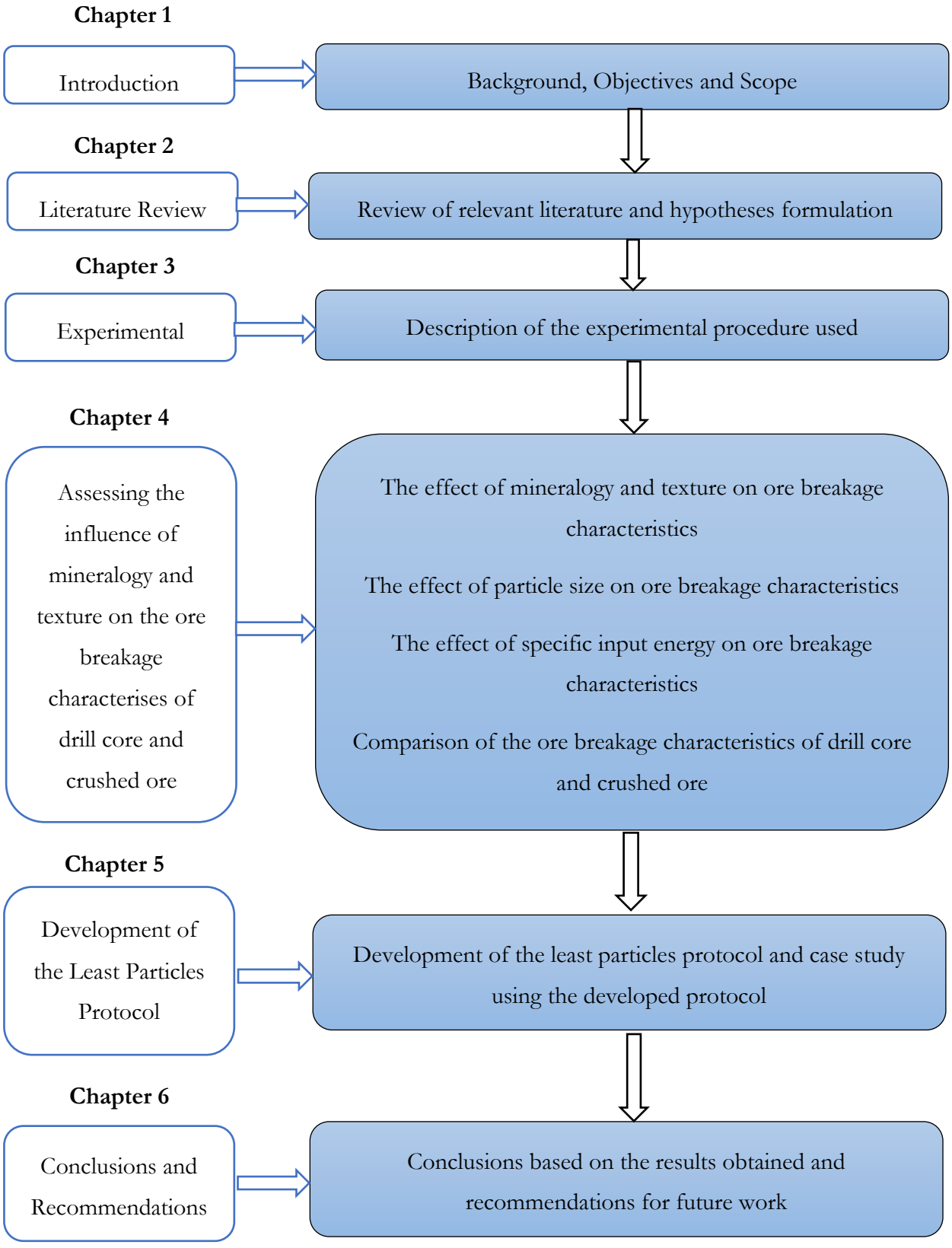

Figure 1-4: Thesis structure.

2. LITERATURE REVIEW

Overview

The purpose of this chapter is to review literature relevant to investigating the relationship between ore texture and the focus areas of geometallurgy, namely energy input required to break ore particles. The chapter begins by looking at comminution fundamental theories related to the energy-size relationship. This is followed by a review of the mechanisms of single impact breakage, single impact breakage characterisation tests and the currently available ore breakage characterisation models with the focus being on the JKRBT, t_{10} breakage model and size-dependant model. This chapter also introduces and considers process mineralogy and texture from the geometallurgical perspective. The chapter concludes with a summary of key findings from the review of literature and the hypotheses formulated after identifying the gap in literature.

2.1 Comminution

2.1.1 Background

Comminution is a key step in Geometallurgical studies and should be considered in any attempt made to link the mineralogical and textural properties of the ore to the process. By definition, comminution in mineral processing is the progressive reduction in the particle size of a solid material until the valuable mineral grains can be liberated from the gangue material using an appropriate separation technique (King, 1994). In a typical mine environment, the comminution circuit consists of a series of crushing and grinding units dedicated to producing the desired particle size and mineral liberation profiles. 'Crushing' refers to size reduction through compression of a rock against rigid surfaces while 'grinding' entails size reduction from abrasion and grinding media (balls, rods etc.) being impacted on the ore (Wills & Napier-Munn, 2006).

Comminution is by far the largest energy consumer in the production of most commodities and precious metals. Comminution equipment alone was found to consume 36% of the total mining energy (Ballantyne & Powell, 2014) while Napier-Munn (2015) suggested that comminution is responsible for 2% of the total world energy consumption. Additionally, it is highlighted that a significant amount of energy is also used indirectly by comminution through the production of grinding media and liners (embodied energy). The root cause of the high comminution energy usage is the extremely low efficiency (~1%) of the conversion of available energy to actual size

reduction; the energy balance is expended as heat and noise (Napier-Munn et al., 1996). As a result of low energy efficiencies, when designing comminution circuits, substantial effort is directed towards knowing and minimizing the energy requirements (Mainza, 2017). As environmental sustainability awareness increases and legislations against the use of energy generated from fossil fuels become more stringent, mining companies are now more than ever trying to reduce their energy consumption and carbon footprint. This has been the catalyst for the development of more energy efficient and economical comminution technologies.

Mining procedures can save a substantial amount of money while reducing the carbon footprint by decreasing electricity usage. To get an overall view of total comminution, drilling and blasting should be included along with crushing and grinding. The high electricity usage associated with the comminution of mineral-bearing ores can be reduced by increasing drilling and blasting efficiencies (Roy et al., 2016). This is typically done by adjusting the explosive charge, drill hole spacing, drill length and drill diameters. When compared, blasting efficiencies are constantly higher than grinding efficiency with crushing being the median between the two (Murr et al, 2015). Murr et al. (2015) also postulated that when blasting is performed efficiently, more internal microcracking results thus increasing energy saving and productivity in downstream processes. However, texture which plays a key role in how the energy is absorbed in the rock and subsequently broken, is often ignored in the discourse.

Tumbling mills are the most widely used size reduction devices in mineral processing and are available as rod, ball, semi-autogenous grinding (SAG) and autogenous grinding (AG) mills. The grinding media used in each varies from rods to balls and other commercially available media, apart from the AG mill in which self-grinding of the ore occurs without the aid of media. SAG mills are predominantly used in metallurgical circuits employed at gold, platinum and copper mines stretching to zinc, lead, silver and nickel processing. Figure 2-1 illustrates the process mechanism for AG and SAG mills. The mill feed composition greatly affects the mill performance as the properties of the feed determine its breakage characteristics. When the feed properties vary in terms of mineralogy and texture, process complications are also introduced as metallurgical circuits are not built to handle these variations in feed composition (Bueno et al., 2013). This is evident in simulators such as the *JKSimMet* and MODSIM which treat the feed composition to the comminution circuit as uniform, resulting in a set of average ore breakage parameters. More recent models now consider differences in ore characteristics (competence and resistance) to reduce the bias in simulated mill performance. However, most existing plants have been designed using average ore body information and in all of this, texture variations have been ignored even in

instances where the data is readily available. The main reason for this could be the lack of information linking texture data to the commonly used design criteria of energy input and ore brokenness.

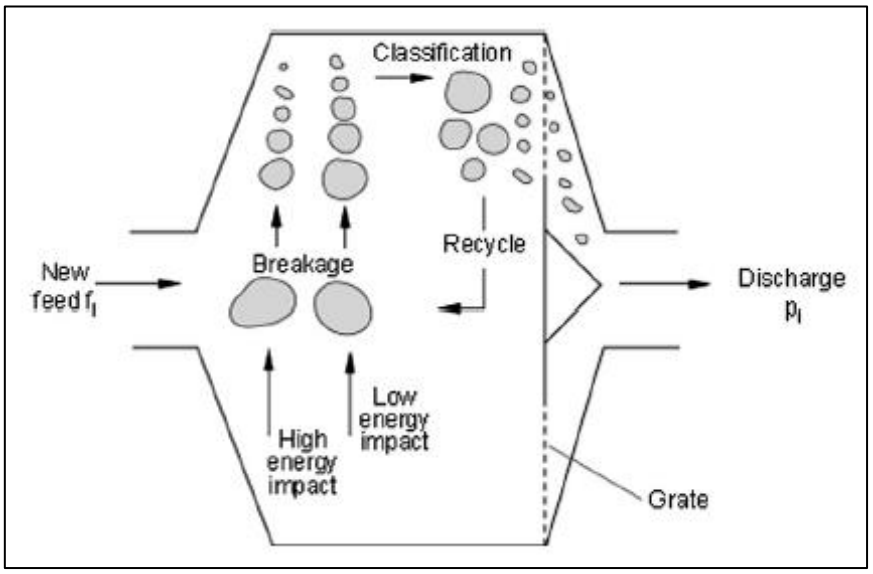

Figure 2-1: Schematic diagram of Autogenous/Semi-autogenous mill process mechanisms (Napier-Munn et al., 1996).

Ore breakage characterisation is a branch of comminution that uses laboratory ore breakage tests to quantify the relationship between specific input energy and the resultant progeny size distribution (Tavares, 2007). The relationship between specific input energy and the resultant progeny size distribution (energy-size relationship) plays a key role in the mineral processing industry's efforts to reduce the comminution energy consumption and carbon footprint. Ore breakage characterisation plays a pivotal role in design, diagnosis and optimization of processing circuits even more so due to an ever-increasing body of literature that acknowledges that ore competence (resistance to breakage) is an important factor affecting circuit performance in terms of energy requirements and resultant progeny characteristics (Zuo & Shi, 2016).

A competent (hard) ore typically has a slower rate of breakage and requires higher energy input for the same size fraction thus leading to increased residence time in the mill. The effect of this is observed as a reduction in the mill throughput and results in accumulation within the mill (Bueno et al., 2013). Numerous authors have reported on the fundamentals and new developments in the ore breakage characterisation field (Bbosa, 2006; Chikochi, 2017; King, 1994; Kojovic & Shi, 2002; Tavares, 2007; Zuo & Shi, 2016;). However, these authors do not consider the influence of texture on the ore breakage characteristics in detail, which this study will address.

2.1.2 Comminution Theories

The energy-size relationship is a key component of comminution research and has its roots in early 19th Century research. As such, a sizeable number of studies have been presented that describe the energy-size relationship. The most popular descriptions for the energy-size relationship were proposed by Walker et al (1837), Rittinger (1867), Kick (1883) and Bond (1952). The general form of comminution was put forward by Walker et al (1837). The proposed equation stated that the energy required to decrease the size of a solid material is directly proportional to the change in size achieved and inversely proportional to the size to the power *n*. The equation proposed by Walker et al (1837) is illustrated by equation 1 where *dE* is the net change in energy, *C* is a material constant, *dx* is the size change, *x* is the dimension of the product and *n* is the exponent.

$$dE = -C\frac{dx}{x^n} \qquad \text{Equation 1}$$

The descriptions for the energy-size relationship proposed by Rittinger, Kick and Bond were based on equation 1 i.e. if the exponent *n* in Equation 1 is replaced by 1, 1.5 and 2 and then integrated, Kick, Bond and Rittinger's equations are obtained. In 1867, Rittinger hypothesised that there is a relationship between the surface area of comminution products and the energy required to achieve the size reduction (Rittinger, 1867). Additionally, the surface area produced is inversely proportional to the particle size as illustrated by Equation 2 where *E* is the net specific energy, X_f is the feed particle size, X_p is the product particle size and *K* is a constant.

$$E = K[\frac{1}{X_p} - \frac{1}{X_f}] \qquad \text{Equation 2}$$

This was followed by Kick (1883) who proposed there is a proportional relationship that exists between the size reduction of a particle, and the work done to achieve the reduction.

$$E = K\ln[\frac{X_f}{X_p}] \qquad \text{Equation 3}$$

Bond (1952) subsequently hypothesised that there is a proportional relationship between the work input and the length of the crack tip produced. Bond added that this work is equal to the difference between the work representing the feed and products (Bond, 1952). The bond work index is a measure of the energy required to reduce the feed size from a given F_{80} to a given P_{80} (Napier-Munn et al., 1996). The bond mill work index is essentially the amount of energy required to reduce the size of the feed material to 80% passing 100 µm. In the mineral processing industry, the bond work index is determined from laboratory scale tests or plant data (Jankovic et al, 2010). Bonds' work index is illustrated by equation 4 where *W* is the work input, *WI* is the work index (ore specific constant), P_{80} is the product 80% passing size and $F_{80}$is the feed 80% passing size.

$$W = 10 * WI * [\frac{1}{\sqrt{P_{80}}} - \frac{1}{\sqrt{F_{80}}}] \qquad \text{Equation 4}$$

All three postulations were assessed by Hukki (1961) who proposed that each equation might be applicable for discrete narrow size ranges. Hukki (1961) suggested that Kick's equation is applicable for crushing, whereas Rittinger's equation is more suited for finer grinding and Bond's equation can be reasonably applied to the range in which ball/rod mills operate in (Jankovic et al, 2010). Historically, the Bond equation is the most widely used for the design of comminution equipment, regardless of its empirical nature (Tavares & King, 1998). It is therefore clear that the influence of ore properties specifically texture, and mineralogy are often not considered during the design of comminution equipment.

2.2 Single Particle Breakage

A rock is a solid aggregate comprised of grains of one or more minerals. For example, granite consists of the minerals quartz, plagioclase and K-feldspar. Rocks break to form progeny particles i.e. particles are subunits of rocks. The mineral grains forming the rock are held together by different types of bonds depending on how the rock was formed. Most mineral grains comprise of a crystalline structure with atoms being arranged in a regular three-dimensional (3D) array (Wills & Napier-Munn, 2006). The exact configuration is a function of the bond size and bond type responsible for holding the lattice structure together. The bonds holding the structure together can be strained by tensile and compressive stresses as illustrated in Figure 2-2. When the strain exceeds the strain limit, the bonds will break.

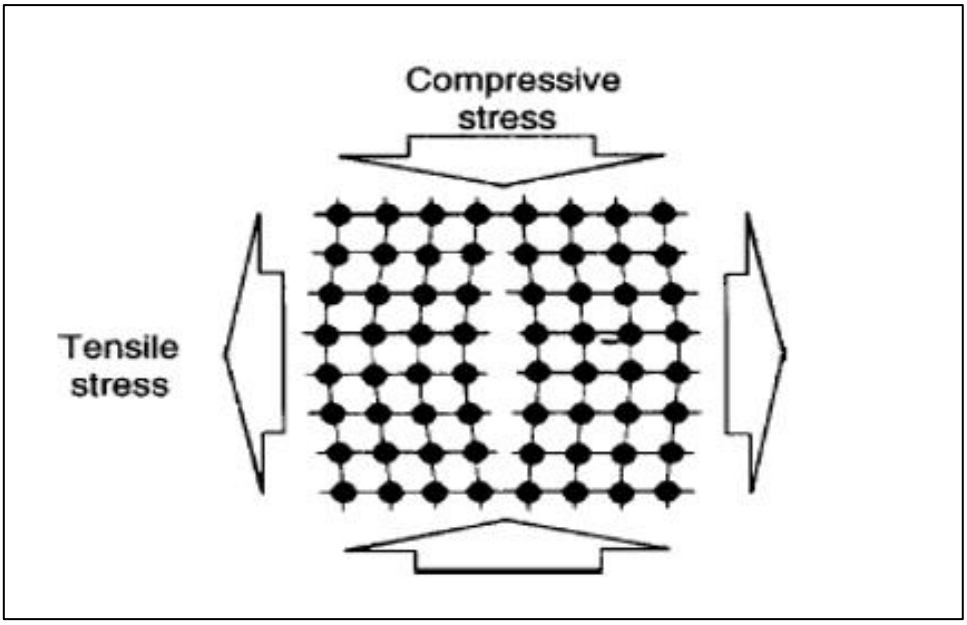

Figure 2-2: Strain of a crystal lattice resulting from tensile compressive stress (Wills & Napier-Munn, 2006).

Particle breakage is a result of a series of micro processes that involve interactions between stressing conditions and material characteristics (Tavares, 2007). A typical breakage event in rock mechanics consists of two main modes i.e. compressive stresses and abrasion/attrition. Disintegration results from the major mode which is the compressive stresses, while abrasion/attrition typically leave the parent particle relatively intact but cause gradual wearing and rounding (Napier-Munn et al., 1996).

When contact is made between the particles and the stressing tools, the applied stress is converted to strain energy and an insignificant amount of plastic deformation. Crack-like damage accumulates within the particle and, beyond a certain point, an unstable microcrack is formed. According to fracture mechanics, if the rate of energy release is greater than the crack resistance, the crack will grow unstably (Tavares & King, 1998). The crack growth is driven solely by the stored strain energy. The parent particle is finally broken into progeny particles when the crack(s) emerge from the particle (Napier-Munn et al., 1996). When fracture occurs, the fracture energy is relatively larger than the dissipative energy. Any excess energy is released as kinetic energy in the progeny fragments. The progeny characteristics (size, shape, distribution and number) are dependent on the characteristics of the initiating flaw (location and size) and the microstructural properties of the material.

2.2.1 Mechanisms of Particle Breakage

Particle size reduction is achieved by one or more particle breakage mechanisms. The exact mechanism that achieves breakage depends on the comminution equipment used and the ore specific properties. Below is a brief review of the possible breakage mechanisms:

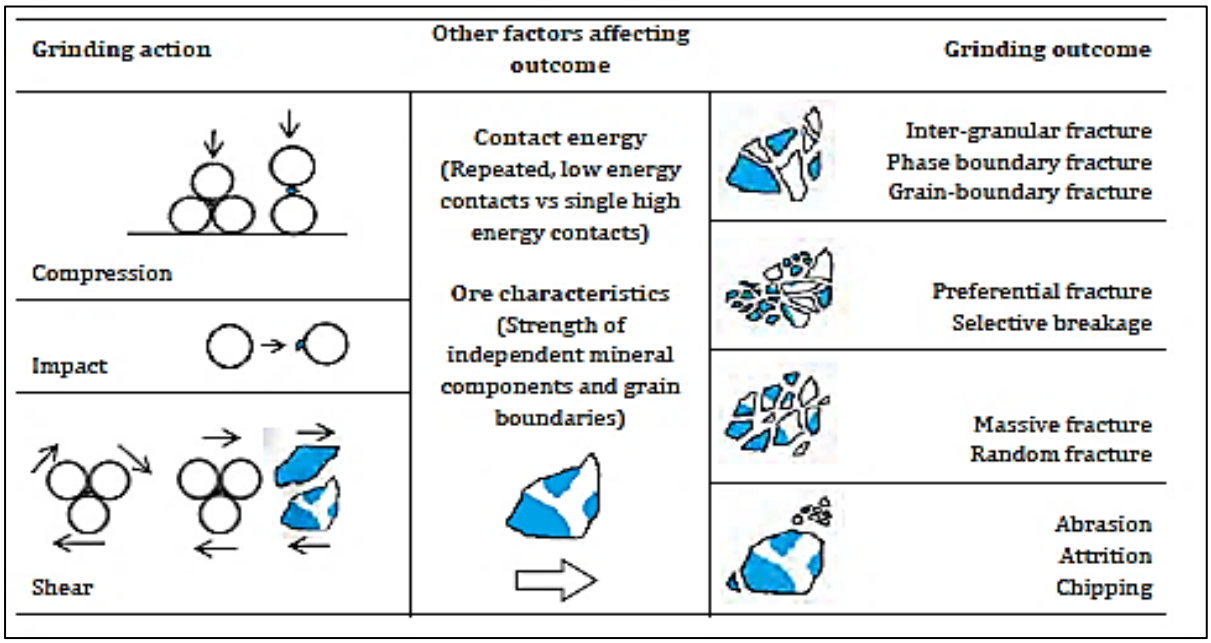

Figure 2-3: Illustration of the breakage mechanisms and the possible breakage patterns. Circles represent grinding media, shaded and unshaded represent the different mineral phases (Little et al., 2016).

Compression

This is a breakage mechanism in which a compressive force is applied to induce particle failure Figure 2-3. Grinding media and larger particles are the driving force for compression breakage. Fracture only takes place when the Unconfined Compressive Strength (UCS) is exceeded (Napier-Munn et al., 1996). The Point Load Test is widely used to characterize individual particle compression breakage behaviour (Broch & Franklin, 1972). The main measurements that can be obtained from compressive tests are the UCS, Poisson's ratio and Young's Modulus. However, with this mode of breakage, it is difficult to measure the specific input comminution energy for breakage and as such particle size distributions are rarely obtained (Schroe, 2016). This type of breakage mechanism is the main breakage mode in jaw crushers, High Pressure Grinding Rollers (HPGRs) and cone crushers.

Shear

When a force acts parallel to a particle surface, this results in shear stress causing surface breakage (Wills & Napier-Munn, 2006). Abrasion and attrition are two forms of surface breakage caused by the application of shear stress on a particle surface. This type of breakage mostly leaves the surface of the large parent particle intact while gradually wearing small particle fragments off the surface of the parent particle (Napier-Munn et al., 1996). Abrasion is a form of size reduction that results from particles inducing shear stress on other particles by moving against each other. This breakage mechanism results in the gradual wearing down of the particles involved (Wills & Napier-Munn, 2006). Attrition is a form of size reduction that occurs when a small particle is trapped between two larger particles or grinding media. The smaller particle is preferentially broken while leaving the larger particles or grinding media intact (King, 2001b). Shear breakage (abrasion and attrition) is the dominant breakage mechanism in stirred mills (Sinnott et al, 2006; Ye et al., 2010; Chaponda, 2011).

Impact

Impact breakage is induced when a compressive stress is applied rapidly to a particulate material resulting in disintegrative fracture (Tavares, 2007). In addition, impact breakage can either be the result of numerous low energy impacts or one high energy impact. Size reduction during a high energy impact is a result of brittle fracture and crushing (King, 2001a). The impact breakage mechanism is dominant in ball mills especially at the toe of the mill (Tavares & King, 1998). Ore breakage characterisation tests mimic the high energy found in ball mills and as such the energy range tested (0.1-2.5kWh/t) is sufficient to cause a single impact breakage (Napier-Munn et al., 1996). Impact breakage can occur on a single particle or on a particle bed such as that found on the base of tumbling mills (Tavares & King, 1998).

Figure 2-4 illustrates the progeny size distribution achieved by different comminution actions. Compressive stresses alone cannot produce a very fine progeny, but rather, a broad spectrum of larger particle sizes. Shear stresses produce a fine progeny with a small size distribution. Impact is an intermediate between the two former comminution stresses and produces a progeny that is characteristic of both shear and compressive stresses (broad spectrum of sizes).

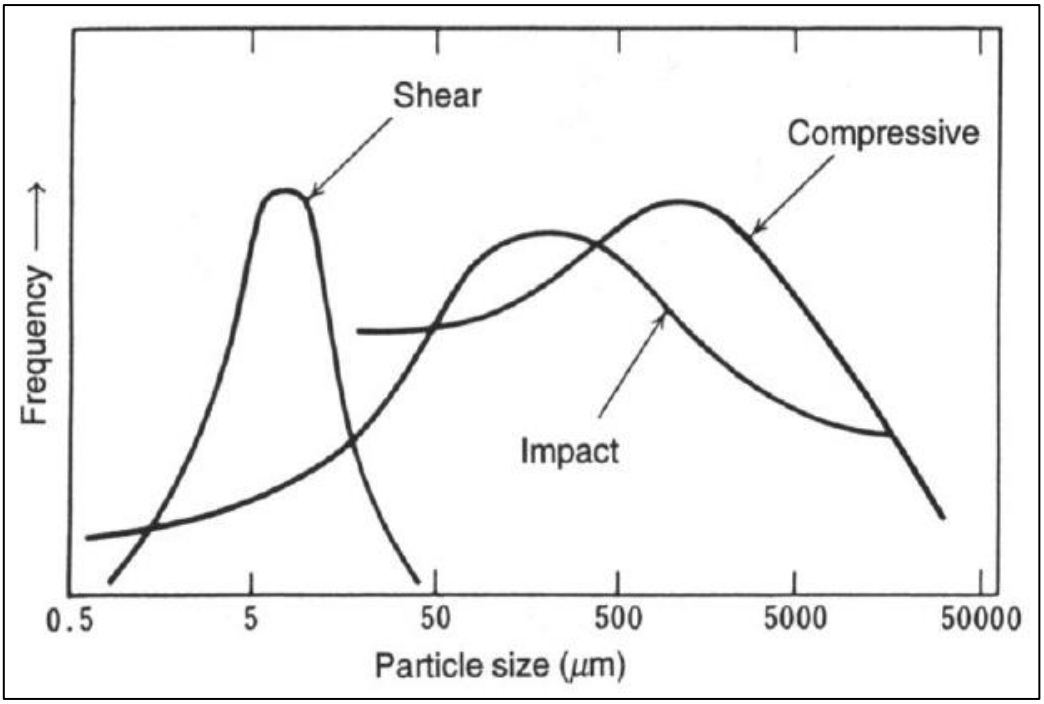

Figure 2-4: Progeny size distribution achieved by different comminution mechanisms (Tavares and King, 1998).

2.2.2 Patterns of Particle Breakage

From fracture mechanics, the broad terms random and non-random are used to describe the fracture patterns that take place under different conditions. When particles within the same size class are broken into a unimodal distribution of finer particles which have the same grade as the initial particle, the term random fracture is used. With random fracture, a particle breaks without showing any preference for breakage of one region over another as depicted in Figure 2-3 (King, 2001a). This term is only applicable when the population balance model is being used for an ore type and the influence of mineralogy and texture is not being considered to affect the breakage pattern (Vassiliev et al, 2008). Any breakage pattern that does not hold the above-mentioned criteria is classified as non-random fracture.

Non-random fracture is described as a fracture pattern that is influenced by the mineralogical and textural compositions of the parent particle and shows preferential breakage of one region over another (King, 2001a). The difference in breakage patterns in non-random fracture are a result of the presence of zones of weakness in the particle structure which are linked to the mineralogical and textural composition of the particle. The work of King & Schneider (1998) grouped non-random fracture as either preferential breakage or phase boundary breakage as it is not typical to

differentiate between the mechanisms in each group. The study stated that differential and selective breakage could be grouped with preferential breakage while boundary region fracture and phase boundary breakage could be grouped together (King & Schneider, 1998).

Preferential breakage Figure 2-3 is a form of non-random fracture in which one mineral phase exhibits the most fragment occurrence of crack branching. Preferential breakage arises from differences in the breakage rates of the minerals present in the ore. Preferential breakage often leads to varying levels of mineral deportment to different size fractions (Vassiliev et al, 2008). Differential breakage occurs when the composition of the parent particle has a direct influence on the progeny size distribution characteristics. Selective breakage transpires from the different degrees of brittleness of the mineral phases present. Particles with a larger content of the more brittle mineral phase exhibit faster rates of breakage. This is because more brittle minerals fracture easily (King & Schneider, 1998).

A phase boundary is the interface between two minerals grains in a multi-component ore (Little et al., 2016). Phase boundary fracture takes place when breakage is frequently along the phase boundary between two minerals rather than through either of the phases due to the existence of weak bonds between mineral grains (Vassiliev et al, 2008). Fracture is induced by high stress concentration at the phase boundary. This phenomenon is less observable directly, but rather inferred from progeny analysis. Additionally, when the particles are analysed, a more than proportionate exposure of the mineral on the surface is a good indicator of phase boundary fracture (King & Schneider, 1998).

The work of Chikochi (2017) who used UG2 ore, showed that chromitite exhibited phase boundary breakage due to its textural properties. The study concluded that UG2 chromitite consisted predominantly of rounded chromite grains contained in a matrix of plagioclase which resulted in chromitite particles breaking along the chromite grain boundary and producing a bimodal progeny size distribution (Chikochi, 2017). Phase boundary fracture therefore depends largely on the ore mineralogical and textural characteristics.

2.3 Single Impact Breakage Tests

Ore breakage characterisation is a key component of the geometallurgical approach and plays a critical role is the design and optimization of comminution circuits. Impact breakage tests are commonly used in ore breakage characterisation as they represent the most elementary process in comminution (Tavares, 2007). Additionally, the impact of falling media has extensively been

reported to be the most effective cause of fundamental fracture in tumbling mills (Kawatra, 2006; Narayanan, 1987). Single impact breakage tests are used to assess the hardness of an ore when it is subjected to an impact load.

Single impact particle breakage is advantageous as it minimizes energy losses due to friction and unsuccessful impacts. Additionally, no losses due to particle to particle interactions exist (Tavares, 2007). Single impact particle breakage tests are utilised to investigate the energy-size relationship, investigate the breakage characteristics of comminution and investigate energy usage and losses during comminution to mention a few. These tests can be classified as low-impact velocity and high-impact velocity. Low impact velocity tests are free fall tests like the Drop Weight Tester and the Twin Pendulum Tester. High impact velocity tests subject impact on a particle by propelling the particle against a hard surface or subjecting the particle to impact from a hard projectile (Split Hopkinson Pressure Bar, Impact Load Cells and the JKMRC Rotary breakage tester).

2.3.1 Twin Pendulum Tester

The twin pendulum device was developed at the Julius Kruttschnitt Mineral Research Centre (JKMRC) as the first device capable of single particle characterisation testing. The device enabled researchers to assess the energy needed for breakage as well as the resultant progeny size distribution (Napier-Munn et al., 1996). Figure 2-5 depicts a schematic of a typical twin pendulum tester.

The pendulum tester is a simple device that makes use of input and rebound pendula to enable breakage of the particle. The input pendulum is released from a known height and impacts the particle which rests between the rebound pendulum and the input pendulum (Napier-Munn et al., 1996). A rope and pulley system guarantee smooth movement of the input pendulum. The rebound pendulum period is measured using a laser detector to compute the remaining energy. This method involves monitoring 25 swings of the rebound pendulum to determine the period loss per swing (King, 2001a).

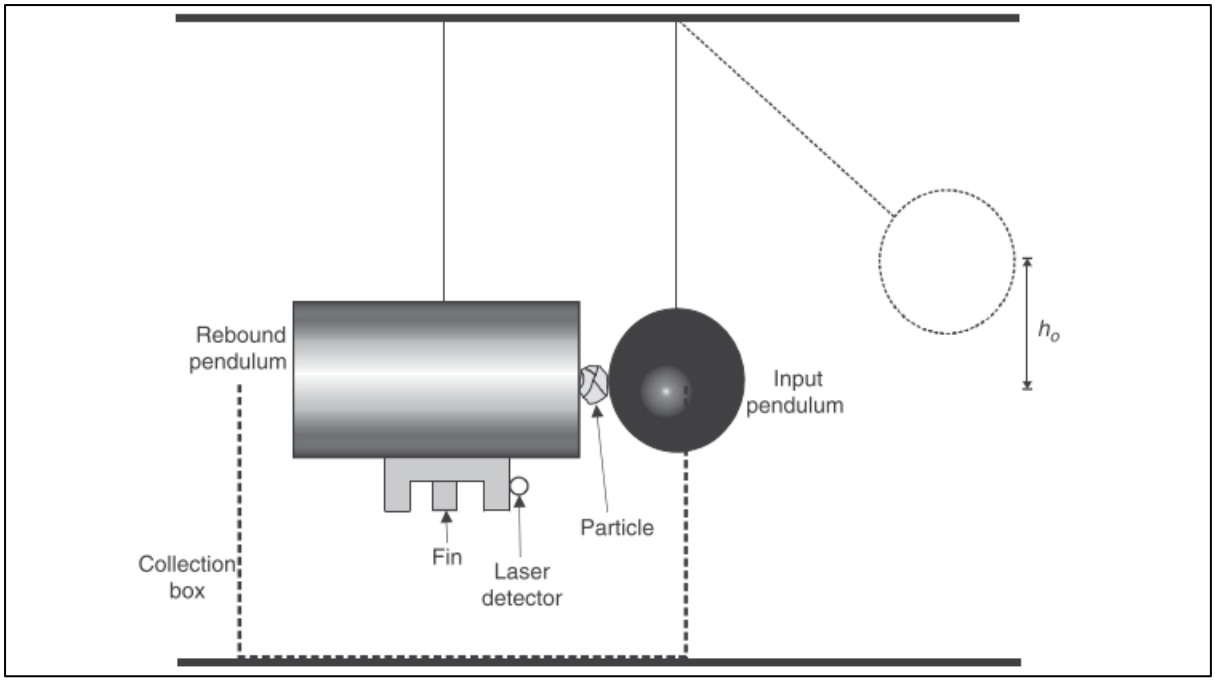

Figure 2-5: Schematic diagram showing a computer-monitored twin pendulum device. The initial pendulum height (h_0) and position of the particle are indicated (Tavares, 2007).

The energy transferred from the input pendulum to the rebound pendulum can be computed as follows (Napier-Munn et al., 1996):

$$E_t = M_r(L - Lcos\theta) \qquad \text{Equation 5}$$

where E_t is the energy transferred from the input to the rebound pendulum, M_r is the mass of the rebound pendulum, L is the pendulum length and θ is the angle through which the rebound pendulum is displaced after impact.

The introduction of this device was advantageous due to its simplicity, both in operation and the resultant data analysis. Additionally, the proportion of the input energy that is used for particle breakage can be calculated using the measurements from the rebound pendulum (Tavares & King, 1998). However, the disadvantages associated with this device are numerous. The biggest disadvantages are the limited energy input and particle size ranges that can be tested. Another major shortcoming is the fact that conducting breakage tests using the twin pendulum device is time consuming (King, 2001a).

2.3.2 Simple Drop Weight Tester

The Drop Weight Tester (DWT) was developed at JKMRC and superseded the Twin Pendulum device. Over time, it has become the most widely used ore characterisation device (De Magalhães & Tavares, 2014). Figure 2-6 provides a schematic of the DWT setup.

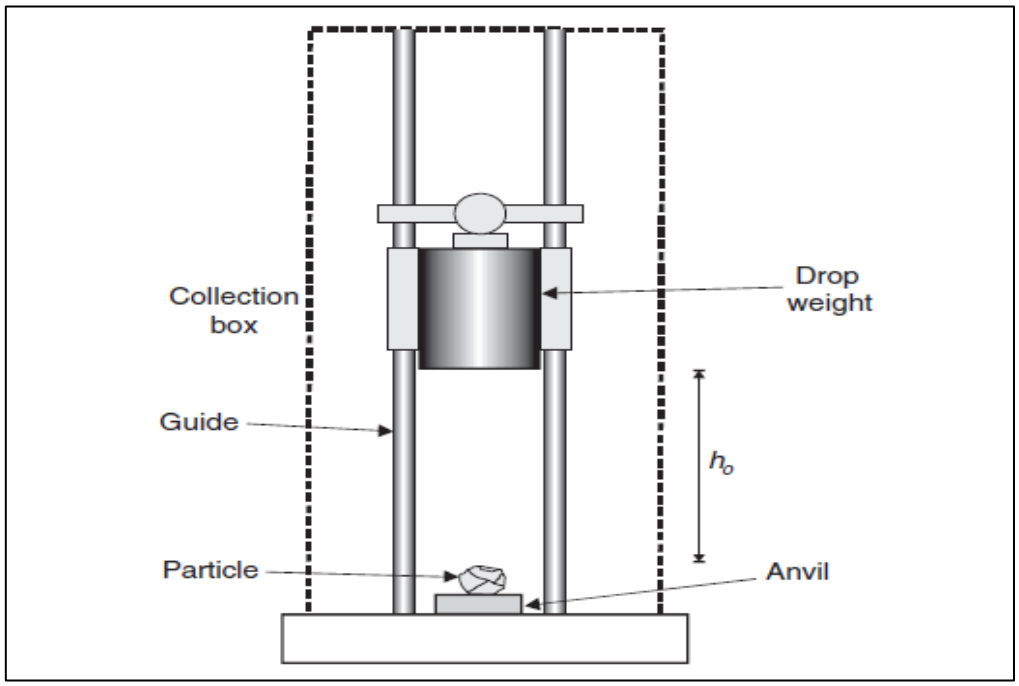

Figure 2-6: Schematic diagram showing the setup of a simple drop weight tester (Tavares, 2007).

The DWT comprises of a simple mechanism that makes use of a drop weight of known mass falling under the influence of gravity from a known height. As the drop weight falls, the potential energy prior to release is converted to kinetic energy which is transferred to a single particle/bed of particles resting on an anvil. Guide rods with minimal friction are used to ensure that the weight falls evenly and therefore impacts the particle uniformly (Tavares, 2007). A Perspex enclosure is mounted directly on a concrete platform to ensure that the resultant product is not lost after impact.

The DWT assumes that the kinetic energy at the point of impact is the same as the initial potential energy of the drop weight before release (conservation of energy). Depending on the particle properties and the energy input, the particle may or may not fracture on impact. After impact, the space left between the weight and the anvil corresponds to the energy not used for breakage. The actual input energy can be computed using the following equation (Napier-Munn et al., 1996):

$$E_{cs} = \frac{0.0272 * h_d (h_i - h_f)}{m} \qquad \text{Equation 6}$$

where h_i is the initial drop weight height, h_f is the final drop weight height, h_d is the drop weight mass and E_{cs} is the specific input energy. Table 2-1 shows a summary of how the DWT energies are calculated from the particle mass, drop height and drop weight mass for different energy-size combinations.

Table 2-1: Illustration of the DWT input values (Data source: UCT inhouse data).

Size Range	Mean Particle Mass	Ecs	Drop Head Mass	Calc Drop Height	Rest Height Adjust	Actual Drop Height
mm	g	kWh/t	kg	cm	cm	cm
63.0 - 53.0	325	0.10	15	80.74	3.17	83.91
	325	0.25	35	86.8	2.55	89.35
	325	1.00	50	95.76	2.09	97.85
45.0 - 37.5	124.33	0.10	50	86.25	2.66	88.91
	123.72	0.25	15	75.81	2.23	78.04
	124.33	1.00	5.3	91.2	1.42	92.62
31.5 - 26.5	45.87	0.10	45	79.26	1.79	81.05
	45.84	1.00	20	84.27	0.88	85.15
	45.71	2.50	5.3	93.68	0.54	94.22
22.4 - 19.0	18.64	0.25	2.5	68.02	1.14	69.16
	18.64	1.00	15	45.69	0.57	46.26
	18.58	2.50	20	85.66	0.36	86.02
16.0 - 13.2	6	0.25	2.5	22.04	0.81	22.85
	6.04	1.00	2.5	88.44	0.5	88.94
	6.02	2.50	15	36.76	0.27	37.03

The development of the DWT improved specific input energy control and allowed for more tests to be run as it is relatively faster than the twin pendulum device (Napier-Munn et al., 1996). The DWT increased the specific input energy range as the initial drop weight height and mass can be changed (0.01-50kWh/t). The shortcoming of the DWT includes the fact that tests are time consuming (De Magalhães and Tavares, 2014). Additionally, the calculations involved in DWT tests do not consider the frictional losses experienced as the drop weight moves down the guide rods (Shi et al., 2009).

2.3.3 Split Hopkinson Pressure Bar

John Hopkinson is credited with developing the Hopkinson bar technique in 1872 as a device for performing stress wave tests. This technique was further refined and altered in 1914 by Bertram Hopkinson (son) as he attempted to quantify the pressure explosives release. To date, numerous modifications have been made to the original Hopkinson bar, however it still maintains the basic functions (Xia & Yao, 2015). The Split Hopkinson Pressure Bar (SHPB) devices that are currently

available can provide information on the damage before fracture and optimum breakage energy. The typical SHPB setup is illustrated by in Figure 2-7.

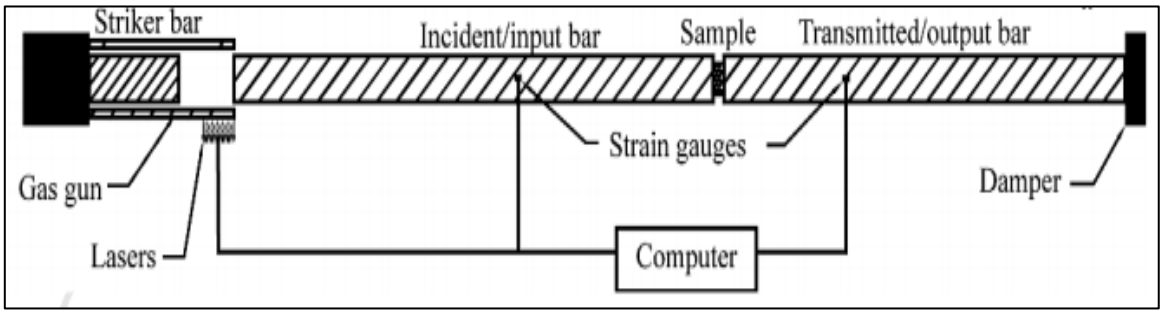

Figure 2-7: Schematic showing the typical SHPB setup (Xia & Yao, 2015).

A typical SHPB device consists of three main parts i.e. the input/incident bar, output/transmitted bar and the striker bar. As depicted in Figure 2-7, the particle being tested is placed in between the transmitted and incident bars. The two bars which are mounted on a frame function by moving only in the longitudinal direction. The bars move in one direction because they are fitted with bearings and bushes (Song & Chen, 2005). The SPHB functions by firing the launcher (gas gun) to hit the striker bar which subsequently impacts the incident bar. The elastic compressive wave generated interacts with the particle placed between the incident and transmitter bars. The remaining longitudinal stress wave produced by the striker reaches the transmitter bar which is embedded with strain gauges. These gauges produce voltage signals proportional to the strain received by the bar which are recorded on a computer (Napier-Munn et al., 1996). The SHPB test produces incident strain energy, specimen energy absorbed and force to fracture energy outputs.

Work by Bbosa et al, (2006) showed that the SHPB is useful when conducting both single and incremental breakage tests. However, test work performed using the SHPB device is time consuming and only works well within a narrow size range. In addition, this device does not allow for particle bed breakage test to be conducted (Song and Chen, 2005).

2.3.4 Impact Load Cell

The Impact Load Cell (ILC) was developed by Reiner Weichest in 1986 at the University of Utah as an ideal way to combine the Split Hopkinson Pressure Bar and Drop Weight Tester for better results (Bourgeois & Banini, 2002). Figure 2-8 depicts the typical setup of an ILC.

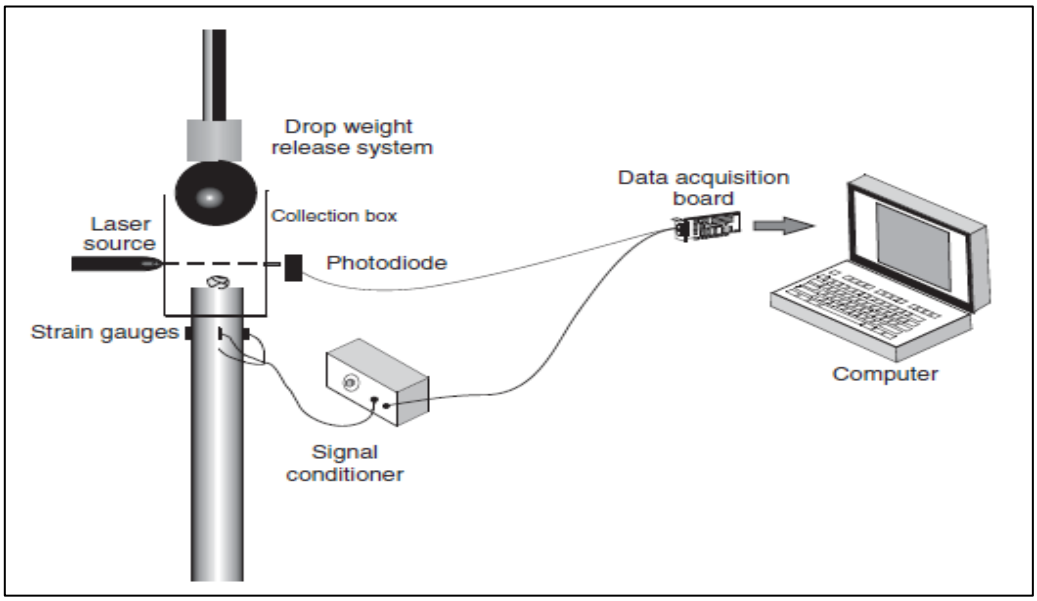

Figure 2-8: Schematic showing a typical impact load cell (Tavares, 2007).

The ILC comprises the DWT mechanism (a weight of known mass dropped vertically from a known height). The weight is used to transfer energy to the particle upon impact. The particle being tested rests on a steel rod which is embedded with solid strain gauges to measure the impact response. The velocity just prior to impact is measured using a laser accelerometer which is mounted about 1mm or less above the particle (Bourgeois and Banini, 2002). At impact, the weight applies a force on the stationary particle which produces a compressive wave. The compressive wave travels through the rod where it is detected by strain gauges (Tavares & King, 1998).

The Short Impact Load Cell (SILC) is a modified version of ILC which has a shorter rod. Particle size range is between the nano to millimetre range (Schroe, 2016). The SILC can be used to measure the particle loading under dynamic compression, compressive force, material stiffness, energy absorbed by the particle and first fracture energy. The advantages of the ILC is that it is capable of productive force-time measurements and can be used to test both single particle and bed breakage. It is also easy to transport and store because of its physical dimensions. However, the input energy range is very limited in this device i.e. it can only be used for low impact energy tests (Bourgeois and Banini, 2002).

2.3.5 Julius Kruttschnitt Rotary Breakage Tester

The Julius Kruttschnitt Rotary Breakage Tester (JKRBT) is a rapid characterisation device that was designed and developed at the Julius Kruttschnitt Mineral Research Centre (JKMRC). This device achieves breakage using controlled kinetic energy (Kojovic & Shi, 2002). The JKRBT was used for rapid ore characterisation tests in-house at the JKMRC before being made commercially available. This device can investigate four of the five DWT size fractions and specific energies ranging between 0.001 - 3.9 kWh/t. In South Africa, only two of these devices have been installed since 2007 – at the *Anglo* and Sibanye Stillwater Research Labs (Zuo & Shi, 2016).

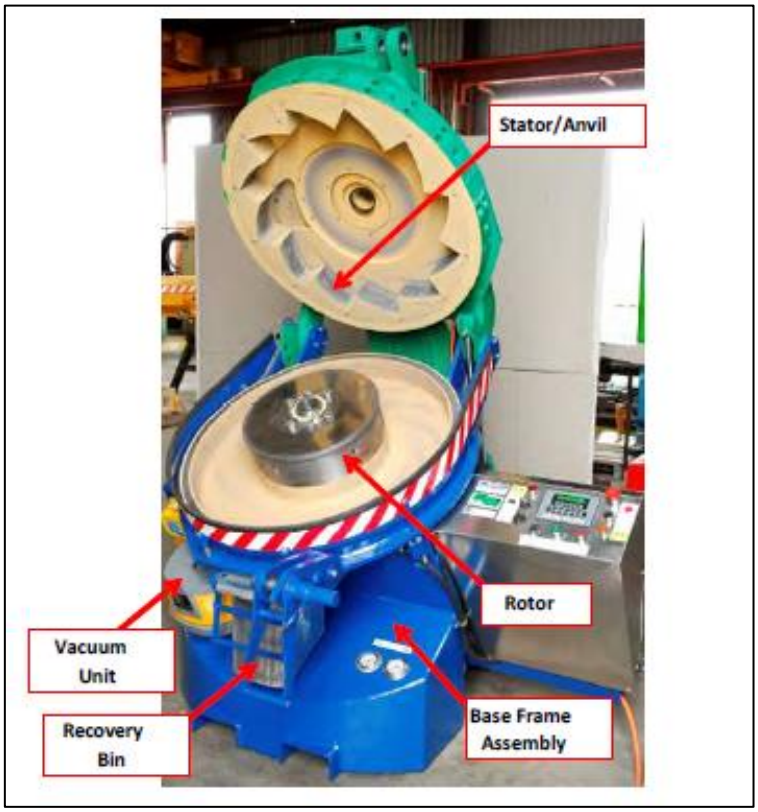

Figure 2-9: Labelled image of the JKRBT (Shi et al., 2009).

The JKRBT uses a rotary-stator impacting system coupled with a feeding system and progeny collection compartments (Kojovic and Shi, 2002). A hand-driven feeder is used to deposit the particles one at a time into the rotor. These particles gain controlled kinetic energy when they are spun round in the rotor (Shi *et al.*, 2009). Impact occurs when the particle is ejected from the rotor and smashes against a circular anvil. Particles can eject from the spinning flywheel at speeds of up to 160 m/s. The energy at which the particle hits the circular anvil is an important parameter and is adjusted by a variable frequency drive which controls the spinning flywheel speed. The resultant progeny falls down the radially inclined device and is collected in a bin by a vacuum (Shi et al.,

2009). The kinetic energy per particle mass is defined as the specific input energy (E_{cs}) for a particular impact. The E_{cs} can be computed by the following equation (Kojovic and Shi, 2002):

$$E_{cs} = \frac{E_k}{m} = \frac{\frac{1}{2} * m * V_i^2}{m} = \frac{1}{2} * V_i^2 \qquad \text{Equation 7}$$

where E_{cs} is the specific input energy (kWh/t), E_k is the kinetic energy (kJ), m is the particle mass (kg) and V_i is the velocity just prior to impact (m/s). Based on equation 7, the specific input energy is solely dependent on the velocity and therefore the particle mass no longer has an influence on the specific input energy.

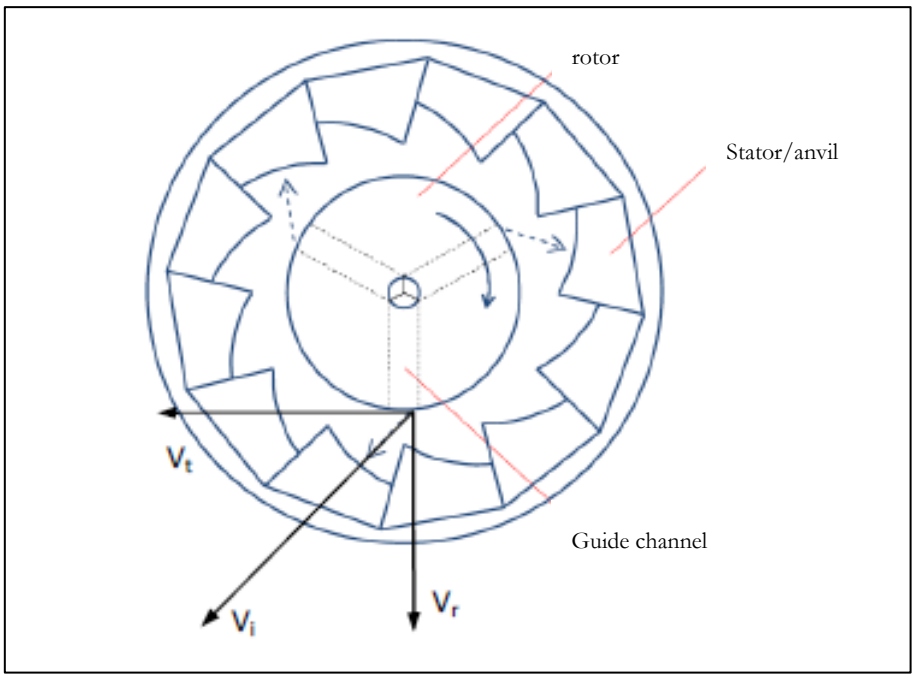

Figure 2-10: The velocity components of a particle when it exits the rotor (Shi et al., 2009).

As depicted by Figure 2-10, the impact velocity (V_i) is a result of the combined effect of the radial and tangential velocity (V_t and V_r) components. The short distance travelled by the particle from the rotor to the anvil and the constant rotor speed lead to the assumption that the velocity of the particle as it exits the rotor is equal to that at the anvil (Bbosa, 2006). The tip speed, theoretically, should be equal to its radial and tangential components (Ballantyne et al, 2015). The impact velocity can therefore be expressed as follows:

$$Vi^2 = Vr^2 + Vt^2 \qquad \text{Equation 8}$$

$$Vi = \sqrt{2Vt} \qquad \text{Equation 9}$$

However, as with any equipment, the transfer of energy is not perfect and therefore 100% energy transfer cannot be assumed. Hence, a calibration factor C is used to account for this inefficiency.

Calibration factors were established for the JKRBT using high-speed video analysis (Shi et al., 2009). The E_{cs} can therefore be computed as follows (Shi et al., 2009):

$$Ecs = \frac{0.5*\left[C*\sqrt{2}*\frac{2*\pi*N*r}{60}\right]^2}{3600} \qquad \text{Equation 10}$$

$$Ecs = 3.046 * 10^{-6} * C^2 * N^2 * r^2 \qquad \text{Equation 11}$$

where E_{cs} is the specific input energy (kWh/t), C is the velocity constant, N is the rotor speed (rpm) and r is the rotor radius (m).

The JKRBT overcame the limitations of previous characterisation devices by reducing the time required to complete the tests and increasing energy input precision (Shi and Kojovic, 2007). When compared, the DWT and JKRBT produce breakage-energy data that is very closely related provided that the size class and ore type are constant as illustrated by Figure 2-11 (Kojovic and Shi, 2002). However, though the JKRBT is a rapid characterisation device, sample preparation is tedious and time consuming due to the amount of sample required and size range specifications needed to complete the full suite of tests. A typical matrix of 12 RBT tests requires 360 particles grouped in small particle size fractions which can prove to be difficult to achieve. Practically speaking, sample availability is a major concern when performing metallurgical testing as numerous tests need to be performed to get a complete view of the metallurgical response of the ore type. This means that very little of the sample is available for ore breakage characterisation. Reducing the amount of sample required for RBT tests would help address these challenges.

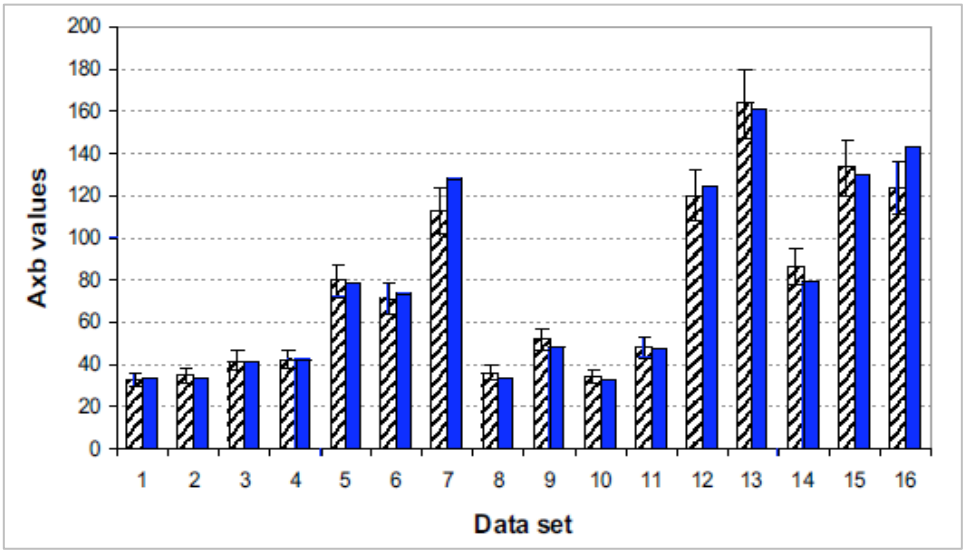

Figure 2-11: Comparison of A*b breakage parameters determined by the DWT and JKRBT. The solid blue bars correspond to the JKRBT results (Kojovic and Shi, 2002). See section 2.5.1 for details on the calculation of A and b.

2.3.6 Comparison of single impact breakage tests

Table 2-2 summarises the advantages and disadvantages of each breakage test. An appropriate ore breakage test should be repeatable, fast, test a wide range including high energy levels and should be able to test a wide size range (Mwanga et al, 2015). Based on these criteria, the JKRBT was chosen as the device to be used for ore breakage characterisation tests as it had the most advantages when compared to other breakage devices.

Table 2-2: Summary of the advantages and disadvantages of each breakage test - adapted from Mwanga et al. (2015).

Ore breakage Test	Advantages	Disadvantages
Twin Pendulum	- Simple to use - Can calculate energy used for actual breakage	- Limited energy range - Limited particle size range - Time consuming - Single particle tests only
Drop Weight	- Improved energy control - Faster that twin pendulum - Wide energy range - Wide size range - Particle bed can be investigated	- Time consuming - Does not consider frictional losses experienced due to guide rods
Split Hopkinson Pressure Bar	- Single impact and incremental breakage test - Faster than DWT	- Time consuming - Narrow size range - Cannot test particle bed
Impact Load Cell	- capable of productive force-time measurements - can test single particles and particle beds - portable	- Limited input energy range - Low energy tests only
JKRBT	- Precise specific input energy control - Repeatability (fast) - Wide specific input energy range - Wide size range - Statistically more valid because of the large number of particles tested - High velocity device	- Sample preparation is time consuming due to the narrow size fractions - One complete test requires 360 particles - Cannot quantify the energy used for breakage - Problems in producing the specific sizes due to limitations in obtaining bulk ore supply - Expensive to acquire

2.4 Data Representation

Particle size is a common parameter used to describe a population of particles. This is useful in developing correlations between benchmark comminution tests and progeny particles size. In industrial comminution circuits, oversize particles are prevented from passing to subsequent processing stages using size classification. These particles are, instead, recycled back into the circuit for further grinding.

The progeny obtained from breakage tests is often characterised on a mass basis. Traditionally, particle size distributions can be determined using a geometric series of √2 screens with decreasing sieve aperture. Screens act as a barrier which can only pass undersize material while oversized material is retained on the screen itself. The breakage progeny is placed onto the top screen with some particles being retained and others progressively moving down the stack of screens. The mass of particles retained on each screen is determined and recorded. The cumulative percentage mass passing a given screen size can be used to plot a progeny particle size distribution, as illustrated by Figure 2-12.

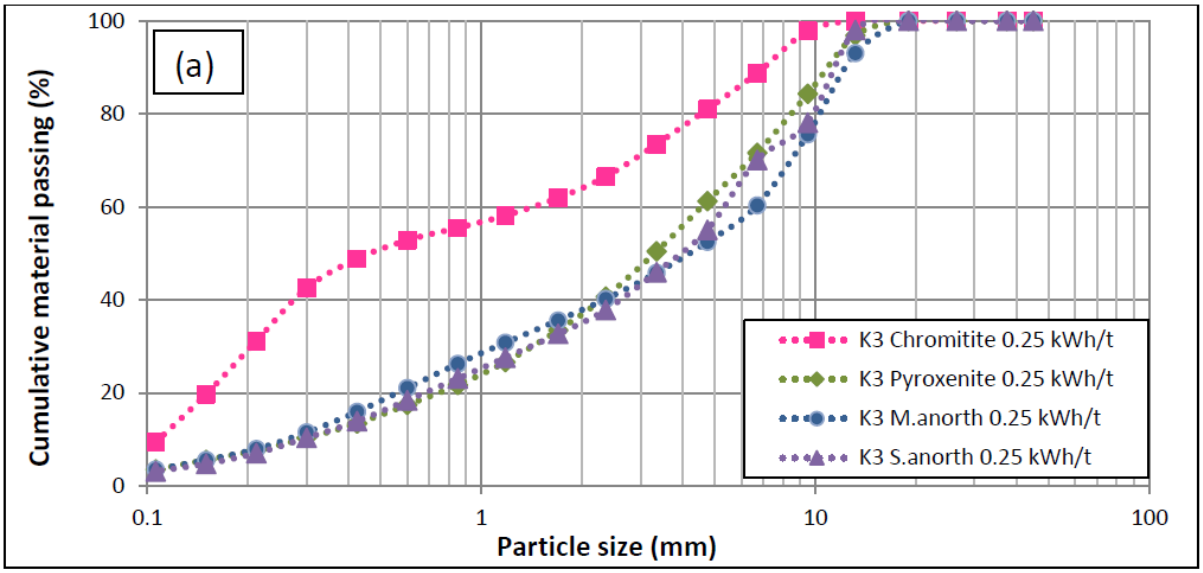

Figure 2-12: An example of a progeny particle size distribution for UG2 ore characterised using the JKRBT. (Chikochi, 2017).

By defining the top size as the maximum (100% mark), any Y-coordinate would correspond to a fraction of the maximum percentage (t). Hence, t_n is a parameter that describes the percentage of material that passes n/t of the feed size. Of all the possible indices, the t_{10} characterisation index is the most widely used in breakage characterisation. The t_{10} index is a fineness parameter that represents product cumulative percent passing one tenth of the feed size. For instance, in Figure 2-12, for a K3 Chromitite feed at 0.25 kWh/t, a t_{10} value of 60 defines that 60% of the particles in

the product are smaller than 1.45mm (one tenth of the geometric mean 14.5mm). A high t_{10} value indicates a finer product, whereas a low value indicates a coarser product (Shi, 2011). Most breakage models make use of the t_{10} parameter to develop a relationship between the specific input energy and progeny sizes.

2.5 Single Impact Breakage Characterisation Models

The relationship between input energy and size reduction has its roots in the early 19th Century (Ballantyne et al, 2015). Much time and effort has been dedicated to understanding the relationship between the energy used for breakage and the resultant progeny size characteristics (Ballantyne & Powell, 2014; King, 1994; Kojovic & Shi, 2002; Tanaka, 1966; Tavares & King, 1998). In ore breakage characterisation, the energy-size relationship is represented by ore breakage characterisation models that are in the form of mathematical equations. Numerous ore breakage characterisation models for single impact breakage have been developed and modified. The most relevant and commonly used models are discussed further in the following sections.

2.5.1 JK Standard t_{10} Breakage Model

This model was developed at JKMRC along with the DWT for analysis of the results obtained from the breakage tester. Of importance is the relationship between t_{10} and E_{cs} which Narayanan (1987) had reported as being linear. The work of Leung (1988) contradicted this by making use of breakage appearance functions to show that the energy-size relationship is exponential. The JK breakage model can be expressed in terms of these two variables as follows:

$$t_{10} = A(1 - e^{-bE_{cs}}) \qquad \text{Equation 12}$$

where t_{10} is the size distribution fineness index (%), A and b are the impact breakage parameters and E_{cs} is the specific comminution energy (kWh/t). The impact breakage parameters A and b are obtained when data is fitted to the model. The A parameter represents the maximum theoretical value of t_{10} i.e., in Figure 2-13 the A value for the "soft" curve is 70. The b parameter controls the shape of the curve and represents the gradient of the curve for low energies – below 1 kWh/t (Napier-Munn et al., 1996).

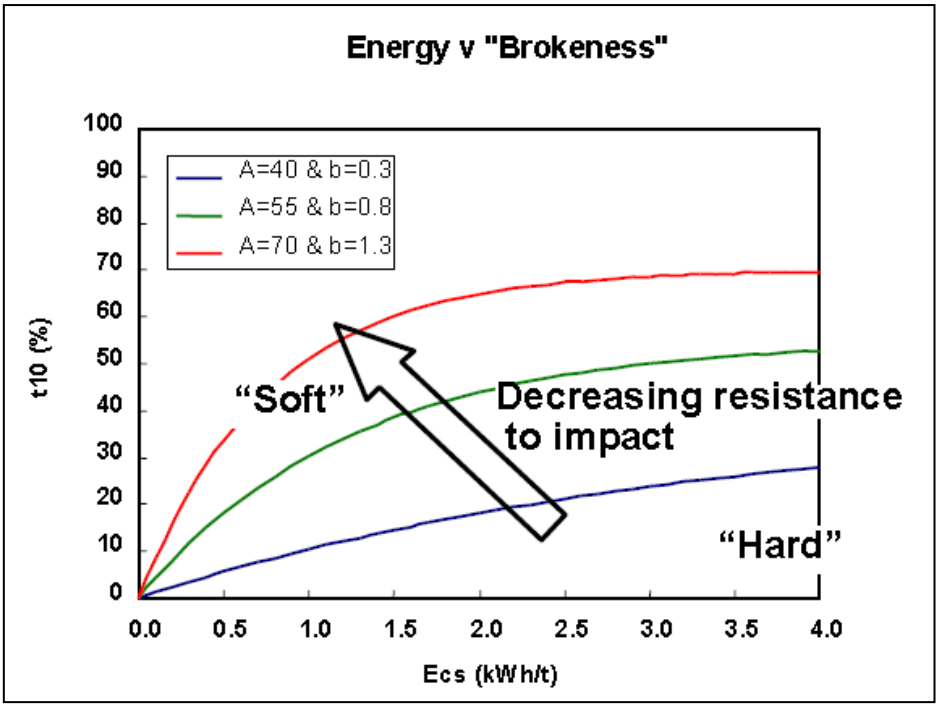

Figure 2-13: Energy vs Brokenness curve (Napier-Munn et al., 1996).

The two parameters A and b have an effect on each other and can be represented as one number i.e. A*b which relates the gradient of the t_{10}-E_{cs} curve at the origin. This can be explained mathematically by taking the derivative as the specific input energy approaches zero as follows:

$$t_{10} = A(1 - e^{-bE_{cs}})$$

$\frac{dt10}{dEcs} = -(Ae^{-bE_{cs}})(-b)$, take derivative and let E_{cs} approach zero

$$\frac{dt_{10}}{dE_{cs}} = -A * -b \qquad \text{Equation 13}$$

$$\frac{dt_{10}}{dE_{cs}} = A * b \qquad \text{Equation 14}$$

In this form, the resistance to hardness can be quantified. As the product A*b becomes smaller (blue curve), the material is said to be hard and having high resistance to impact. As the product A*b becomes larger (red curve), the material hardness and thus, resistance to fracture decreases as illustrated in Figure 2-13. The A*b parameter obtained for any ore can be compared and classified on the typical hardness scale (Table 2-3) provided in Napier-Munn et al. (1996).

Table 2-3: Typical hardness values during impact breakage (Napier-Munn et al., 1996).

Hardness	Very Hard	Hard	Medium	Soft	Very Soft
A x b	<30	30-38	38-67	67-127	>127

2.5.2 George Banini Breakage Model

The JK breakage model proved to be practical, however, a poor predictor across a large size range. This is because the model does not consider particle size and mass. Work by Bourgeois and Banini (2002) demonstrated that the hardness parameters (A and b) did not remain constant across a large size range. Therefore, an improved version of the JK model that included particle size was proposed by George Banini who used Bourgeois' drop weight data. The Banini model can be expressed as follows (Bourgeois and Banini, 2002):

$$t_{10} = 100 * \left[1 - \left(\frac{1}{\left(1+\left(\frac{\ln(E_{SV}+1)}{\alpha\wedge\infty^{-1}\, d^{-n}}\right)\right)^{\beta\infty}}\right)\right] \qquad \text{Equation 15}$$

where d is the particle diameter (mm), E_{sv} is the volumetric specific energy (kWh/m) and $a\infty$, $\beta\infty$, n are parameters to be fitted to the test data.

2.5.3 Vogel and Peukert Breakage Model

Single particle impact tests are used to determine material properties which, when combined with impact energy and initial particle size, allow for the description of the breakage probability and thereafter the breakage function for different minerals (Vogel & Peukert, 2003). Vogel and Peukert developed a model that considered the effects of particle size and ore properties on breakage. This model was largely based on both Hertzman theories of contact and Weibull statistics and can be expressed as follows (Vogel and Peukert, 2003):

$$S = 1 - e^{[-fmat*x*k(W_{m,kin}-W_{m,min})]} \qquad \text{Equation 16}$$

Where s is the breakage probability, $W_{m,min}$ is the theoretical minimum energy, W_{cri} is the critical energy value, x is the initial particle size and $k*(W_{m,kin} - W_{m,min})$ is the total mass specific input energy.

2.5.4 Particle Weakening Breakage Model

Tavares and King (1998) put forward a model that described the effect of multiple impacts on particle fracture using the Hertzman contact theory and continuum damage mechanics. This model only requires one experimental parameter, therefore, requires less experimental effort. The required parameter is material-dependent. The Particle Weakening model provides a link between progressive weakening of a particle after repeated impact and damage accumulation (Francioli et al., 2014). The model can be expressed as follows (Tavares and King, 1998):

$$D_n = \left(\frac{2\gamma}{2\gamma - 5Dn + 5} * \frac{E_{k,n}}{E_{n-1}}\right)^{\frac{2\gamma}{5}} \qquad \text{Equation 17}$$

where D_n is the damage accumulated at the nth impact, $E_{k,n}$ is the strain energy specific, E_{n-1} is the energy required to break the particle and γ is the damage accumulation constant. It is worth noting that this model will not suit our needs as it considers multiple impacts instead of single impact.

2.5.5 Size-Dependent Breakage Model

The main drawback of the JK breakage model is that it uses one set of A and b parameters for all particle sizes. The use of fixed parameters implies that particle size has no influence on breakage characteristics which is incorrect (Tavares, 2007). Vogel and Peukert (2003) claimed that their model could be used to quantitatively describe the breakage distribution function, however, failed to prove it. Furthermore, the breakage probability is less important than the progeny size distribution after breakage (Shi and Kojovic, 2007). The drawback was dealt with when Shi & Kojovic (2007) introduced the JK size-dependent breakage model. They modified the Vogel and Peukert model to describe the breakage index as a function of the net cumulative energy, particle size and mineral properties. This model is advantageous as it allows for direct quantification of the size effect on breakage. The size-dependent breakage model was initially only available for in-house use at the JKMRC until it was fully published in 2015. This model is based on the historically proven t_{10} concept and can be described by the following equation (Shi and Kojovic, 2007):

$$t_{10} = M[1 - e^{[-fmat*x*k*(E_{cs} - E_{min})]}] \qquad \text{Equation 18}$$

where t_{10} is the cumulative percentage passing 1/10 of the initial size (%), M is the maximum t_{10} for the material (%), E_c is the mass specific impact energy (J/kg) and E_{min} is the threshold energy (J/kg). Equation 18 can further be expanded into parameters that can be measured and constants as follows (Ballantyne et al, 2015):

$$t_{10} = M[1 - e^{[-3.6*p*d^{1-q}*k*(E_{cs} - E_{min})]}] \qquad \text{Equation 19}$$

where d is the feed particle size (mm), k is the number of repetitive impacts, E_{cs} is the specific input energy (kWh/t), E_{min} is the energy threshold (kWh/t) ,M is the maximum t_{10} for the material being subjected to breakage (%), p is the material characteristic parameter (t(kWh)$^{-1}$ (mm)$^{q-1}$) and q describes size effects on breakage (0-1). Table 2-4 shows a description of the meanings of some of the parameters mentioned above.

Table 2-4. A guide on the physical meaning of the q-value (Ballantyne, Peukert & Powell, 2015).

q	(1-q)	d(1-q)	Meaning
1	0	unity	Diminishing particle size effect
0	1	d	Indicates strong particle size effect on breakage
<0	>1	dn	Very strong particle size effect
>1	<0	d-n	Larger particles are more competent

The specific energy required to produce the desired t_{10} can thus be computed as follows (Ballantyne et al, 2015):

$$E_{cs} = \frac{\ln\left(1-\frac{t10}{M}\right)*3.6p*d^{1-q}*k*E_0}{-3.6p*d^{1-q}*k} \qquad \text{Equation 20}$$

To compute the theoretical energy required for a particle size (d) to generate the desired t_{10} (k = 1 and E_0 = 0 for a high energy single impact breakage):

$$E_{cs} = \frac{\ln\left(1-\frac{t_{10}}{m}\right)}{-3.6p*d^{1-q}} \qquad \text{Equation 21}$$

2.6 Factors affecting ore breakage characteristics

Various factors influence particle breakage characteristics: the stressing intensity, particle size, particle shape, mineralogy, texture, porosity, fracture network and, to a lesser extent, the particle moisture content have been identified as being influential in the particle breakage. These are discussed in more detail in the following subsections.

2.6.1 Stressing Intensity

The stressing intensity (input energy) is recognized as the most significant variable controlling ore breakage. Following Kick's law (equation 3), as the input energy increases, there is an increase in crack density and propagation up to the fracture threshold after which fracture takes place. When contact is made between the particle and the stressing tool, the input energy is converted to strain energy. As the input energy is increased, the strain energy becomes significantly greater than the crack resistance leading to crack propagation. The parent particle is finally broken into progeny particles when the crack(s) emerge from the particle. Therefore, increased input energy results in faster breakage rates (Tavares, 2007).

Generally, increasing the input energy causes an increased degree of fineness on the progeny. However, this relationship exhibits asymptotic behaviour where maximum fineness is achieved i.e. indefinite fineness is not produced even at maximum energy input. This is due to the ability of fine particles to agglomerate (Tavares and King, 1998).

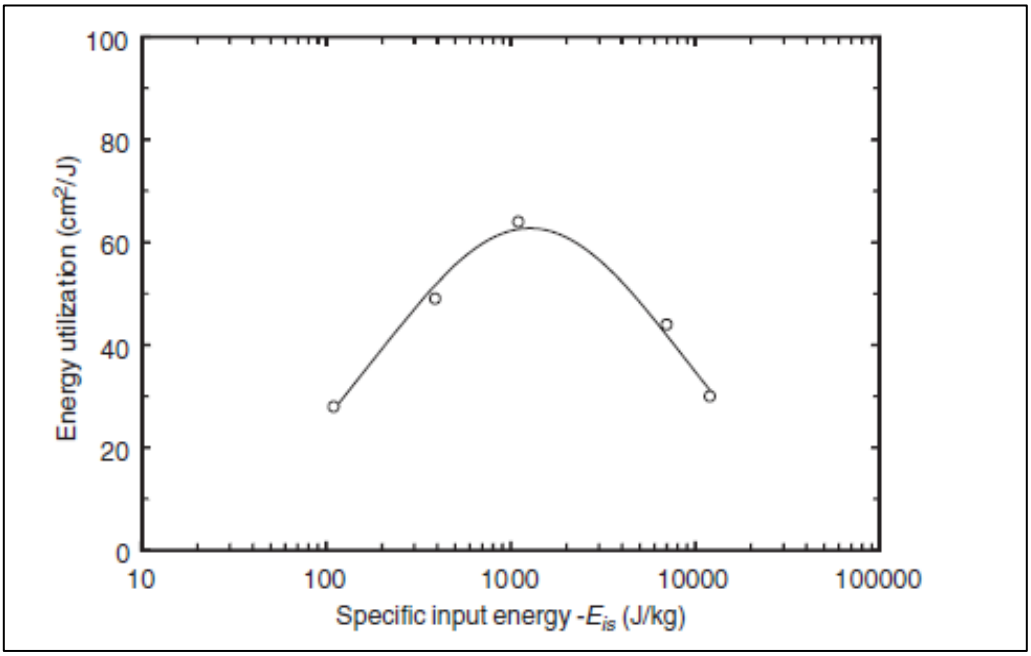

Figure 2-14: Relationship between the specific input energy and the energy utilisation (Tavares, 2007).

The relationship between the specific input energy and the energy utilisation is depicted by Figure 2-14. It is observed that an optimum is reached in terms of energy utilization i.e. 100% fracture probability. On either side of the curve, inefficiency exists. If less energy than the particle fracture strength is supplied, no fragmentation takes place as it cannot overcome the energy barrier. If too much energy is supplied, most of it is lost to friction. During single impact breakage, excess energy beyond the particles fracture energy is contained in the kinetic energy of the progeny. If this kinetic energy is directed to a surface, secondary breakage occurs further reducing the progeny particle size. The relationship between the progeny size distribution and the specific input energy is depicted in Figure 2-14 (Shi et al., 2009).

The work of Genç et al (2004) used the DWT procedure to investigate the influence of input energy on the resultant progeny distribution. The test work was carried out using 4 ore types (colemanite, quartz, copper and limestone) in narrow size fractions between -5.6mm to +55mm at increasing energy levels. The results obtained strongly conformed to Kicks hypothesis i.e. an increase in input energy within the same particle size range results in an increase in the fineness of the product size distribution.

A study by Chikochi et al (2017) investigated the breakage properties of 4 variations (chromitite, pyroxene, spotted anorthosite and mottled anorthosite) of Bushveld PGE ore grab samples using the JKRBT. The results presented conformed to Kicks law as illustrated by Figure 2-15. As the t_{10} is the indicator of the degree of breakage, a higher t_{10} value points to more fine progeny particles being generated. This result was consistent for all size fractions tested. Chikochi et al (2017) explained that an increase in the impact energy leads to a stress increase within the particle leading to a higher rate of crack propagation and rupture to form finer products.

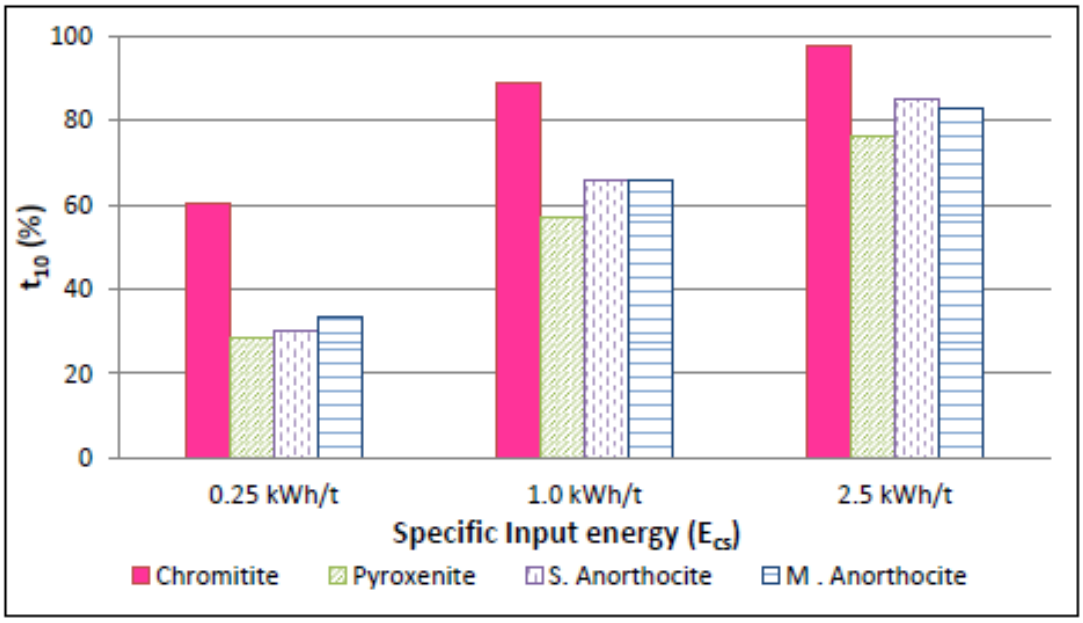

Figure 2-15: Effect of input energy on the degree of breakage of various UG2 rock types for (-16.0 + 13.2 mm) particles.

2.6.2 Particle Size

The feed particle size has long been recognized as one of the main factors affecting ore breakage. A study by Shi & Kojovic (2007) questioned the reliability and sensitivity of the historically used t_{10} model to changes in particle size. The fact that the t_{10} model does not consider the particle size effect is problematic especially in the design and modelling of SAG mills where particle sizes vary widely. The authors proposed the size dependent model which is a modified version of the Vogel and Peukert breakage model that takes a form similar to the t_{10} model but incorporates the particle size effect (equation 18). The proposed breakage model was validated using in house DWT data comprising 8 sample sets of 3 variations of quarry material tested at various energy levels and size fractions within the standard DWT ranges. The progeny obtained from the breakage tests was sized and modelled using both the t_{10} model and the proposed size dependent model. The authors

reported that the size dependent model was a better fit for the data than the t_{10} model. It was also observed that at the same energy, particles with smaller sizes required more energy for form a finer progeny.

Grain boundaries, cracks, flaws and pores are characteristics of any solid particle. A particle will begin to deform and crack when the stress concentration experienced within the particles varies across the particle (Shi & Kojovic, 2007). The authors explained that a smaller particle contains fewer grain boundaries and flaws due to its smaller size and volume. Such a particle requires a higher impact energy for cracks to result from these flaws. To turn into cracks. In general, the larger the particle size (more flaws), the less the energy required to break the particle (Shi & Kojovic, 2007).

In another study conducted by Norazirah et al. (2016) the effect of particle size was investigated. The standard DWT procedure was used on pegmatite (coarse grained igneous rock) ore from a quarry. The ore was screened into three size fractions (-5mm – 6.3mm, 6.3mm-10mm and 10mm-14mm) and tested at three energy levels (1.0kWh/t, 1.5kWh/t and 2.5kWh/t). The results obtained confirm to those found by Shi and Kojovic (2007). It was observed that at the same energy (1kWh/t) as the particle size increases from 5mm to 10mm, the degree of breakage increases from ca. 14% to ca. 27% i.e. larger particles require less energy to break due to abundance of cracks and flaws in their structure.

2.6.3 Particle Shape

In the same study conducted by Norazirah et al. (2016), the effect of particle shape on ore breakage was also investigated. The standard DWT procedure was used on pegmatite however the sample was separated into two distinct groups (flaky and equidimensional). The results reported show that under the same conditions, the t_{10} of the flaky particles is higher than that of the equidimensional particles for all test conditions. Particle fracture is a result of crack formation, propagation and subsequent rupture. However, this only takes place if the applied stressing intensity is higher than the stress threshold. The authors attributed the observed phenomenon to the flaky particles having a thinner cross-sectional area therefore making crack initiation and propagation easier for flaky particles (Norazirah et al, 2016).

Chandramohan et al (2010) studied the influence of particle shape on ore fracture. It was noted that the breakage models currently available do not incorporate the effect of particle shape on breakage behavior. The experimental method used classified particles according to their aspect

ratio (shortest length divided by the longest length) to separate the sample into two distinct particle shape groups (flakes and non-flakes). The authors defined flakes as elongated, flat particles and non-flakes as spherical particles. The flakes were then further divided according to orientation as depicted in Figure 2-16.

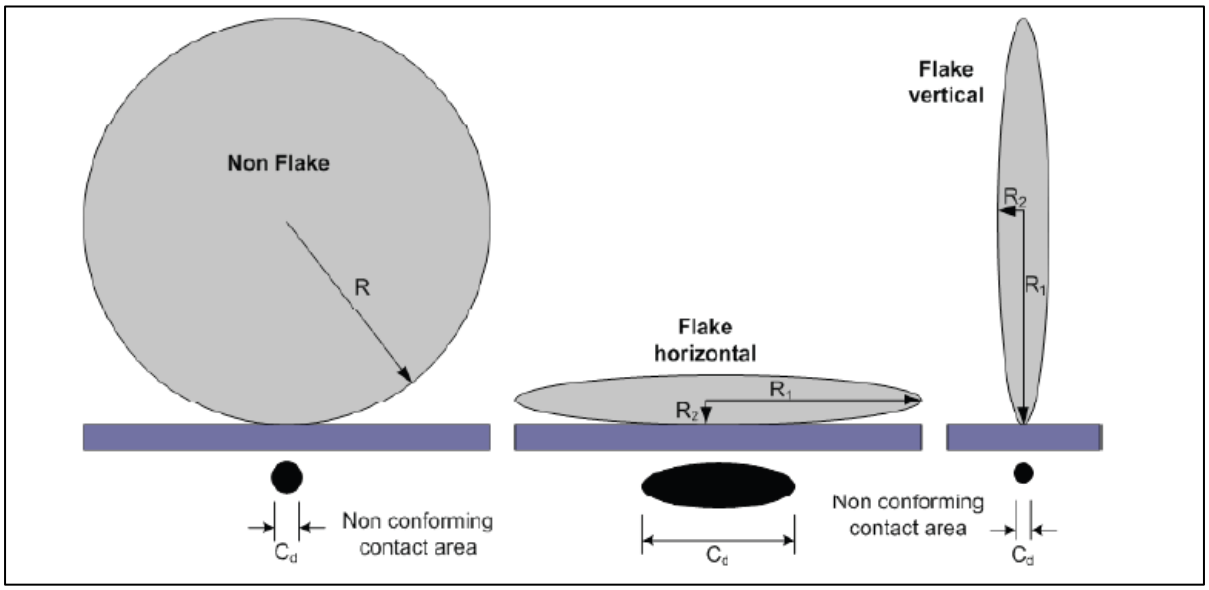

Figure 2-16: Non-conforming contact areas for each particle shape (Norazirah et al. 2016).

Controlled DWT tests were conducted using quarry granite feed at 3 energy levels for all 5 size fractions (no repeats) for each of the 3 particle shapes under investigation. The resultant progeny was sized using root 2 screens. Chandramohan et al (2010) used the size dependent breakage model to obtain the ore competence indicator for each particle shape. It was reported that horizontal flakes were the least competent, vertical flakes were the most competent and the competence of non-flakes was in-between the two. The authors reasoned that the energy absorption is a function of the particle shape because energy transfer takes place at the point of contact. Therefore, particles with larger surface areas exposed for contact require less energy to break (Chandramohan et al, 2010). The shape and contact area therefore control breakage. This work contributed toward knowledge by showing that it is possible to utilize the variations in hardness of different particle shapes to reduce comminution energy.

A study by Bbosa et al (2006) focused on the influence of particle shape on the breakage behavior of rounded and angular particles of a Bluestone ore. The experimental procedure was carried out at various size fractions and energy levels using the Split Hopkinson Pressure Bar tester. It was reported that though the fracture energy range is similar for the two particle shapes, rounded particles absorb more energy than angular particles and therefore have a greater probability of breakage. However, the author indicated that there were insufficient samples tested for a strong

statistical significance to be established. It is also worth noting that stereology (parallel bands formation) and the loading direction are also important, however they are beyond the scope of this work.

2.6.4 Mineralogy and Texture

Mineralogy affects the ore breakage properties because it has a direct effect on the hardness of the ore. It is an accepted fact that an ore is only as hard as its constituent minerals and their associated relative abundance within the ore. Mohs hardness scale is an accepted quantitative scale that ranks various minerals according to their scratch resistance. The scale ranges from 1-10 with 1 being the softest (talc) and 10 being the hardest (diamond) as shown in Table 2-5. Though numerous mineral hardness measures are available (Knoop hardness test, Vickers hardness test, Schmidt hammer test etc.), Mohs hardness test was chosen for this study because it is the most readily accessible as well as the abundant availability of data for various minerals. The hardness of an ore can therefore be considered to be a function of the mineral hardness and its relative abundance. Relating these two properties, it follows that are ore with a greater abundance of harder minerals will show greater resistance to breakage than an ore which contains less of the hard minerals and more of the softer minerals for an equivalent texture.

Table 2-5: Mohs Hardness Scale (webminerals, n.d.).

Mineral	Mohs Hardness
Talc	1
Gypsum	2
Calcite	3
Fluorite	4
Apatite	5
Orthoclase	6
Quartz	7
Topaz	8
Corundum	9
Diamond	10

A study by Yildirim et al. (2014) focused on developing a relationship between ore hardness and mineralogy using the SILC device. This study focused on the mineral proportions in each ore caused during copper ore formation. The findings of this work showed that there is a relationship between mineral grades and the process alternation index (PAI). Additionally, a linear correlation between the ED50 of force and the first fracture distribution obtained from single impact breakage tests (Yildirim et al., 2014).

Various concepts used in texture studies are illustrated by Figure 2-17. Interlocking, cemented (matrix supported) and glass mineral grain boundary types are shown in Figure 2-17a. The difference between interlocking grain boundaries and matrix supported grain boundaries lies in the fact that the former shows clear contact between the individual minerals comprising the rock while in the later individual minerals are contained in a larger mineral or matrix support.

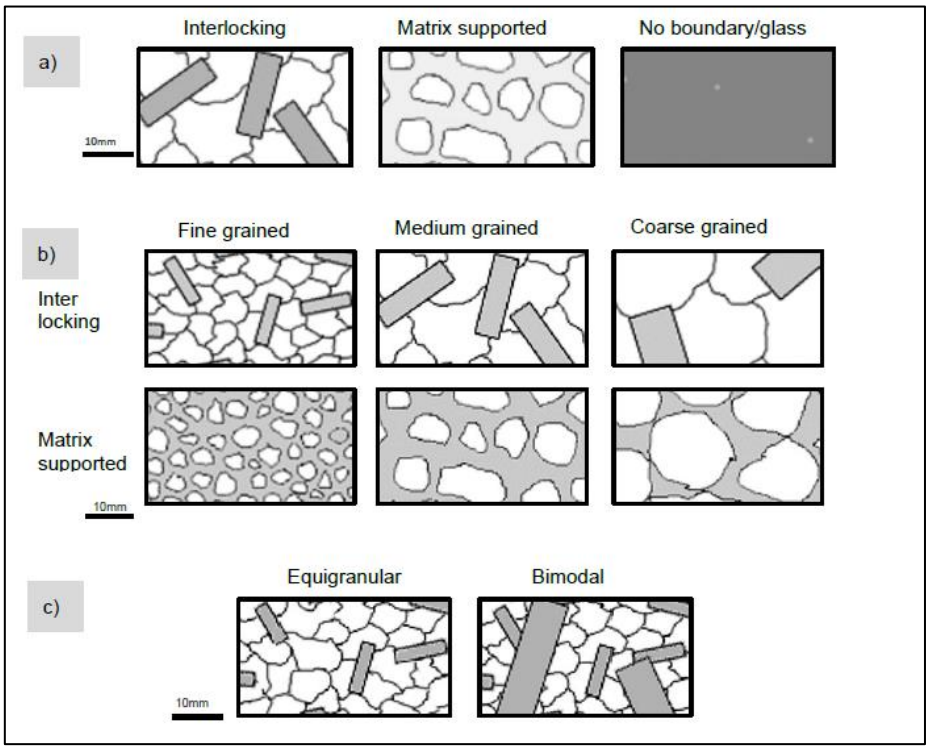

Figure 2-17: Illustration of a) mineral grain boundary type, b) mineral grain size definition and c) Mineral grain size comparison (adapted (Jardine, 2016)).

Grains in various rocks are not distributed randomly in space, but rather organised into clusters, layers and chains (Higgins, 2006). Grain size distribution is described using two main terms i.e. equigranular distribution and inequigranular (bimodal) distribution as illustrated in Figure 2-17c. Equigranular distribution refers to a sample containing mineral grains of approximately the same size (uniform size) while inequigranular distribution refers to a sample containing mineral grains varying considerably in size, usually resulting from different minerals being constituents of the same rock sample.

It is worth noting that grain descriptions such as interlocking and equigranular are all qualitative textural descriptors, whereas measurements of grain size or grain shape distributions are quantitative textural descriptors. Mineral grain size is described as a measure of the space occupied by the grain within the rock (Petruk, 2000). Qualitatively, grain size can be classified as fine, medium and coarse grained for both interlocking and matrix supported grain boundary types as

illustrated in Figure 2-17b. In this study, grain size will be described quantitatively with the following correlation between the quantitative and qualitative descriptions:

- Fine grained rocks have very small grains, each < 1mm across. Because of the minute size of the grains, they are invisible to the naked eye but can be identified under microscopic observation.
- Medium grained rocks have individual grains that are visible and between 1-5mm across.
- Coarse grained rocks have individual crystals that are clearly visible to the naked eye and can be anywhere between 5 millimetres to a few millimetres.

Grain size has a significant influence on the ore breakage characteristics. If the mineralogy and porosity are kept constant, a texture with smaller grains exhibits greater strength than a rock comprised of larger grains. This relationship was established by the work of Nelson (1983). Nelson reported on the results of the grain size-strength relationship after conducting tests using Navajo Sandstone. The report concluded that rock strength is dependent on grain size. This was explained to be a result of an increase in surface area and contact area per unit volume by reducing the grain size. An increase in contact area results in less stress being experienced by each grain as the load can be distributed over numerous contacts. Nelson also noted that this relationship was only valid for unaltered rocks.

Similarly, the investigation by Eberhardt et al (1999) focused on the effect of mineral grain size on the strength of rocks. The effect of grain size on crack initiation and propagation was investigated using samples that were mineralogically similar but however had different grain sizes (coarse grained pegmatite, medium grained grey granite and fine grained granite). Unconfined Compression Stress tests were conducted, and strain gauge measurements were taken to monitor the fracture process. The results presented show that the mineral grain size greatly influences crack propagation. The paper reported that increasing the grain size led to larger intergranular cracks and larger grain boundaries which promote crack propagation and extension by provided continuous paths of weakness (Eberhardt et al, 1999). This means that an increase in grain size leads to a decrease in rock strength and therefore an increase in the ore competence parameters.

This was later confirmed by the work of Akram & Bakar (2007) who conducted UCS tests using salt range ores (limestone, siltstone and sandstone variations) with different grain sizes. A similar trend to that of Eberhardt et al (1999) was observed. The authors attributed the results to an increase in the surface area available for contact due to the decrease in grain size. An increase in contact area results in less stress per unit area due to distribution of the stress across the increased

contact area. Smaller grains lead to a decrease in porosity and therefore more tightly held particles which are harder to break (Akram & Bakar, 2007).

2.7 Mineral Liberation

Mineral liberation is an important ore characteristic which occurs during the comminution step and prior to separation of the valuable material from gangue. Liberation therefore allows for valuable minerals to be separated from the gangue materials to concentrate the minerals (Becker et al, 2016). Feed ore liberation characteristics are important as they determine how much grinding is required i.e. how much energy is required to break down the feed material to a size that maximises liberation of the target mineral. Engineers rely on liberation data to determine how much of the target mineral or gangue mineral is fully liberated to avoid overgrinding (Becker et al, 2016). Additionally, liberation data gives an idea of the distribution of unliberated material and gangue to ensure that the appropriate steps are taken to liberate the target minerals.

The degree of liberation is determined by the mineralogy of the ore being processed and the concentration process being used. In reality, not all particles grades and sizes recover equally resulting in a need to find the optimum liberation and recovery (Bradshaw et al., 2019). Additionally, technoeconomic and environmental factors also tend to influence the desired degree of liberation at which a plant will operate at (Bradshaw et al., 2019).

2.7.1 Defining and Measuring Mineral Liberation

A liberated particle is defined as a particle that contains only one mineral (Bradshaw et al., 2019). It therefore follows that if a particle has two or more minerals, it is defined as unliberated. Composite particles contain mixtures of particles while locked particles have no surface exposure of the mineral (Bradshaw et al., 2019). The definition of liberation depends on the separation process being used i.e. a particle is said to be liberated if the valuable mineral will respond predictably during the separation process (Mariano & Annieli, 2016). Composition and textural data should accompany all liberation data to allow for the prediction of how unliberated particles will respond to each separation process. The effect of texture on the recovery of unliberated minerals is illustrated by Figure 2-18. The three particles illustrated contain similar compositions; the differences in particle texture result in different separation techniques to allow access to the target mineral locked within unliberated particles.

	Which unliberated particle texture allows the valuable phase to be recovered? (All particles are same grade.)		
Typical particles of valuable (dark phase) and gangue (light phase) shown in cross-section.	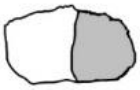	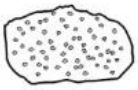	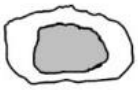
By flotation	✓ Recovered	✖ Not recovered	✖ Not recovered
By density separation	✓ Recovered	✓ Recovered	✓ Recovered
By leaching	✓ Recovered	✖ Not recovered	✖ Not recovered

Figure 2-18: Effect of texture on liberation (Evans & Morrison, 2016).

Liberation data can be obtained through a variety of measurement techniques. One of the most common contributors to liberation databases is the use of measurements in polished sections. This method entails taking measurements from polished sections of particles using an optical microscope or Scanning Electron Microscopy (SEM). This method preceded the particle counting method used in the early days of mineralogy which involved the labour-intensive counting of the number of particles that were locked or liberated as seen under an optical microscope by a mineralogy expert. However, due to technological developments, liberation data can more accurately and more quickly be obtained using relatively new technology like SEM-based mineralogy systems. It is also worth noting that the same techniques are used in the quantification of texture. For specific cases, microtomography is used to determine 3D liberation.

Numerous authors have reported on the effect of texture and specifically grain size, on the liberation properties of different ore types. Bérubé & Marchand (1984) reported on the effect of size reduction on mineral liberation using iron ore. In the published report, the authors noted that the mineral liberation within the same size fraction was independent of the degree of fineness if the particles were finer than 210 μm. It was also noted that for particles coarser than 210 μm, mineral liberation varies with different stages of size reduction (Bérubé & Marchand, 1984). Work conducted by Mariano et al (2016) using a variety of ore with differing mineralogical and textural properties established that particle liberation and distribution is independent of the amount of breakage applied as well as the breakage method (crushing or impact or any other) used to achieve breakage.

Existing work reports that mineral grain size and type i.e. ore texture, influences mineral liberation. Petruk (2000) reported that poor liberation within the same size class was observed in ores in

which the mineral grains were strongly bonded to each other, for instance, fine grained ores. The same author also stated that higher liberation within the same size class is achieved when the mineral grains are weakly bonded. Additionally, Petruk observed that the mode of size reduction in weakly bonded ores was by preferentially breakage along grain boundaries as opposed to the random breakage observed when dealing with ores that have strongly bonded grains (Petruk, 2000).

Tungpalan et al, (2015) showed a correlation between the grain size and mineral recovery. It was reported that coarser material showed greater liberation characteristics and therefore higher liberation in the same particle size fraction.

2.7.2 Common Mineral Characterisation Devices

Auto-SEM technology is commonly used for mineralogical classification. Popular forms of this technology are the QEMSCAN, Mineral Liberation Analyser (MLA), TIMA-X (by Tescan), Mineralogic (by Zeiss) and AMICS. Auto-SEM allows for quantitative mineralogy and produces a vast array of information for each sample analysed. This information includes, but is not limited to, mineral association, ore grain size, bulk mineralogy, liberation, elemental deportment, particle size and shape, grain relationships and grain distributions. According to Petruk (2000), SEM technology releases electron beams under high vacuum which irradiate the material being processed. The material responds by returning backscattered electrons and X-Rays which are read by the SEM detectors.

Currently, QEMSCAN is one of the most widely used technology to obtain mineralogical data in educational institutes and mining houses. The QEMSCAN machine uses the same principle as SEM, however, graphite particles are added to the mineral sample to avoid the touching of particles. Additionally, the surface of the sample is coated with graphite to improve conductivity. Before the slide is examined, particles are sectioned, hardened and polished (Petruk, 2000). During analysis, an electron gun scans the particles to obtain X-ray counts which are compared to reference files on the computer linked to the system. As with any form of technology, Auto-SEM technology has a few disadvantages, including:

- Long scanning time depending on the mineral characteristics required
- Cost of acquisition
- Particles less than 0.5µm are not identifiable
- Stereological error caused by measuring of sections

XCT has been around for over 40 years but mainly has medical applications to visualize the interior of solid objects. According to Ketcham & Carlson (2001), the XCT works by exposing the sample under investigation to incident X-Rays. This then attenuates X-rays which are proportional to the mineral density and atomic number. The XCT comes equipped with two X-ray tubes, though only one is used at any one moment depending on which is needed. The first tube emits a strong x-ray beam and the second is responsible for softer x-ray beams (Jardine, 2016). It is also worth noting that to obtain a final image with high resolution, the sample should be placed as close as possible to the tubes emitting the beams. Table 2-6 provides an overview of the common techniques used in obtaining mineralogical and textural information. For this study the QEMSCAN device will be used for all mineralogical and textural classification. QEMSCAN was selected over XCT because XCT does not provide a definitive mineral ID. Additionally, the data analysis when using QEMSCAN is simpler than when using XCT.

Table 2-6: Advantages and disadvantages of common techniques used in obtaining mineralogical and textural information (adapted from Voigt (2017)).

Technique	Dimensions	Mineralogy	Texture	Advantages	Disadvantages
Chemical Assays	None	✓		- Cheapest to run - Relatively Fast	- Cannot extract textural information
Optical microscopy	2D	✓	✓	- Easy to use - Easy data interpretation	- Only manual use possible - Time and energy intensive - Limitations in the sizes that be resolved
X-Ray Diffraction (XRD)	None	✓		- Quantitative information - Low cost of ownership - Easy sample preparation	- Does not allow for extraction textural information
Auto-SEM	2D	✓	✓	- Automated - Data analysis is simple - Both mineralogy and texture can be investigated	- High cost - Long scanning time
X-Ray Computed Tomography (XCT)	3D	✓	✓	- Very high resolution - Non-destructive in nature - Can view the internal structure	- Slow sample turnaround - High cost to own - No definitive mineral ID

2.8 Summary of Key Literature and Hypotheses

The processing of complex heterogenous ores is becoming more common due to the depletion of the 'simple' to process ore. Textural variability is a key component of ore heterogeneity. Mineral grain size is a pivotal part of textural variability. The effect of mineral grain size on ore breakage has not been widely reported. This is likely due to challenges associated with estimating grain size.

Grain size has a significant influence on the ore breakage characteristics. Studies have shown increase in the surface area available for contact due to the decrease in grain size. An increase in contact area results in less stress per unit area due to distribution of the stress across the increased contact area. Smaller grains lead to a decrease in porosity and therefore more tightly held particles which are harder to break.

Comminution energy usage is the extremely high due to the low energy conversion efficiency. Because of this, when designing comminution circuits, substantial effort is directed towards knowing and minimizing the energy requirements. Ore breakage characterisation is a key component of the geometallurgical test work and plays a critical role is the design and optimization of comminution circuits. Ore breakage characterisation tests are usually performed using crushed ore as opposed to drill core. The use of drill core in ore breakage characterisation would be beneficial as it is available months ahead of the time of mining.

The JKRBT is more accurate and the test work less time consuming than its predecessors. However, the sample preparation is tedious and time consuming due to the amount of sample required and size range specifications needed to complete the full suite of tests. Practically speaking, sample availability is a major concern when performing metallurgical testing as numerous tests need to be performed to get a complete view of the metallurgical response of the ore type. This means that very little of the sample is available for ore breakage characterisation. The least particles protocol seeks to address these concerns by reducing the amount of sample required to carry out a full suite of tests. This protocol also seeks to obtain similar ore competence parameters (within 2%) to the standard procedure while using minimal samples i.e. less than 30 particles per test.

Based on the literature reviewed, the following hypotheses were formulated:

1. Drill core samples are routinely available months ahead of time and can therefore be used for mineral processing planning. It is hypothesized that drill core particles will produce a coarser product than crushed particles. This is because crushed particles are angular in shape whereas drill core particles are cylindrical thus offer less contact surface for energy absorption.

2. Textural variability is a key component of ore heterogeneity. The most important factor in textural variability is grain size. It is therefore hypothesized that an ore with a coarse grained texture will break to form a finer progeny than an ore with a fine grained texture. A reduction in grain size results in an increase in surface area and contact area per unit volume. An increase in contact area results in less stress being experienced by each grain as the load can be distributed over the numerous contacts.
3. Though the JKRBT is a rapid characterisation device, the sample preparation and progeny screening are still time and energy consuming. It is hypothesized that an abridged test can be performed using a fewer number of particles to obtain similar ore competence parameters to the standard procedure while using minimal samples. Additionally, this abridged test can be applied on a different ore type despite its mineralogical and textural composition.

3. MATERIALS AND METHODS

Overview

This chapter describes the procedure designed to address the objectives defined. The Julius Kruttschnitt Rotary Breakage Tester (JKRBT) was applied in this work for ore breakage characterisation. The sample selection and preparation methods are described in this chapter. This is followed by a description of the standard JKRBT ore breakage characterisation procedure prior to the introduction of the procedure used to investigate the feasibility of using fewer particles for an abridged ore breakage characterisation test. The techniques used to quantify mineralogy and texture are also described in this chapter.

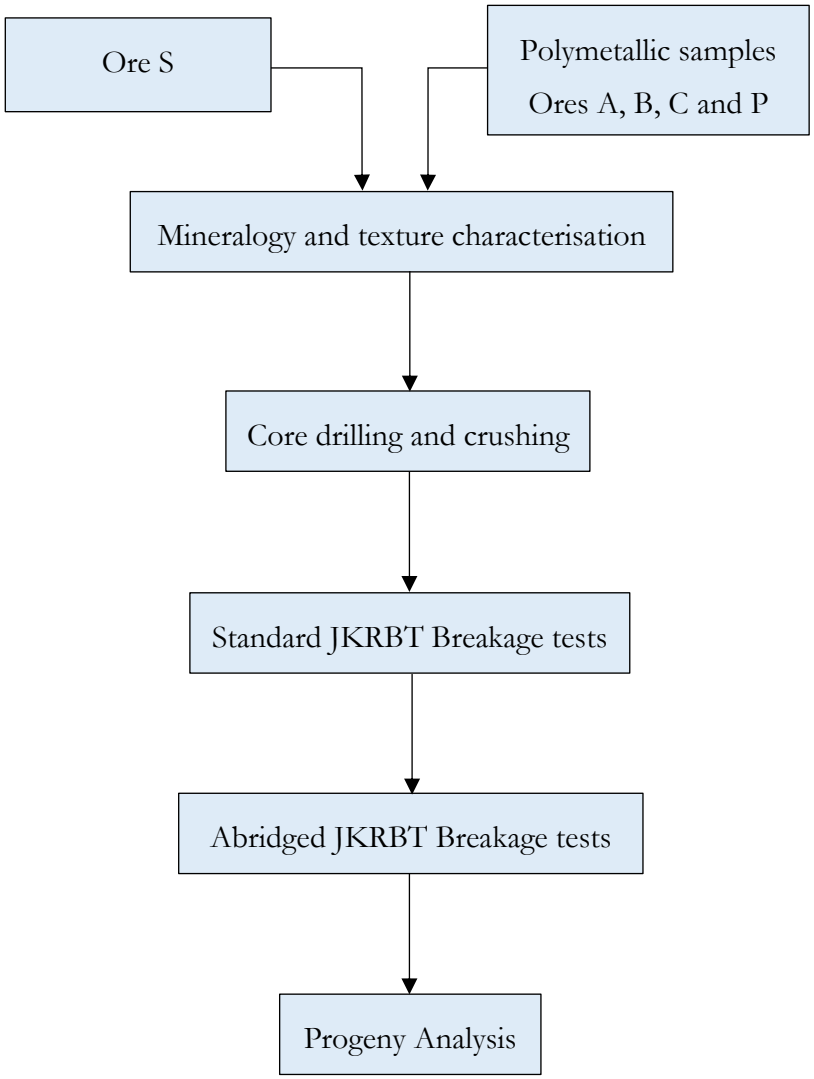

Figure 3-1: Overview of the experimental procedure followed.

3.1 Apparatus

3.1.1 The JKRBT

The JKRBT was the ore breakage characterisation device of choice in this project; a decision driven by the numerous advantages associated with the JKRBT over other devices like the drop weight tester. Advantages of using the JKRTB include increased precision of energy input and the short time required to run a single test as highlighted in Table 2-2. Using this device, a wide energy range (0.001-3.8 kWh/t) can be investigated. Additionally, the particle size range that can be investigated (13.2-45mm), is within the drill core diameters that can be obtained with the range of drill bit heads available on the market.

Figure 3-2: The JKRBT used for test work in this project.

Several factors affect ore breakage properties; however, this project will focus mainly on the effect of texture, mineralogy, particle shape, initial particle size and the specific input energy on ore breakage properties. To obtain statistically valid data throughout the operating ranges of the JKRBT, a standard test consists of 3 energy levels (low, medium and high) tested on 3-4 particle size fractions (small, medium, large and very large). This makes it possible to investigate the energy-size relationship using methods developed from the pendulum and drop weight tester. The same procedure can be used for both drill core and crushed ore, allowing comparison of ore breakage

properties for both sample preparation methods. Likewise, the procedure can be repeated for different ore types to compare their ore breakage properties.

3.1.2 QEMSCAN

The QEMSCAN device was selected to for mineralogical classification in this project. QEMSCAN uses Auto-SEM technology which allows for quantitative mineralogy and produces a vast array of information for each sample analysed. This information includes, but is not limited to, mineral association, ore grain size, bulk mineralogy, mineral liberation, particle size and shape, grain relationships and grain distributions. Once acquired, this information is readily available and have the potential to be very useful.

Figure 3-3: QEMSCAN 650F located at the University of Cape Town.

QEMSCAN has several advantages over other techniques used to obtain mineralogical information. The main reasons QESCAN was chosen was due its ability to provide both qualitative mineralogical and textural information as opposed to optical microscopy and chemical assays which only provide mineralogical information. Additionally, the energy and sample turnaround time required to run samples are greatly reduced when using QEMSCAN as opposed to its

predecessors. Finally, the data outputs from QEMSCAN are simple to analyse using the iDiscover software.

3.1.3 Additional Apparatus

The following apparatus was also used to prepare the samples and carry out the experimental procedure:

- Shibuya R2231 Diamond Coring Machine – used to obtain drill core pieces from the bulk rocks.
- Labex (5 x 3") jaw crusher – used to reduce the particle sizes of the bulk rock to fit the size range required for ore breakage characterisation tests using the JKRBT.
- Gilson vibrating screen shaker – used to sieve the particles into the narrow size classes to be tested.
- XRD – Used to quantitatively validate the mineralogical results obtained from QEMSCAN.
- Zeiss optical microscope – used to take magnified photographs of the ore samples used.
- Precisa-XB4200C weighing scale – used to weight the progeny before and after breakage testing and screening.
- Fritsch Analysette 3 PRO vibrating sieve shaker – used to sieve the progeny particles to obtain a progeny particle size distribution.
- $\sqrt{2}$ series of screens (45mm – 0.106mm) with a diameter of 200mm – used in conjunction with the vibrating sieve shaker.

3.2 Sampling and Sample Preparation

3.2.1 Sample selection

Ore breakage characterisation tests are usually performed using crushed ore as opposed to drill core. Crushed ore that can be used for characterisation tests is available after mining and as such very little can be done to inform the mineral processing of this mined ore after ore breakage characterisation. The use of drill core in ore breakage characterisation would be beneficial as it is routinely available months ahead of the time of mining. This means that when performed, the ore

breakage characterisation test results can be used to better manage ore variability and optimise the plant prior to processing of the ore thus maximizing recovery.

A 500kg Malmesbury Shale sample was obtained from a local quarry in the Durbanville area of the Western Cape Province, South Africa. The ore was sampled directly from the quarry pit and obtained in block form, with each side measuring ~300mm. The blocks of ore were transported to the Civil Engineering laboratory at the University of Cape Town (UCT). Shale was selected because of its relative homogeneity and fine grained texture which makes it more likely to produce consistent ore breakage results. It is commonly used in the construction industry due to its strength and homogeneity. Additionally, shale has already been well studied (Bbosa, 2006).

150kg of four different polymetallic sulfide ores was obtained from the Black Mountain Complex (BMC) which is located in the Aggeneys-Gamsberg Ore district, Northern Cape, South Africa. This deposit covers an area of approximately 300km^2 (Bailie et al, 2007), with its most Western section being the focus of this study. For brevity, the four ores obtained from the Black Mountain Complex were then assigned the names ore A, B, C and P. Ores A to C have been previously described (Gordon, 2019). The sampling exercise involved going into the underground mine shaft, channel sampling and bringing the selected ore to the surface. The sampled ore was then transported to the Centre for Minerals Research (CMR) laboratories at UCT.

3.2.2 Preparation of drill cores

Drill cores were extracted from shale samples using the Shibuya R2231 Diamond drill core machine (Figure 3-4). Diamond tipped drill bit heads suitable for wet coring were purchased from a local supplier. The drill bits heads had inner diameters of 16mm, 20mm and 27mm. To obtain a drill core from a rock sample, the block being drilled was placed on a flat surface directly below the drill bit as illustrated in Figure 3-4. Water flows through the drill bit head to the point of contact between the drill bit head and the rock surface, providing lubrication and acting as a coolant for the coring process. The lever on the drill core machine was used to slowly lower the drill bit head as it progressively made its way through the rock sample. To complete the drilling process, the drill bit head was raised using the lever. The core from the rock sample was then obtained inside the hollow space of the drill bit head.

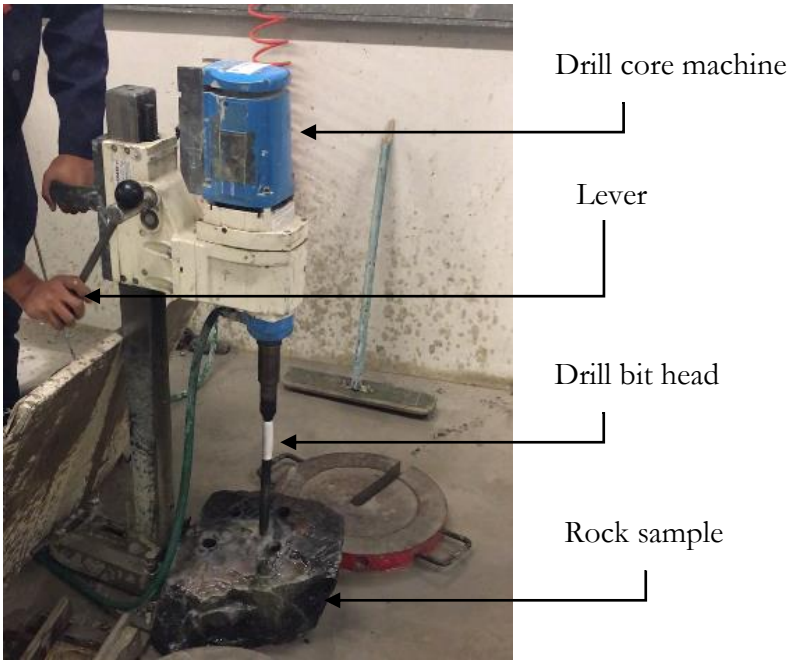

Figure 3-4: Operator using the Shibuya R2231 Diamond drill core machine.

To avoid breaking the cores inside the drill bit head, the coring process was stopped when the drill bit was about 150mm (maximum) into the rock sample (Figure 3-5a). The cores from the rock samples were carefully examined for any visible cracks. This was done to maintain the integrity of the drill cores. The cylindrical drill core pieces for each rock type were then cut into cylindrical drill core particles each with a height of 20mm as illustrated in Figure 3-5b. This was done for all drill core particle produced for this study. The drill core particles for each rock sample and size were bagged, labelled and stored in a sealed dry bucket.

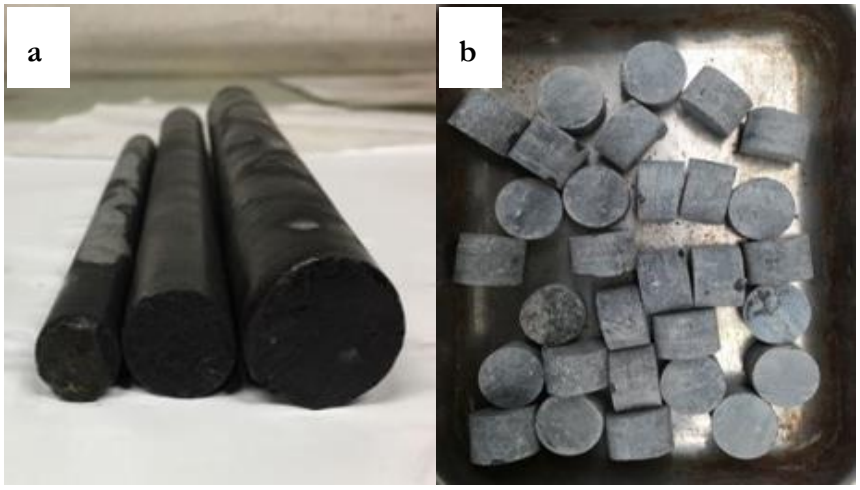

Figure 3-5: (a) Fresh drill core pieces 150mm in length and (b) cut 20mm core particles.

In the case of the polymetallic ore sample, the drill coring was performed by a local company called Hardcore Drilling. The same drill coring procedure was applied as before, obtaining cylindrical

particles of core with a height of 20mm for each ore type. The drilling process however consumed most of the available sample as the blocks were narrow thus producing drill cores with a maximum height of 50mm. This meant more drill holes had to be drilled to obtain enough cores to make up the required number of particles to be tested for each ore type. The residual material after the drill coring process only allowed for one test to be conducted with crushed particles for each ore type as indicated in Table 3-1.

3.2.3 Preparation of crushed ore

The residual material from the drill coring process was packed and transported to Thyssenkrupp Industrial Solutions, Gauteng, South Africa for crushing.

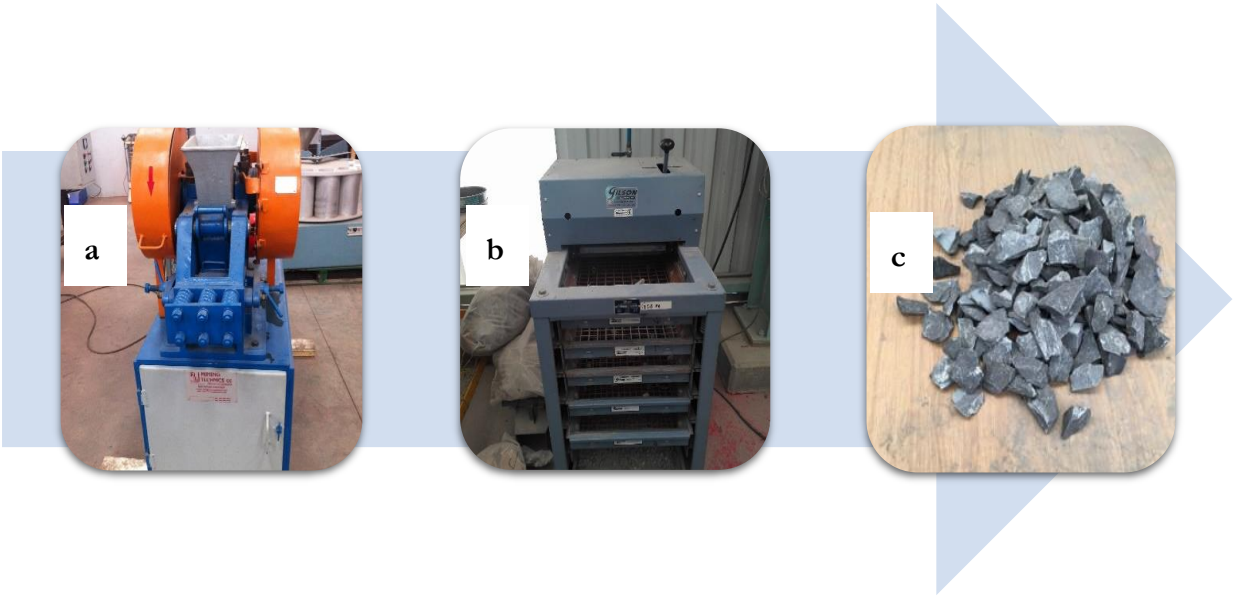

Figure 3-6 (a) The Labex jaw crusher used to reduce the particle size to sub 45mm (b) Gilson Vibrating screen shaker (c) Shale crushed particles (-45+37.5mm).

The Labex laboratory jaw crusher was used to crush the rocks to a size of 45mm and below. The crushed material was sieved using the Gilson vibrating screens shaker to obtain the narrow size fractions shown in Table 3-1. The crushed particles in each size fraction were bagged and labelled for further use.

Table 3-1: Summary of the particle size fractions tested in this project.

Size Fraction (mm)	Drill bit inner diameter (mm)	Shale		Polymetallic	
		Crushed	Drill Core	Crushed	Drill Core
-45.0+37.5	-	✓	×	×	×
-31.5+26.5	27	✓	✓	×	✓
-22.4+19.0	20	✓	✓	✓	✓
-16.0+13.2	16	✓	✓	×	✓

3.3 Ore Breakage Characterisation Procedure

The JKRBT used in this work is located at the Sibanye Stillwater research and development laboratories. Sibanye Stillwater is in the Marikana area which is about 50km from Rustenburg in the North West province, South Africa. The full suite of breakage tests on an ore type typically consists of a series of tests on four particle size fractions at three energy levels as shown in Table 3-2. In the case of drill cores, only the bottom three size classes could be investigated due to limitations in the size of diamond drill bit heads that could be obtained from the market.

Table 3-2: Summary of the specific input energy levels tested in this project.

	Specific input energy			
Size Fraction (mm)	0.1 kWh/t	0.25 kWh/t	1.0 kWh/t	2.5 kWh/t
-45.0+37.5	✓	✓	✓	
-31.5+26.5		✓	✓	✓
-22.4+19.0		✓	✓	✓
-16.0+13.2		✓	✓	✓

3.3.1 The standard JKRBT ore breakage characterisation procedure

The standard RBT test procedure included in the devices user manual (JKTech, 2012) and was used in this test work. A summary of the procedure is given in this thesis:

Calibration and pre-start-up checks: Before any tests are carried out, the RBT calibration accuracy needed is verified. This is done by measuring the diameter of the rotor and comparing it to the diameter calibrated for (0.45m). If the diameter of the rotor is not 0.45m, the rpm speed calibration is adjusted accordingly using equation 10 and equation 11 shown in chapter 2. The RBT used in this test work had a rotor diameter of 0.45m thus no recalibration was required. The pre-start up checks that are included in the procedure after checking for calibration are:

- Switch on the compressed air and open the valve connected to the RBT
- Switch on the fan to aid ventilation in the workspace
- Check the oil and pressure levels on the RBT gauges.
- Switch on the main RBT power and allow booting procedure to take place (approximately 30 seconds)

Test protocol: The following protocol was used with 30 particles per test.

1. Enter the desired energy level in kWh/t on the control panel. This will be converted to rpm automatically (Figure 3-7).

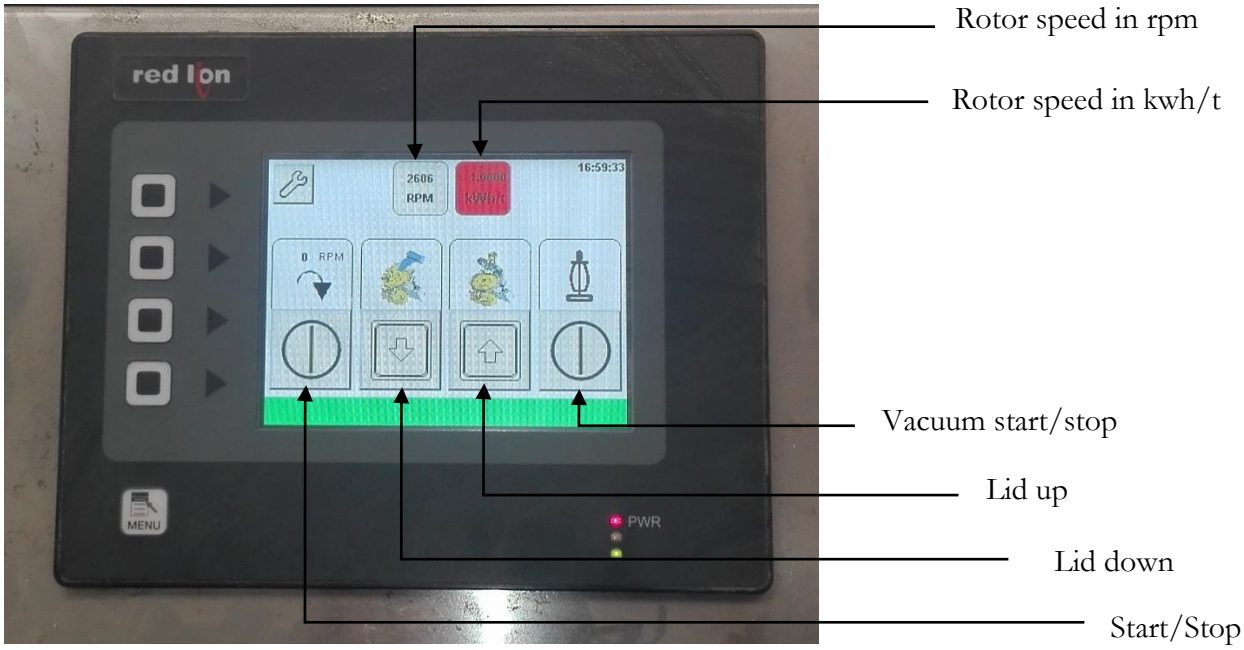

Figure 3-7: RBT control panel

2. Press the "Vacuum Start" button followed by the "Start" button.
3. Monitor the indicator on the RBT lid which will turn white, signalling that the rotor has reached the set rpm.
4. Use the hand feeder to feed particles at a rate of 1 particle per 2 seconds or longer. This ensures that only single particle impact breakage is taking place.

Figure 3-8: Operator feeding particles into RBT

5. Make sure with every turn of the hand feeder, you listen out for the sound of the inserted particle impacting the anvil.
6. Feed all 30 particles into the RBT and stop the machine by pressing the "Start/Stop" button when complete.
7. Wait for the rotor to brake and reduce the speed. The indicator on the RBT lid will turn white, showing that the rotor has completely stopped.
8. Use the control panel to lift the RBT lid and secure it in the lifted position using a steel bar.
9. Use a paint brush to clean the progeny material from the sides of the anvil and guide it into the collecting bin. This minimizes the material losses and increases the accuracy of the test.
10. Remove the collecting bin and empty the contents into a plastic bag.
11. Weigh the mass of material in each bag and compare it to the initial particle mass. If the breakage loss is >2%, repeat the test.
12. Change the energy level and repeat steps 1-11.

3.3.2 The least particles protocol

The JKRBT is more accurate however the sample preparation is tedious and time consuming due to the amount of sample required and size range specifications needed to complete the full suite of tests. Practically speaking, sample availability is a major concern when performing metallurgical testing as numerous tests need to be performed to get a complete view of the metallurgical response of the ore. This is the motivation for developing an ore breakage characterisation test protocol that uses minimal samples to extract indices that can be used in design and optimisation studies.

Shale was chosen to develop the minimal particle protocol due to its fine grained texture and homogeneity. In developing the protocol, all the steps of the standard procedure were followed except Step 6. Instead of using 30 particles for each test, 5 particles were used per test allowing for arithmetic summing and progression. This was done for both crushed particles and drill core particles and repeated 6 times for each energy level and size fraction combination in the full suite matrix as shown in Table 3-3.

Table 3-3: Least particles protocol experimental matrix (note 5p6 represents 5 particles x 6 tests).

	Specific input energy			
Size Fraction (mm)	0.1 kWh/t	0.25 kWh/t	1.0 kWh/t	2.5 kWh/t
-45.0+37.5	5p6	5p6	5p6	
-31.5+26.5		5p6	5p6	5p6
-22.4+19.0		5p6	5p6	5p6
-16.0+13.2		5p6	5p6	5p6

3.4 Progeny Analysis

3.4.1 Sieving procedure

The progeny from the ore breakage characterisation tests was analysed to determine the particle size distributions, bulk mineralogy, grain size, grain distribution, particle counts and liberation data. The progeny material from the breakage tests was transported back to the UCT CMR Lab 2B for sieving. The material was sieved using the root two series of screens (Napier-Munn et al., 1996). The root two screen series consist of 19 screens with aperture sizes ranging from 0.106mm to 45mm. The screens used had a diameter of 200mm. Each sample was weighed before screening and emptied into the top screen. The stack of screens was placed on the vibrating sieve shaker,

covered and secured in position. The vibrating sieve shaker program was set to an amplitude of 1.9 and a screening time of 10 minutes, which is enough for the sieving of coarse material, was chosen. When the shaker stopped, the mass of material retained on each screen was recorded and the sample was repacked and stored for further analysis.

3.4.2 Mineralogical Characterisation Procedure

Mineralogical analysis was carried out using the QEMSCAN device located in the New Engineering Building, UCT. Not all the breakage samples were selected for QEMSCAN analysis due to the high cost and long scanning time required for such work. Samples were selected based on the matrix shown in Table 3-4. Mineralogical analysis was carried out to explore the following relationships:

1. The mineralogical variations between the ore types used in this study (◆).
2. The mineralogical variations as the specific input energy increased while keeping the particle size fraction constant (✸).
3. The mineralogical variations as the particle size is increased while keeping the specific input energy constant. (★).

Table 3-4: Matrix of samples selected for mineralogical analysis.

	Specific input energy		
Size Fraction (mm)	0.25 kWh/t	1.0 kWh/t	2.5 kWh/t
-45.0+37.5		★	
-31.5+26.5		★	
-22.4+19.0	✸	✸★◆	✸
-16.0+13.2		★	

The samples selected for mineralogical and textural analysis where then prepared according to the following procedure.

1. The selected sample was dry screened for 10 minutes into 1 size fraction - +1.7mm.
2. A micro-riffle was used to split the sample into 4g aliquots.
3. The aliquot is mixed with 4g of graphite with a size one fraction below the sample size. This minimizes contact between particles in the sample.
4. Make 30mm round blocks and 70 x 70mm square blocks with a height of <20mm.

for use as shown in Table 3-5.

Table 3-5: Block mould sizes used and measurement details

Progeny size fraction	Block type	Measurement Details
+6.7mm	70 x 70mm	2500 µm field size, 15 µm pixel size
+1.7mm	70 x 70mm	2500 µm field size, 15 µm pixel size
+0.425mm	30mm round	1500 µm field size, 15 µm pixel size

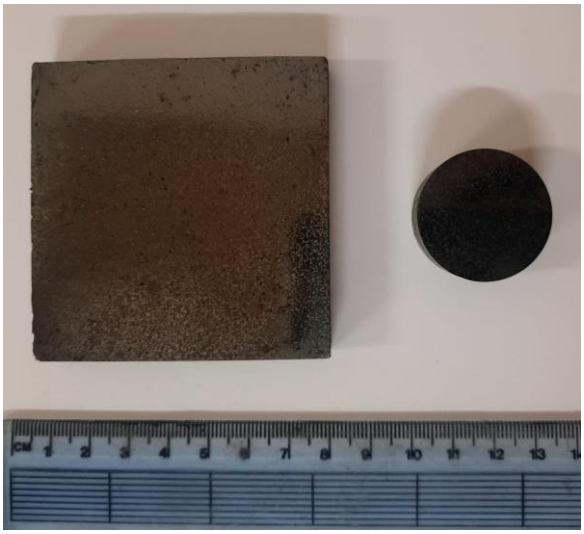

Figure 3-9: Image showing samples of the blocks used

5. Label and lubricate block moulds.
6. Add the sample into the moulds. Also add resin and stir continuously.
7. Place in vacuum chamber for 5 minutes.
8. Place printed labels on mould.
9. Add more resin and put back in the vacuum for 5 more minutes. This removes any trapped air bubbles.
10. Cure overnight in an oven at 30°C.
11. Remove the mould from the oven when cured. This is followed by polishing which consists of grinding and polishing steps until a 1µm polish is achieved.
12. Remove any loose grains by gently washing with soap.
13. Place the mould in an ultrasonic bath for ten minutes.

14. Rinse the mould with ethanol while making sure to minimize scratching of the mould surface.
15. Leave in a 30ºC oven to dry for 1 hour.
16. An optical microscope is used to check the quality of the final polish thus ensuring that there are no plucked grains or visible cracks.
17. The mould is the put in an emitted carbon evaporator to carbon coat it. The carbon coat serves to diffuse electrons off the sample surface.

Duplicate moulds of each sample were placed in the QEMSCAN sample chamber for analysis. Though for most of the samples only the +1.7mm size fraction was used, all three size fractions shown in Table 3-5 were used for one sample (medium size fraction at 1 kWh/t) in all the ore types used. The QEMSCAN was run using pre-set parameters including a voltage of 25kV and a beam current of 10nA. Upon completion, the results obtained were analysed using the iDiscover software which allows simple extraction of relevant data trends. iDiscover classifies elemental measurements obtained by the QEMSCAN device into mineralogical species according to an inbuilt mineral library. This library can be user-specified using the SIP (Species Identification Protocol) which is compared to the elemental information obtained for matching entries. QEMSCAN measurements were postprocessed by field stitching large particles, as separating touching particles using inbuilt processors. Thereafter, the mineral grades, grain sizes (as equivalent spherical diameter), false colour images and liberation data was extracted.

XRD was used to validate the data obtained from QEMSCAN for ore P and S. Samples were prepared by micronizing the sample in ethanol as per standard method. A Bruker D8 Advance diffractometer with CoKα radiation was used for the analysis. The samples were scanned over a 2θ angular range of 10 to 80°, with a step size of 0.02° and counting time of one second per step. Minerals were identified using Bruker EVA software and quantified by the Rietveld refinement method using TOPAS.

The material used in this project and this study build into a larger ongoing project at UCT with several individuals completing a different section of the project. The validation of QEMSCAN results for this material was done using XRF and XRD. This information is reported in a master's thesis by Mr Henry Gordon (Gordon, 2019).

4. THE EFFECT OF MINERALOGY AND TEXTURE ON ORE BREAKAGE CHARACTERISTICS

Overview

This chapter presents and discusses the results obtained for the ore breakage characterisation tests carried out on ore samples using the standard JKRBT test procedure. The chapter begins with a review of the mineralogical and textural characteristics of each ore type followed by an analysis of the progeny particle size distributions obtained. The degree of breakage for the tested ores are then compared and discussed to assess the influence of mineralogy and texture. The results obtained from fitting the breakage data to the t_{10} breakage model and size dependant breakage model are then presented. The comparison between the ore breakage properties of drill core and crushed ore is highlighted throughout the chapter. A discussion of the results obtained concludes the chapter.

4.1 Introduction

Four polymetallic sulfide ores (ore A, ore B, ore C and ore P) and a Malmesbury Shale (ore S) were obtained from two mineral deposits in South Africa. These ores were selected based on their mineralogical and textural differences which have an influence on the breakage characteristics of each ore. Four particle size fractions of crushed ore and drill core particles were prepared for ore breakage characterisation as summarized in section 3.3.2 and section 3.3.3. This makes it possible to investigate the energy-size relationship using methods developed from the pendulum and drop weight tester. The ore breakage characteristics were investigated using the standard JKRBT test procedure outlined in Section 3.4 and the progeny sieved to obtain particle size distributions. From the particle size distributions, the degree of fineness in the form of a t_{10} was obtained. The t_{10} breakage model and size dependent breakage models were used to investigate the energy size relationship which is the main objective of ore breakage characterisation (Napier-Munn et al., 1996). The material was analyzed using QEMSCAN to obtain the mineralogical and textural properties of the ores. The results are presented in the following sections. For brevity, in this thesis each of the size fractions will be referred to as follows:

- -45.0+37.5mm - Very Large/VL
- -31.5+26.5mm - Large/L

- -22.4+19.0mm - Medium/M
- -16.0+13.2mm - Small/S

4.2 Mineralogy

An investigation into the bulk mineralogy of the ores was conducted. Thereafter, false colour images were obtained to show the visible characteristics of the particle. Five different ore types were used in this work. However, the four polymetallic sulfide ore types had similar mineral components while shale had different mineral components. Thus, separate mineralogical descriptions are given focussing on mineral composition.

Table 4-1: Bulk Mineralogy for all five ore types (Data for ores A, B and C from Gordon (2019)).

	Mineral Mass %				
Mineral	Ore A	Ore B	Ore C	Ore P	Ore S
Sphalerite	3.1	2.6	0.6	2.8	-
Chalcopyrite	1.6	2.0	0.6	15.2	-
Galena	0.5	0.5	6.4	0.1	-
Pyrrhotite	2.0	2.0	0.8	12.0	-
Pyrite	1.1	0.9	1.0	2.4	0.1
Magnetite	57.1	53.8	58.8	55.9	-
Quartz	6.8	6.8	2.5	9.8	31.4
Grunerite	5.5	3.5	0.6	0.1	-
Pyroxmangite	21.0	26.2	27.7	0.3	-
Apatite	0.9	0.7	0.5	0.4	0.3
Mica	-	-	-	-	44.3
Chlorite	-	-	-	-	4.3
Feldspar	-	-	-	-	19.0
Rutile	-	-	-	-	0.6
Other	0.4	1.0	0.6	1.2	0.2
Total	100.0	100.0	100.0	100.0	100.0

Table 4-1 illustrates the relative mineral abundance as a wt.% in the ore samples investigated in this study. The difference in the mineralogy of the polymetallic ores and ore S is evident as ore S consists mostly of mica, quartz and feldspar while the polymetallic ores are rich in magnetite and pyroxmangite (except ore P which is the most chalcopyrite and pyrrhotite rich). Comparing ores A-P, it was noted that they all contained above 50% magnetite with ore C containing the most magnetite (58.8%) and ore B containing the least (53.8%). Looking at all five ore types used in this study, there are only three minerals common to all i.e. pyrite, quartz and apatite. Ore S is the richest

in quartz but also contains the least pyrite when compared to the other ore types. All five ore types have less than 1% apatite. Although ore A and ore B have similar mineralogical characteristics, ore B can be distinctly defined by being more pyroxmangite rich than ore A while containing less grunerite.

It was also noted that though all the polymetallic ores contained pyroxmangite, ore P contained the least amount (0.3%) compared to ores A-C which all contained above 20% pyroxmangite. Another noticeable difference in the polymetallic ores was that only ore P contained above 12% of the minerals chalcopyrite and pyrrhotite which are only contained in small amounts in the other polymetallic ore types (A-C). Looking at the galena content of the ores, it can be seen that ore C has the highest galena content (6.4%) compared to the other ores which only contain trace amounts of galena (less than 1%).

4.3 Texture

QEMSCAN and the optical microscope images were used to obtain both a qualitative and quantitative description of the texture of the ores used in this study. As previously mentioned, texture in this study refers only to the mineral grain size distribution.

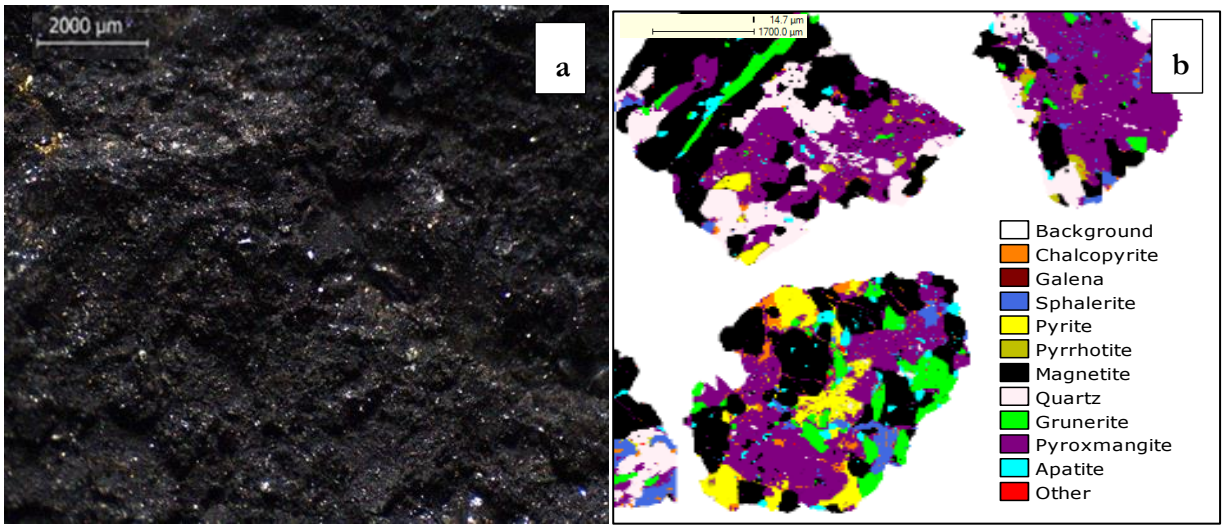

Figure 4-1: a) Optical microscope image and b) QEMSCAN false color image obtained for ore A.

From Figure 4-1b, chalcopyrite in association with magnetite can be observed. Galena, pyrite and small amounts of sphalerite are present as well. In addition, medium size grains of apatite are also observed. A compositional layering texture that is well defined can be observed in ore A. The texture also shows an association of fine-banded magnetite and pyroxmangite mineral grains.

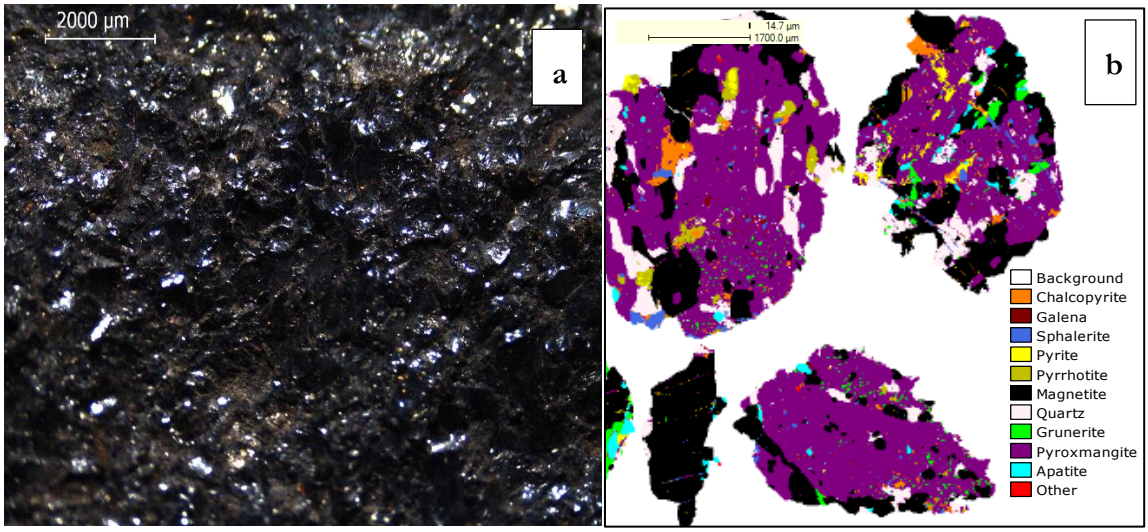

Figure 4-2: a) Optical microscope image and b) QEMSCAN false color image obtained for ore B.

Figure 4-2 shows an optical microscope image and QEMSCAN false color image for ore B. Ore B is defined by the association of fine grained grunerite with pyroxmangite. Coarse grained chalcopyrite is present in association with magnetite. Where present, apatite is associated with magnetite. Characteristics of ore B texture include the presence of coarse grained sphalerite and chalcopyrite overprinted on a fine to medium grained banded texture.

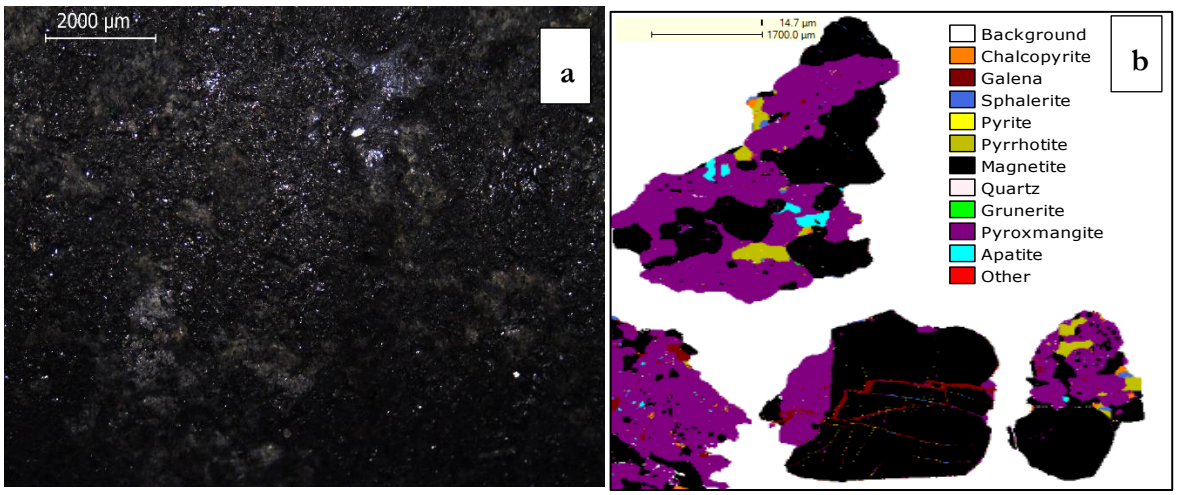

Figure 4-3: a) Optical microscope image and b) QEMSCAN false color image obtained for ore C.

Figure 4-3 shows an optical microscope image and QEMSCAN false color image for ore C. Ore C is defined by the presence of pyroxmangite and massive magnetite grains. Additionally, the dominance of pyroxmangite over grunerite is most pronounced in ore C. Coarse grained pyrite and galena are associated with coarse-banded magnetite. The texture of ore C is foliated and exhibits banding with alternating layers of different mineral compositions as exhibited in Figure

4-3b.Figure 4-4 shows an optical microscope image and QEMSCAN false color image for ore P. Massive particles of magnetite and chalcopyrite can be observed. Chalcopyrite and pyrrhotite occur in association with magnetite. Relative amounts of quartz and sphalerite are also visible occurring mainly in association with each other.

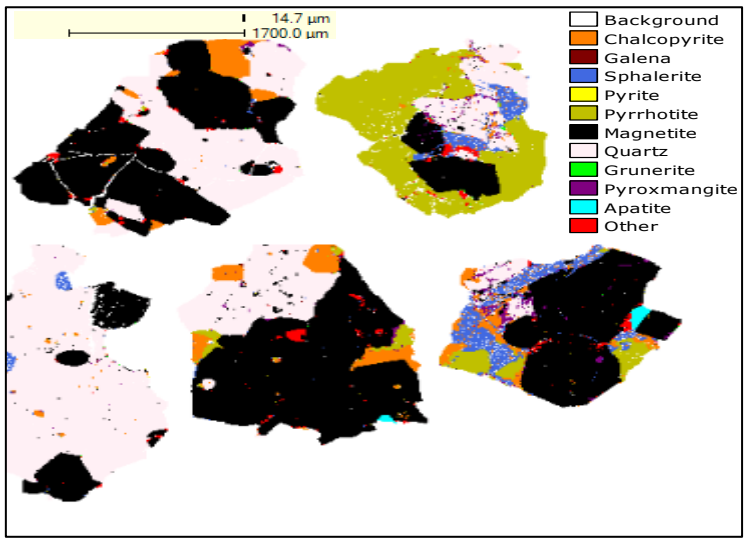

Figure 4-4: False colour image obtained for ore P.

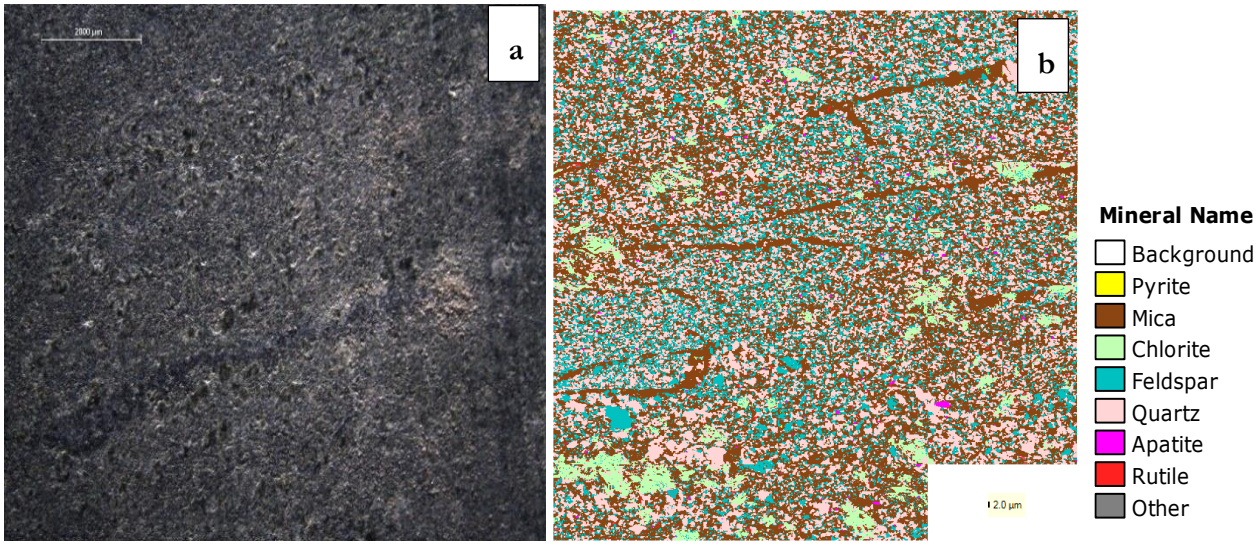

Figure 4-5: a) Optical Microscope image at 10x magnification b) QEMSCAN false colour image for ore S.

Ore S is a metamorphized sedimentary rock which is dark-greyish in colour, consisting predominantly of mica, quartz and feldspar. It occurs within the metamorphic aureole which is the zone of thermal metamorphism close to contacts with the intrusive granites of the Cape Granite Suite (Cole et al., 2014). As illustrated in Figure 4-5a, ore S is considered to have a homogenous and fine grained texture. Some larger crystals can be seen embedded in the fine grained matrix as

shown by the QEMSCAN false colour image (Figure 4-5b). It can be seen that larger chlorite minerals (light green false colour) sit within a matrix of fine grained biotite (brown false colour) and quartz (light pink false colour).

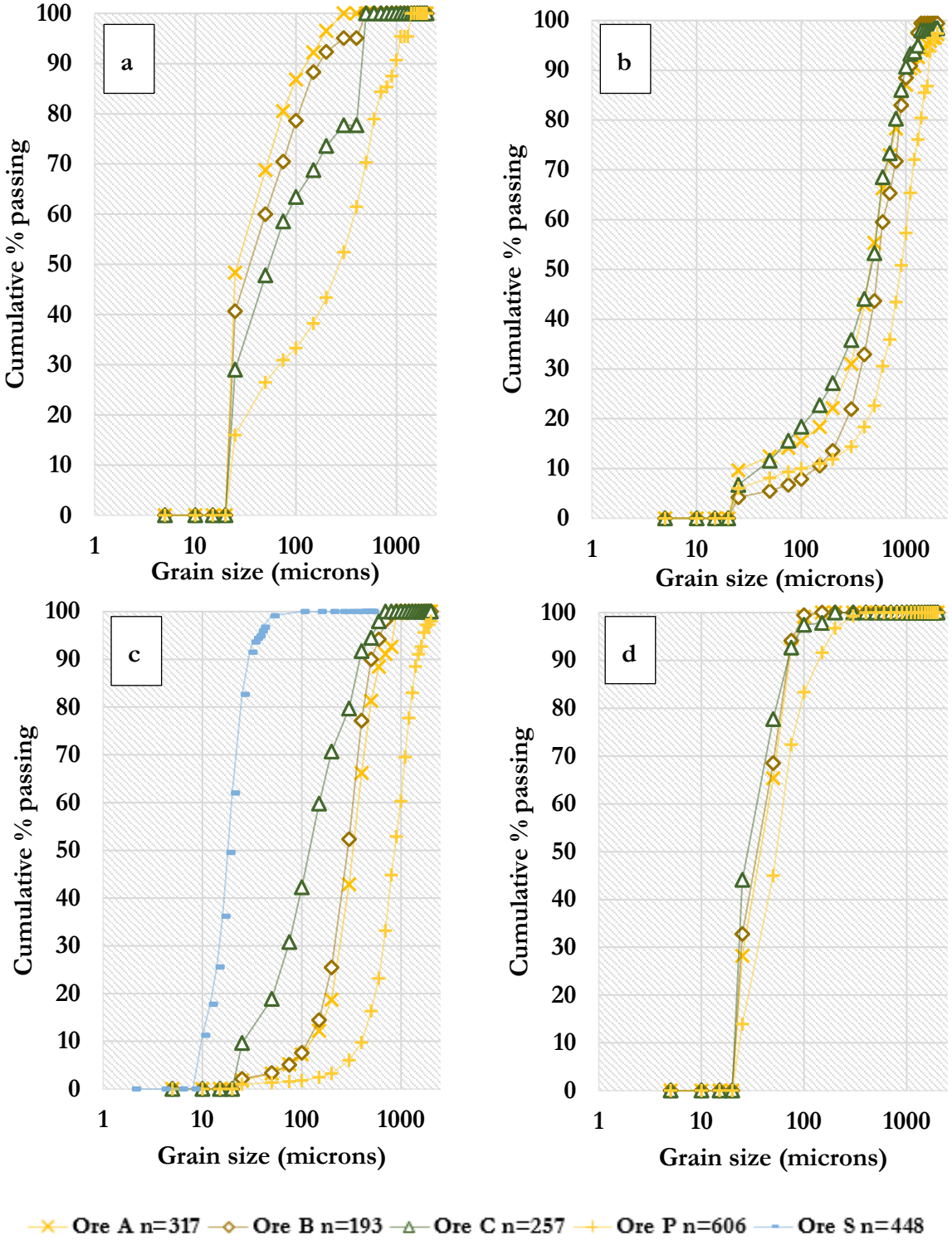

Figure 4-6: Grain size distributions for a) chalcopyrite, b) Magnetite c) Quartz and d) pyrrhotite for all ore types where n represents the number of particles measured.

Grain size distributions for six minerals namely chalcopyrite, magnetite, quartz, pyrrhotite, mica and feldspar were obtained for the ores used in this study. These six minerals were selected because as shown in the previous section, they are the bulk of the minerals found in the ores used. Figure 4-6 shows grain size distributions for the minerals found in the polymetallic sulfide ores and ore S (quartz only) while Figure 4-7 shows the grain size distributions for mica and feldspar which are only found in ore S.

Table 4-2: Summary of the d_{50} an d_{90} parameters for the minerals investigated in each ore.

	d_{50} (microns)				
	Ore A	Ore B	Ore C	Ore P	Ore S
Chalcopyrite	38	60	75	375	-
Magnetite	650	650	600	810	-
Quartz	400	380	140	950	19
pyrrhotite	45	45	35	75	-
Mica	-	-	-	-	22
Feldspar	-	-	-	-	11
	d_{90} (microns)				
Chalcopyrite	150	200	600	1000	-
Magnetite	1050	1000	1000	1700	-
Quartz	700	700	575	1500	28
Pyrrhotite	75	75	75	145	-
Mica	-	-	-	-	18
Feldspar	-	-	-	-	40

Comparing the graphs shown in Figure 4-6, it was observed that ore P consistently had the largest d_{50} for all four minerals investigated. The same trend was evident when looking at the d_{90}s of each ore. This means that it had the larger grain sizes compared to the other ore types. From Figure 4-6b and Figure 4-6d, it can be seen that the grain sizes of the magnetite and pyrrhotite found in the four polymetallic ores are similar though the grains of ore P were consistently slightly larger. While looking at Figure 4-6a, some difference in grain size are observed with ore A having the smallest chalcopyrite grains and ore P having the largest chalcopyrite grains. The grain sizes of quartz which is found in all five ore is shown in Figure 4-6c. It was observed that ore S, has the smallest d_{50} and therefore smallest quartz grains when compared for the polymetallic sulfide ores. Additionally, of the polymetallic sulfide ores, ore P had the largest d_{50} followed by ores A and B which had similar d_{50}s while ore C had smaller quartz grains than the other polymetallic sulfide ores but smaller grains than ore S. The d_{50} and d_{90} parameters for each mineral investigated in the ores are summarized in Table 4-2.

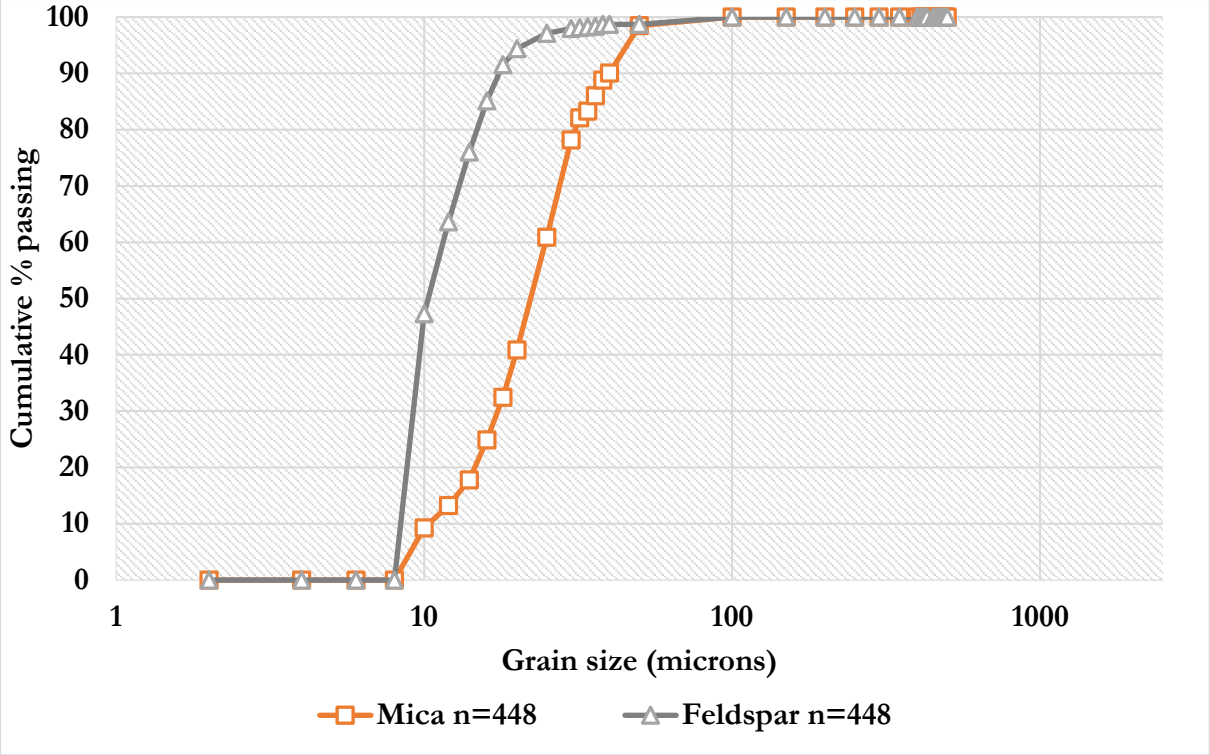

Figure 4-7: Grain size distributions for Mica and feldspar for ore S.

The grain size distributions of the minerals found in ore S only (mica and feldspar) are depicted in Figure 4-7. Comparing the d_{50}s of these minerals and the ones in the polymetallic ores shown inFigure 4-6, it is evident that all the minerals found in ore S (including quartz) had the smallest grain sizes. Additionally, the grain size of quartz found in ore S is smaller than the mica and feldspar grains found in the same ore. These findings will have implications on the ore breakage characteristics, and this will be shown in following sections.

4.4 Particle Size Distributions

From the sieving of the ore breakage progeny (see appendix A for raw screening data), progeny particle size distributions (PSD) in the form of cumulative percentage of the progeny material passing a certain particle size were plotted. This was to assess the effect breakage had on the progeny particle size. PSDs were plotted for all the energy-size combinations tested. PSDs obtained for both crushed ore particles and drill core particles were compared where available.

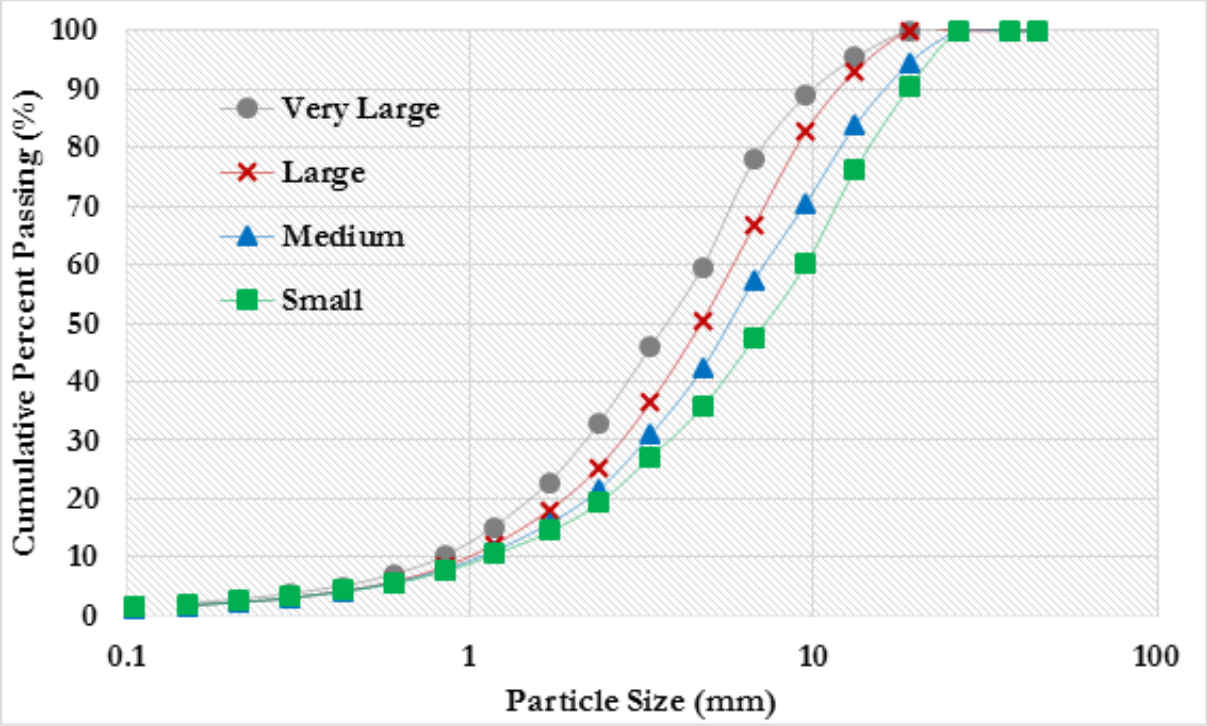

Figure 4-8: Comparison of the particle size distributions for all size classes of crushed ore S at 1 kWh/t.

Figure 4-8 shows a comparison of the particle size distributions for all size classes of crushed ore S at 1 kWh/t. The PSDs show that if the specific input energy is kept constant, the progeny particle size becomes coarser as the initial particle size decrease. On the graph, this can be seen by the PSDs shifting more to the right as the particle size gets smaller. For example, the cumulative percent passing corresponding to a particle size of 10mm was 90%, 85%, 72% and 62% for the very large, large, medium and small size classes respectively. The same trend was observed for all other ore types and at all energy levels.

Figure 4-9 shows a comparison of the particle size distributions for the medium size class of ore S at all energy levels for both crushed ore and drill core. It can be seen that as the specific input energy is increased, there is a related increase in the fineness of the progeny. This is illustrated as an increase in the cumulative percent passing a certain screen size. For example, for drill core at a particle size of 10mm, the cumulative percent passing was 18%, 53% and 82% for the 0.25kWh/t, 1.0kWh/t and 2.5kWh/t energies respectively. This means that as the energy increased, the progeny fineness increased thus more material was able to pass each size. A similar trend was observed for all size classes tested. The same trend was also present in the particle size distributions obtained for all polymetallic ores A-P (refer to appendix B for additional PSDs).

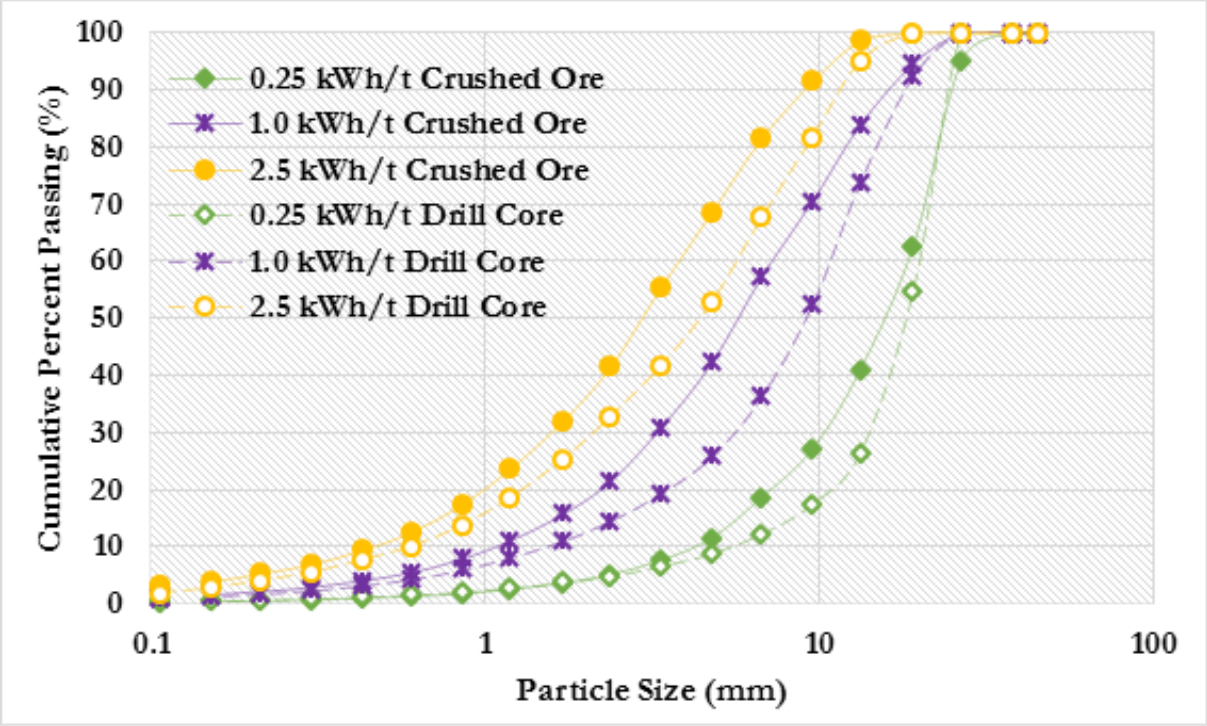

Figure 4-9: Comparison of the particle size distributions for the medium size class of ore S at all energy levels for both crushed ore and drill core.

Figure 4-9 shows that when tested at the same energy-size combination, drill core particles produced a coarser progeny that crushed particles. From Figure 4-9, at 2.5kWh/t, the PSD for drill core lies to the right of the PSD for crushed ore which shows an increase in the coarseness of the progeny particles. For a particle size of 10mm, at 2.5kWh/t, this corresponds to a cumulative percent passing of 92% and 82% for crushed ore and drill core respectively. This indicates that a greater degree of progeny fineness is achieved for crushed ore particles than drill core particles. This trend is also consistent in for all size classes and ore types tested (refer to appendix B for additional PSDs).

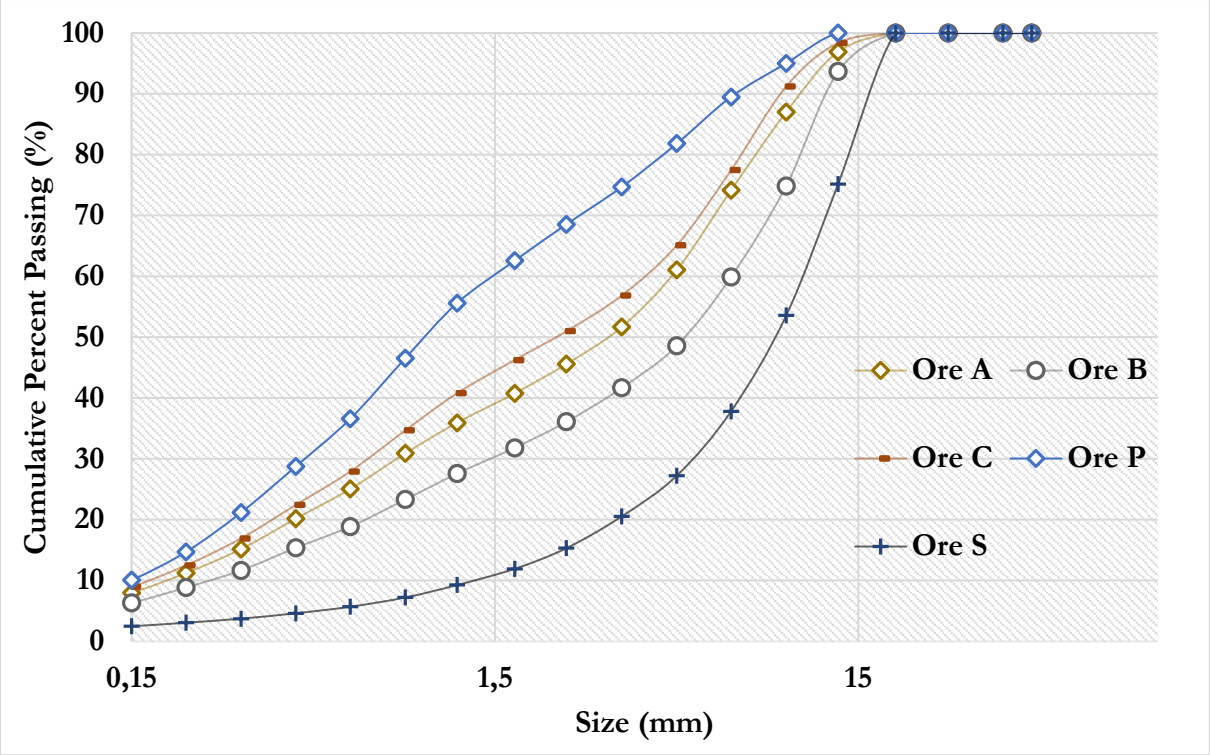

Figure 4-10: Comparison of the particle size distributions for the medium size class of all ore types at 1 kWh/t (drill core).

Figure 4-10 shows a comparison of the particle size distributions for the medium size class of all ore types at 1 kWh/t (drill core). It was observed that at the same energy (1 kWh/t), ore P produced the finest progeny of the five ores while the ore S produced the coarsest. Ore C produced a progeny that was finer than ore A, but coarser than ore P. All ore types produced a progeny that was finer than the progeny produced by ore S. This result was found to be consistent for the other energy-size combinations tests for crushed ore and drill core where available.

4.5 Degree of Breakage

The degree of breakage is described using the t_{10} which represents the percentage of progeny particles that pass one tenth of the initial feed particle size (Napier-Munn et al., 1996). The t_{10} is widely accepted as a measure of "brokenness" to obtain this degree of breakage. Figure 4-11 illustrates a comparison of the degree of breakage (t_{10}) achieved for crushed sample of ore S at all energy-size combinations. No error bars are shown as repeats were not conducted. This was valid as the number of particles used for each energy-size test allowed for statistically valid data to be obtained (Napier-Munn et al., 1996).

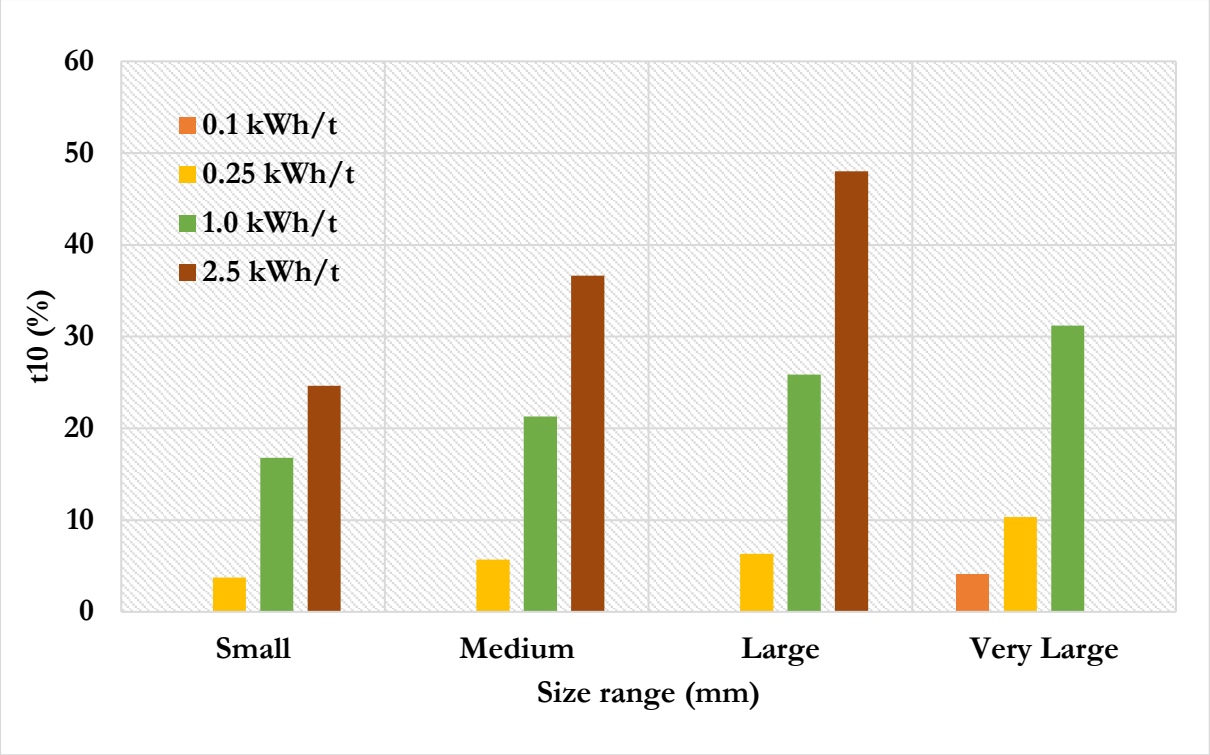

Figure 4-11: A comparison of the degree of breakage achieved for crushed ore S particles.

Comparing the results shown in Figure 4-11, it was observed that as the initial particle size increased while keeping the specific input energy constant, there was an increase in the t_{10}. For example, at 1kWh/t, the t_{10} for crushed ore particles in the small, medium, large and very large size classes were 16.80%, 21.28%, 25.86% and 31.19% respectively. It should also be noted that the very large size class was the only one tested at 0.1kWh/t as specified in the JKRBT test matrix and therefore stands out as singular point. The results observed show that a smaller particle size produces a coarser progeny than a larger particle at the same specific input energy. The same trend is observed at all energy levels tested and is also consistent for drill core particles. The same trend was also observed in all ore types tested (refer to appendix B). The observed trend was expected as grain boundaries, flaws and pores are characteristics of any solid particle (Shi & Kojovic, 2007). A particle will begin to deform and crack when the stress concentration experienced within the particles varies across the particle. A smaller particle contains fewer grain boundaries and flaws by virtue of its smaller size and volume. Such a particle requires a higher impact energy for cracks to result from these flaws. In general, the larger the particle size (more flaws), the less the energy required to break the particle and vice versa (Shi and Kojovic, 2007).

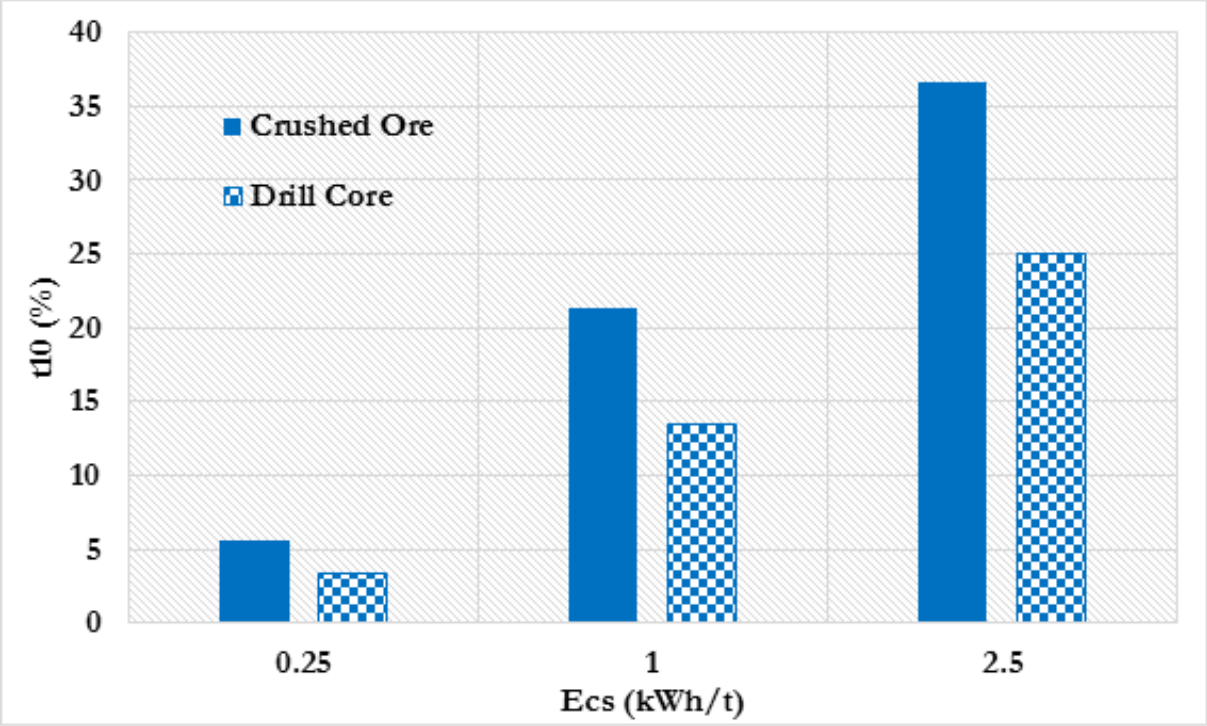

Figure 4-12: Comparison of the degree of breakage for medium size ore S crushed ore and drill core particles at all energy levels.

From Figure 4-12, it is observed that the t_{10} value increases as the specific input energy increases within the same initial particle size class, indicating an increased generation of fine particles at higher energy levels. The trend is consistent for all the size classes and ore types tested (appendix B). The consistently finer progeny obtained translates into higher t_{10} values for all energy levels. Looking at Figure 4-12 for example, the t_{10} for crushed ore S at a specific energy input of 0.25kWh/t, 1kWh/t and 2.5kWh/t were 5.68%, 21.28% and 36.64% respectively. A similar trend is also observed with drill core particles. The observed trend is expected as an increase in specific input energy results in increased stress within the particle, resulting in increased crack density which speeds up crack propagation and fracture leading to smaller particles being formed (Tavares and King, 1998).

Figure 4-12 shows that drill core particles consistently produced a lower t_{10} value than crushed particles at the same conditions. For example, at 2.5 kWh/t, the t_{10} values for drill core particles and crushed ore particles were 19.49% and 24.63% respectively. The same trend is also observed across all size classes and ore types tested. The differences in t_{10}s for crushed and drill core particles can be attributed to the relationship between the energy applied and crack propagation. At constant energy, a particle with a higher number of cracks will rupture more readily than a particle with fewer cracks. Crushed particles likely have a higher crack density per unit volume than drill core particles due to the crushing process which leads to pre-weakening of the particles (Tavares, 2007).

Drill core particles have less cracks as they were freshly extracted from the rock and not exposed to external stressing forces before their use in the impact breakage tests. Upon application of a stressing force above the stress threshold, particles with a higher crack density will fracture more easily because of a higher rate of crack propagation due the numerous paths of weakness available.

The observed trend may also be attributed to differences in the particle shape between the drill core particles (cylindrical) and crushed particles (angular) as shown in Figure 3-5b and Figure 3-6c respectively. Particle shape influences ore breakage characteristics as energy absorption occurs at the point of contact between the stress and the particle surface (Norazirah et al, 2016). Angular particles have a larger surface area exposed for contact than cylindrical particles and, therefore, require less energy for breakage to occur (Chandramohan et al, 2010). Similar results were found by Chikochi (2017) who compared the ore breakage characteristics of Run-of-Mine and drill core samples of UG2 ore.

Looking back at the hypothesis presented in chapter 2, it was hypothesized that drill core particles will produce a coarser product that crushed particles. The observations made in this study showed that drill core particles consistently produced a coarser progeny than crushed ore particles. The results obtained were attributed the difference in the particle shape as explained by Norazirah, et al. (2016). This therefore proved hypothesis 2 put forward for this study.

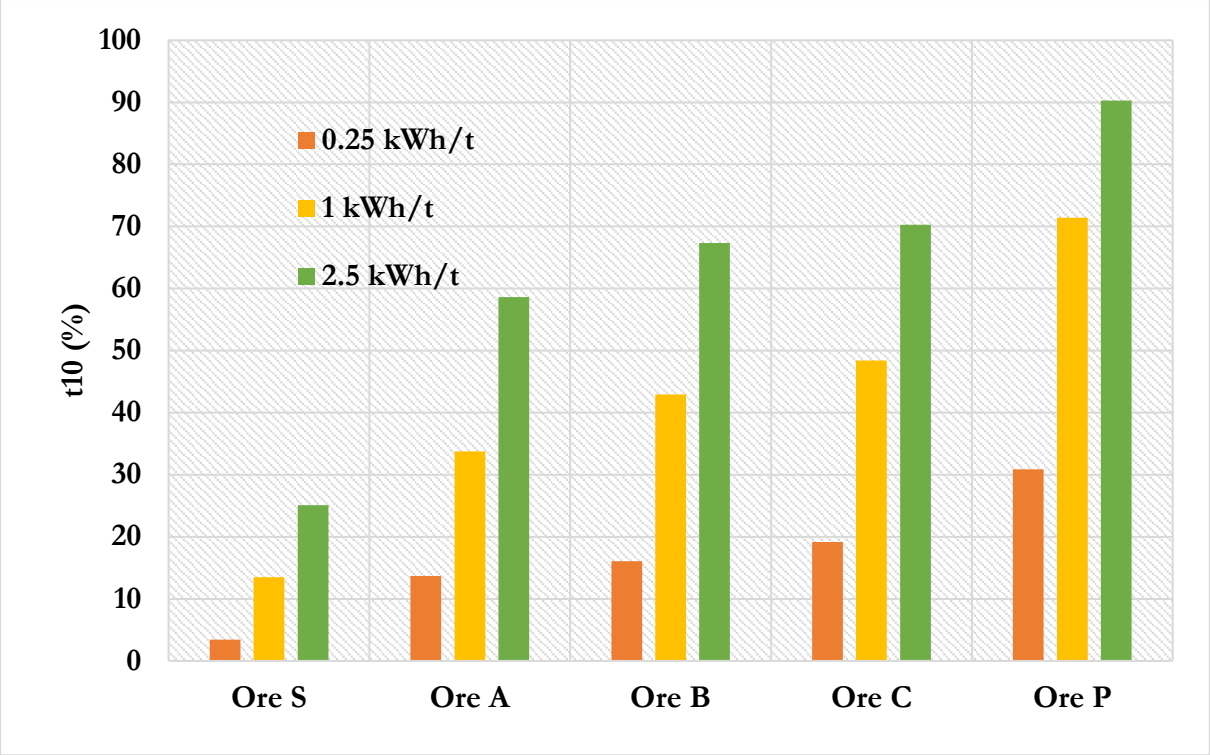

Figure 4-13: A comparison of the degree of breakage for the medium size class for all ore types tested (drill core).

It was also observed that the t_{10} increased from ore S to ore A to ore B to ore C and finally ore P. For example, the t_{10} for medium sized drill core particles at 2.5 kWh/t for ore S, ore A, ore B, ore C and ore P were 25.09%, 58.64%, 67.35%, 70.27% and 90.31% respectively. As previously mentioned, a higher t_{10} corresponds to a finer progeny. These findings are therefore in accordance with the PSD's obtained which showed the same trend.

4.6 Energy-Size Relationships

The main objective of ore breakage characterisation is to quantify the relationship between the specific input energy and the progeny size. The relationship between the E_{cs} and t_{10} is represented by ore characterisation breakage models. This work will investigate the application of two breakage models namely the historically used t_{10} breakage model and the more recent size-dependent breakage model. This was done to obtain the ore competence indicators which are a reliable way to compare the ore breakage characteristics of different ore types. The results are presented in the following sections.

4.6.1 The t_{10} breakage model

The t_{10} based model was fitted to the RBT data using nonlinear regression with the aim of obtaining the ore competence parameters A and b. This was done by comparing the experimentally obtained t_{10} (from the sieving data) to the t_{10} predicted by the t_{10} based model using arbitrary values for A and b to begin with. The difference between the predicted and experimental t_{10} values is summed. A and b are then fitted to the data to provide the least root mean square error (RMSE). Figure 4-14, Figure 4-15, Figure 4-16, Figure 4-17 and Figure 4-18 show the RBT data fitted to the t_{10} breakage model for Ore S, ore A, ore B, ore C and ore P respectively. The solid black lines represent the values predicted by the t_{10} based model based on the accepted A and b values for each ore type.

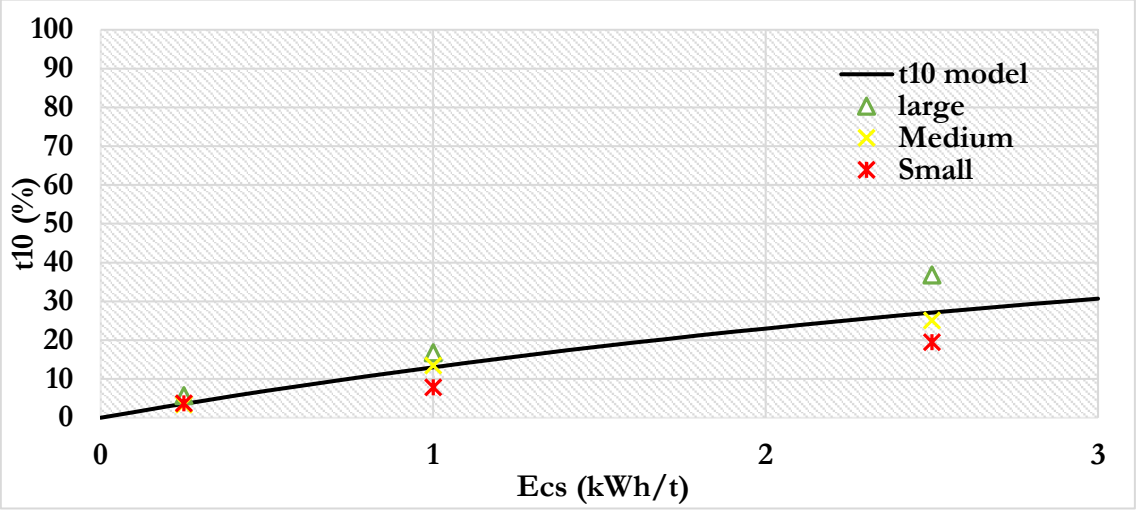

Figure 4-14: RBT data fitted to the t_{10} model for Ore S (drill core)..

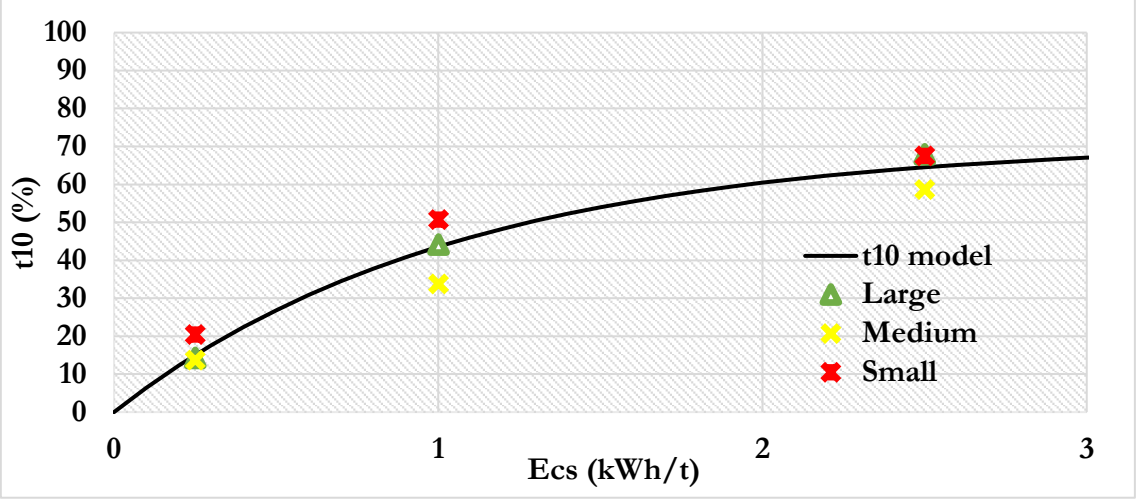

Figure 4-15: RBT data fitted to the t_{10} model for polymetallic ore A (drill core).

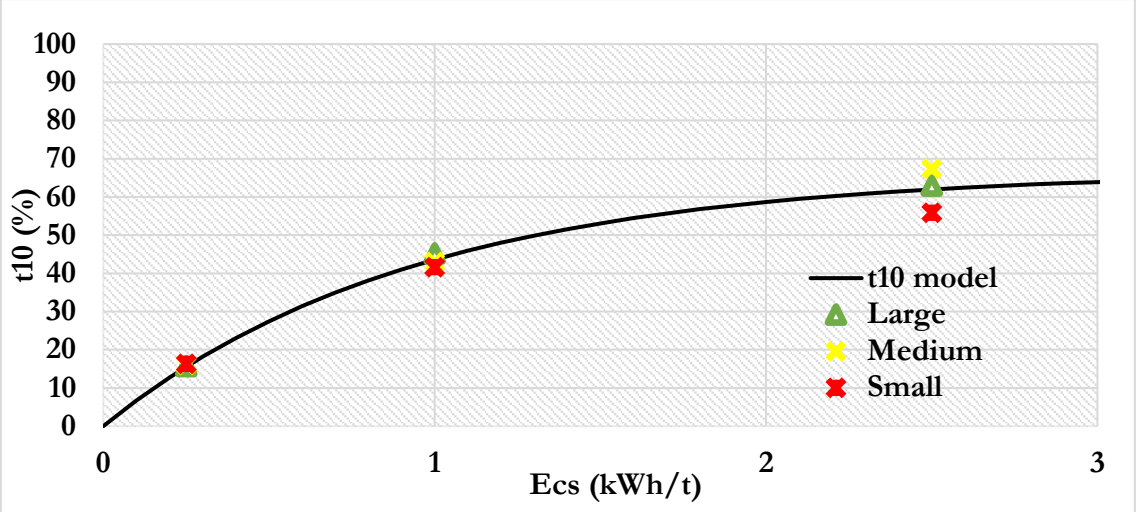

Figure 4-16: RBT data fitted to the t_{10} model for polymetallic ore B (drill core).

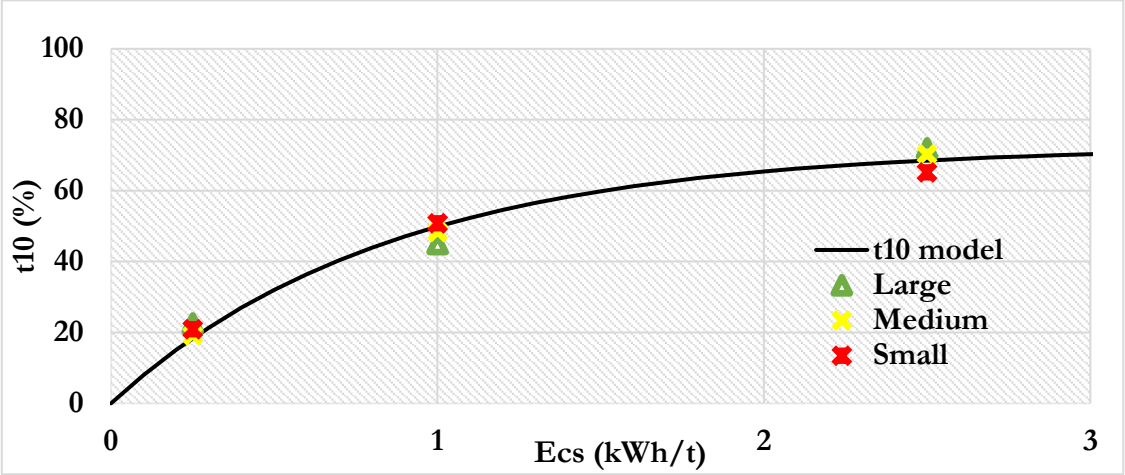

Figure 4-17: RBT data fitted to the t_{10} model for polymetallic ore C (drill core).

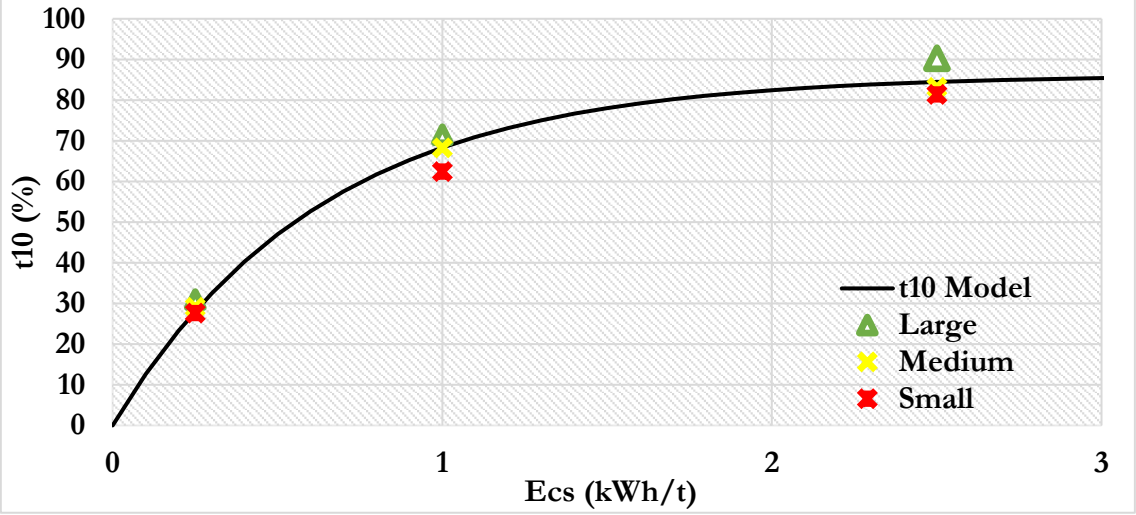

Figure 4-18: RBT data fitted to the t_{10} model for polymetallic ore P (drill core).

From Figure 4-15, it was observed that the t_{10} based model correctly predicted that the t_{10} value increased as the specific input energy increased. The same trend was observed for all ore types tested. This was expected as at higher energy inputs; a greater degree of breakage is achieved due to increased stress concentrations within the particle. However, a point is reached where any further increase in specific input energy does not result in any additional breakage being achieved. This is seen by the model prediction plot reaching a maximum value and beginning to plateau.

The maximum t_{10} reached corresponds to the A parameter which was 56.16%, 71.16%, 66.64%, 72.44%, and 86.14% for ore S, ore A, ore B, ore C and ore P respectively. A higher A value indicate a greater degree of breakage being achieved at higher energies. This was the case with the ores S, A, C and P. However, the A parameter obtained for ore B was not expected as ore A would be expected to have the lowest A value as it shows the greatest resistance to breakage. A possible explanation for this may be that though a higher A value indicates a greater degree of breakage, the progeny material resulting from the breakage was not fine enough to report to sizes below the t_{10}. Because of this, ore A can still be classified as the hardest of the three ore types as shown by the overall breakage parameters (Axb).

Also of importance is the b parameter which is related to the material stiffness and corresponds to the gradient for the linear part of the model prediction curve (Napier-Munn et al., 1996). The b parameter for ore S, ore A, ore B, ore C and ore P was 0.26, 0.95, 1.06, 1.17 and 1.57 respectively. As expected, ore S had the lowest b value thus implying that ore S particles had a greater resistance to deformation than polymetallic ores A, ore B, ore C and ore P.

Table 4-3: Summary of ore competence indicators for each ore type using the t_{10} based model (DC refers to drill core particles while CP refers to crushed ore particles) – classification from Napier-Munn et al. (1996).

Ore Type	Preparation	A (%)	b	A*b	Classification
Ore S	DC	56.17	0.26	14.8	Very hard
	CP	42.54	0.79	33.6	Hard
Ore A	DC	71.16	0.95	67.4	soft
	CP	77.89	1.02	79.1	soft
Ore B	DC	66.64	1.06	70.7	soft
	CP	74.23	1.12	83.1	soft
Ore C	DC	72.44	1.17	84.4	soft
	CP	82.98	1.25	104	soft
Ore P	DC	86.14	1.57	136	Very soft
	CP	92.37	1.76	162	Very soft

The most important ore breakage indicator to be considered when using the t_{10} based model is the Axb parameter which shows gives the overall picture of the ore competence or resistance to breakage. The Axb parameter corresponds to the gradient of the t_{10} based model curve at the origin i.e. when the specific input energy is 0 kWh/t. The higher the Axb indicator, the more readily the ore will fracture i.e. the ore shows less resistance to breakage. Axb values can also be compared to the typical ranges prescribed by Napier-Munn et al. (1996).

Table 4-3 summarizes the ore competence parameters for all ore types tested. The Axb value for drill core samples of ore S, ore A, ore B, ore C and ore P was 14.8, 67.4, 70.7, 84.4 and 136 respectively. These values show that ore P is the least competent (highest Axb) while ore S is the most competent (lowest Axb). The same trend was true was observed for crushed ore however crushed ore consistently had a higher Axb value than drill cores. It is also worth noting that the difference between the ore B and ore A Axb values is relatively small. According to the typical ranges prescribed by Napier-Munn et al. (1996) and found in Table 2-3, crushed ore S was classified as "hard" (30<Axb<38) while drill core ore S was classified as very hard (Axb<30). Additionally, ore A, ore B and ore C were classified as "soft" (67<Axb<127) while ore P is classified as "very soft" (Axb>127).

4.6.2 The Size-Dependent breakage model

The main drawback of the t_{10} breakage model is that it uses one set of A and b parameters for all particle sizes. The use of fixed parameters implies that particle size has no influence on breakage characteristics which is incorrect (Tavares, 2007). This also goes against the experimental t_{10} values obtained previously which show a decrease in the t_{10} as the particle size decreases at the same energy. The Size-dependent breakage model is therefore more advantageous as it allows for direct quantification of the size effect on breakage (Shi & Kojovic, 2007).

The experimentally obtained breakage data was fitted to the size dependent model (SDM) which allowed for the particle size effect to be explored. For fitting purposes, some parameters of interest in the SDM included k (number of impacts) which was assumed to be 1 due to only single impact breakage taking place. The energy threshold (E_{min}) was assumed to be zero as no historical incremental breakage data could be accessed for the sample. This assumption was based on the work of Zuo and Shi (2015) which validated this assumption for high t_{10} values such as those exhibited by the breakage data.

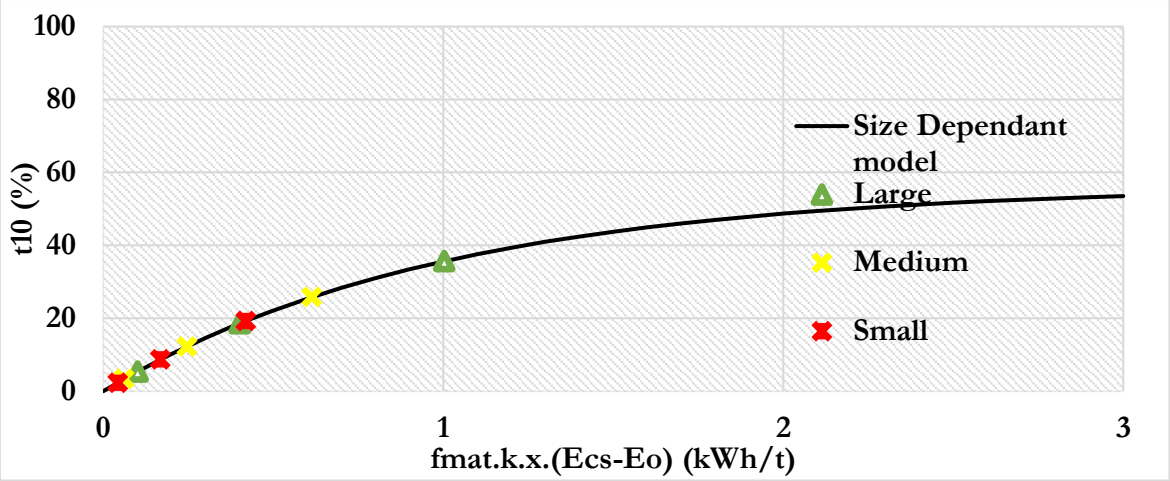

Figure 4-19: RBT data fitted to the Size-dependent model for ore S (drill core)..

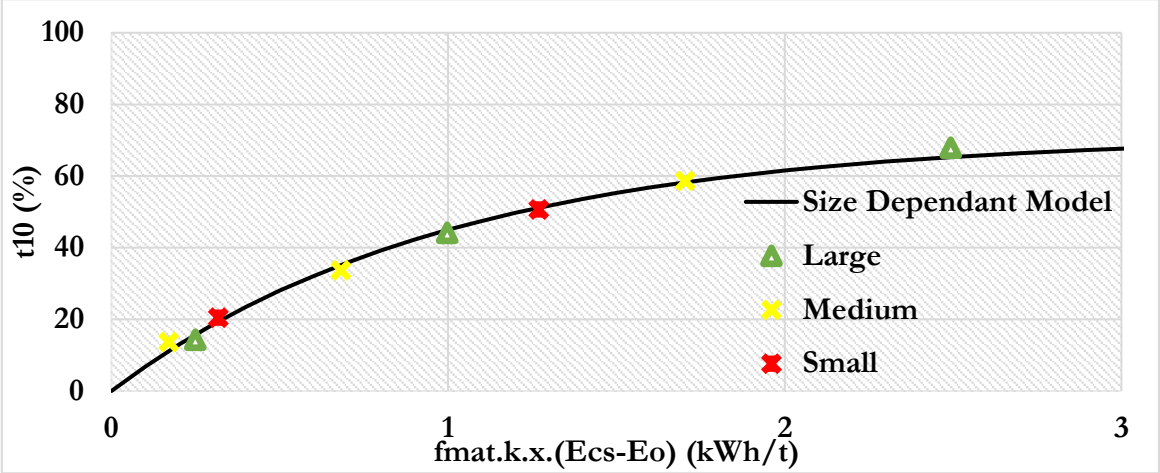

Figure 4-20: RBT data fitted to the Size-dependent model for ore A (drill core).

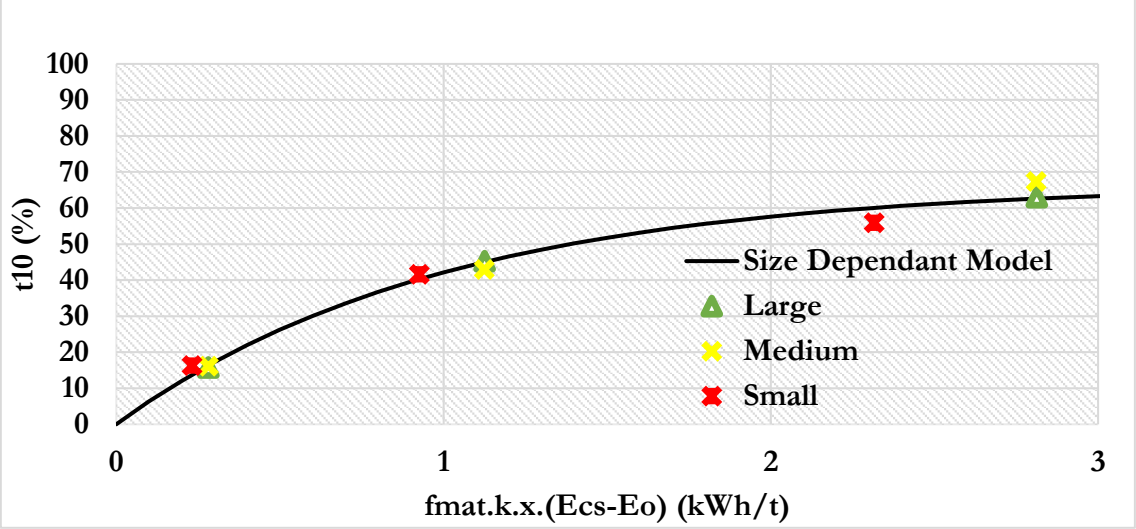

Figure 4-21: RBT data fitted to the Size-dependent model for ore B (drill core).

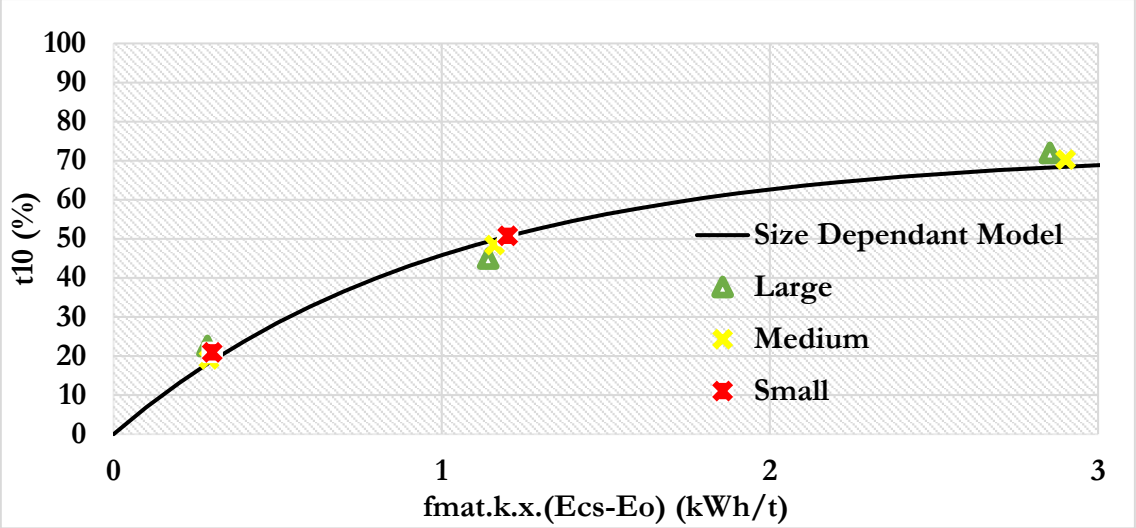

Figure 4-22: RBT data fitted to the Size-dependent model for ore C (drill core).

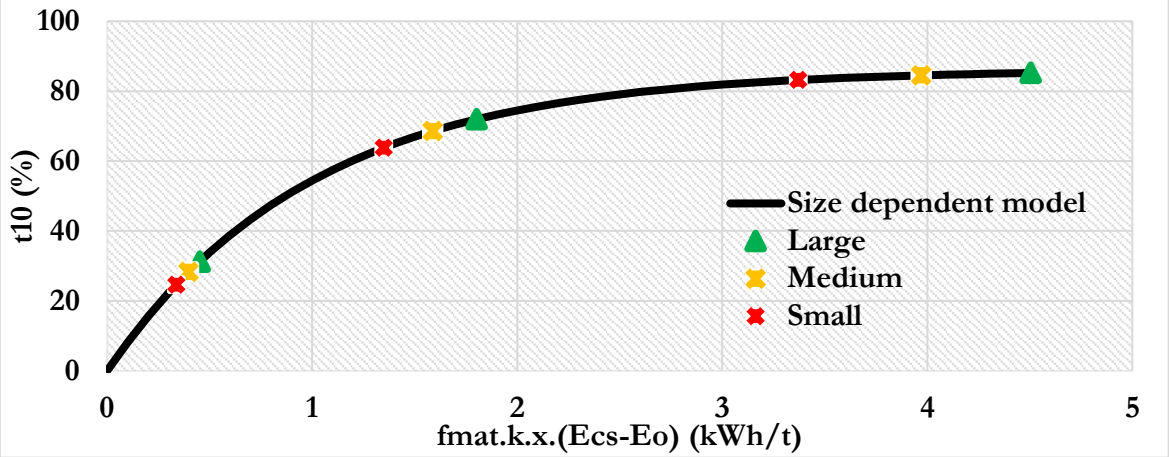

Figure 4-23: RBT data fitted to the Size-dependent model for ore P (drill core).

Figure 4-19 - Figure 4-23 show the ore breakage data fitted to the size-dependent model for ore S, ore A, ore B, ore C and ore P respectively, where the solid black lines represent the values predicted by the model. Figure 4-18 – 4-20 show that higher energy inputs result in a greater degree of breakage due to increased stress concentrations within the particle. As with the t_{10} model, a maximum t_{10} value is reached which in the case of the SDM corresponds to the M-parameter. The M-parameters were 56.16%, 71.16%, 66.64%, 72.44%, and 86.14% for ore S, ore A, ore B, ore C and ore P respectively which was found to be the same as the A value from the t_{10} based model (Table 4-4).

Table 4-4: Summary of the ore competence indicators for each ore type using the size-dependent model (drill core).

		Mean particle size (mm)			
		28.9	20.6	14.5	
Ore Type	M (%)	3600.M.F_{mat}.x			RMSE
Ore S	56.3	81.3	69.6	67.5	3.1
Ore A	71.16	289.4	255.5	174.7	4.49
Ore B	66.64	313.5	269.7	269.9	7.28
Ore C	72.44	325.3	302.6	297.6	8.81
Ore P	86.1	559	493	418	6.58

The ore competence indicator when using the SDM takes the form of 3600.M.f_{mat}.x. This competence indicator is different for each size class as f_{mat} changes with each size class. The higher the indicator, the more readily the ore will fracture i.e. the ore shows less resistance to breakage. The SDM ore competence indicators are shown in Table 4-4. It was also observed the ore competence indicators decreased with a decrease in the initial parent particle size. This trend was seen in all ore types tested. The results obtained show the effect of initial particle size on the breakage characteristics where grain boundaries and flaws are characteristics of any solid particle. A particle will begin to deform and crack when the stress concentration experienced within the particle varies (Norazirah, Fuad and Hazizan, 2016). Small particles typically contain fewer grain boundaries and flaws due to their smaller size and volume, leading to an increase in the minimum energy threshold (Shi and Kojovic, 2007). Larger particles, therefore, require less energy to break due to abundance of cracks and flaws in their structure.

Table 4-5: Comparison of the ore competence parameters of crushed ore and drill core for each ore type (medium size class).

	Crushed ore	Drill Core
Ore Type	3600.M.F_{mat}.x	
Ore S	109.7	69.6
Ore A	284.6	255.5
Ore B	299.3	269.7
Ore C	374.3	302.6
Ore P	548	493

Table 4-5 shows a comparison of crushed ore and drill cores for each ore type investigated. The results showed that crushed ore consistently had higher values of 3600.M.F_{mat}.x than drill cores in all cases. For example, ore C had ore competence indicators of 374.3 and 302.6 for crushed ore and drill core respectively. These results show that crushed ore shows less resistance to breakage than drill core.

4.7 Mineral Liberation

The main function of comminution circuits is to liberate the targeted valuable minerals from the gangue minerals. The liberation of valuable minerals is an essential step as downstream beneficiation of the valuable minerals is not possible if they are not liberated. The work of Wightman et al (2008) and Vizcarra (2010) showed that the liberation of minerals in a given size fraction was independent of the mode of comminution used. Additionally, the authors found that the liberation characteristics of the ore were a function of the mechanical properties of each mineral rather than the breakage mode used.

Liberation analyses were conducted on various samples to determine and compare the liberation characteristics of the samples after breakage using the JKRBT. This study investigated the liberation characteristics of various samples in order to understand the differences in liberation for:

- Ore A, ore B, ore C and ore P
- Drill core and crushed ore

The results are presented in the following sections and focused on tracking the liberation of chalcopyrite, quartz, magnetite and pyrrhotite only. Liberation data for ore S was not obtained because the mineral grain sizes are so small, it can be assumed nothing would be liberated anyway. In this study, three liberations groups will be used i.e. locked (0-29%), middling (30-89%) and liberated (90-100%). Figure 4-24 shows a comparison of the liberation profiles for four minerals found in drill core particles of ores A, B, C and P.

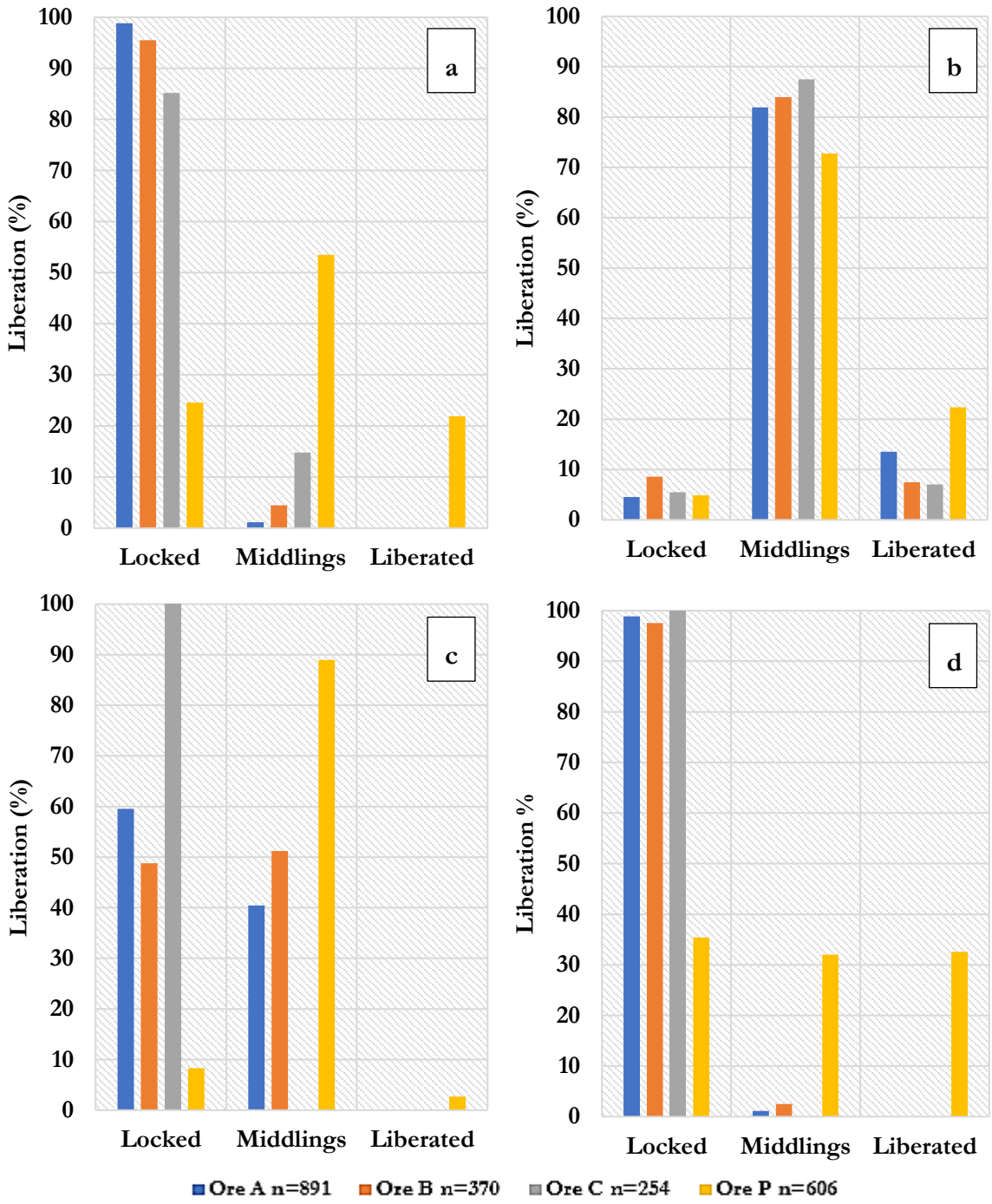

Figure 4-24: Comparison of the mineral liberation for medium size particles at 1 kWh/t for a) chalcopyrite, b) magnetite, c) Quartz and d) pyrrhotite in ore A, ore B, ore C and ore P (drill core only) where n indicates the number of particles counted and locked (0-29%), middling (30-89%) and liberated (90-100%).

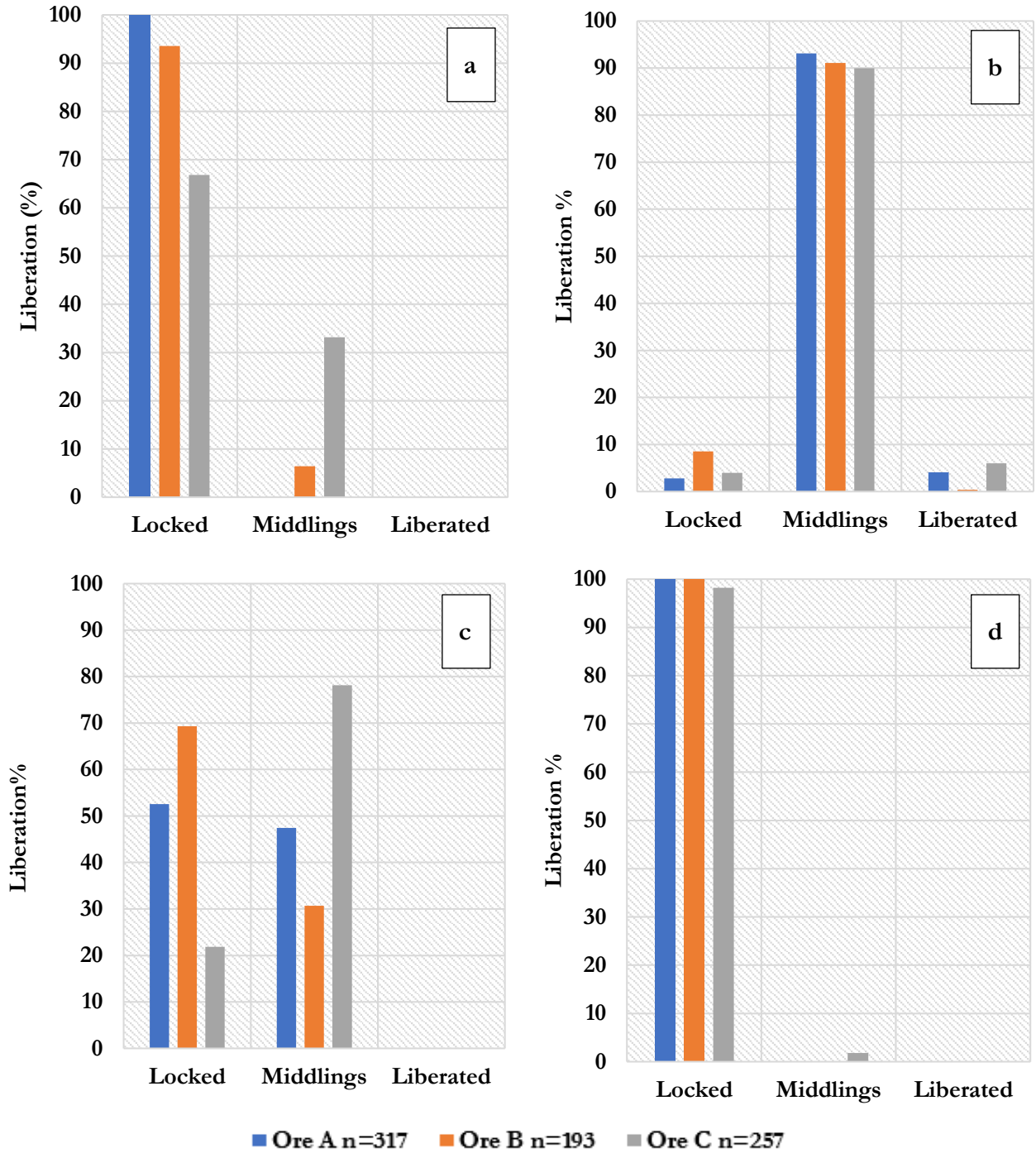

Figure 4-25: Comparison of the mineral liberation for medium size particles at 1 kWh/t for a) chalcopyrite, b) magnetite, c) Quartz and d) pyrrhotite in ore A, ore B and ore C (crushed ore only) where n indicates the number of particles counted and locked (0-29%), middling (30-89%) and liberated (90-100%).

From Figure 4-24a, it can be seen that drill core ore A samples had the greatest proportion of chalcopyrite minerals still locked (99%) and no particles were fully liberated (0%). This is as opposed to ore P which had the least locked (25%) and the greatest proportion of fully liberated

particles (22%). Additionally, ore P had the highest proportion of middling (53%). A similar trend also observed for crushed ore particles (Figure 4-25a), however in this case ore C has the least locked and most middling. The observed trend was expected as ore P showed the least resistance to breakage when compared to the other three ore types. The observed liberation trend can be attributed to the grain size distribution of each ore type. Ore P larger chalcopyrite grains as opposed to the other polymetallic sulfide ores. Fine grained particles have higher resistance to breakage and thus liberation due to the increased surface area available for contact which results in less stress per unit area as the stress is distributed evenly over the numerous contacts. This means that at the same energy levels, finer grained particles exhibit less breakage and therefore less liberation of valuable minerals as illustrated in Figure 4-24.

A comparison of Figure 4-24 and Figure 4-25 shows that crushed ore particles exhibited slightly more liberation than drill core particles under the same conditions. For example, the liberated proportion for ore C in drill core and crushed ore was 2% and 12% respectively. This means that crushed ore showed greater liberation than drill core particles. The same trend is observed for all ore types tested. This trend was expected as the breakage data obtained showed that crushed ore produced a finer progeny than drill core particles under the same conditions. As the degree of fineness increases, so does the liberation of manganese minerals. Therefore, the higher degree of liberation observed, corresponding to increased fineness, was attributed to the differences in crack density and particle shape between the two particle types.

4.8 Discussion

The results observed and presented in previous sections can be attributed to the grain size distribution of the constituent minerals for each sample as presented in Figure 4-6 and Figure 4-7. Grain size distributions for six minerals namely chalcopyrite, magnetite, quartz, pyrrhotite, mica and feldspar were obtained for the ores used in this study. These six minerals were selected because they are the bulk of the minerals found in the ores used.

As observed in Figure 4-6, ore P had the largest grains while ore S had the smallest d_{50}s and therefore smallest grains. The polymetallic ores A-P had similar grain sizes for magnetite and pyrrhotite. In terms of chalcopyrite, it was observed that ore A had the smallest chalcopyrite grains and ore P having the largest chalcopyrite grains. Quartz which was dominant in ore S, was found to be smallest in ore S. Additionally, of the polymetallic sulfide ores, ore P had the largest d_{50}

followed by ores A and B which had similar d_{50}s while ore C had smaller quartz grains than the other polymetallic sulfide ores but larger grains than ore S.

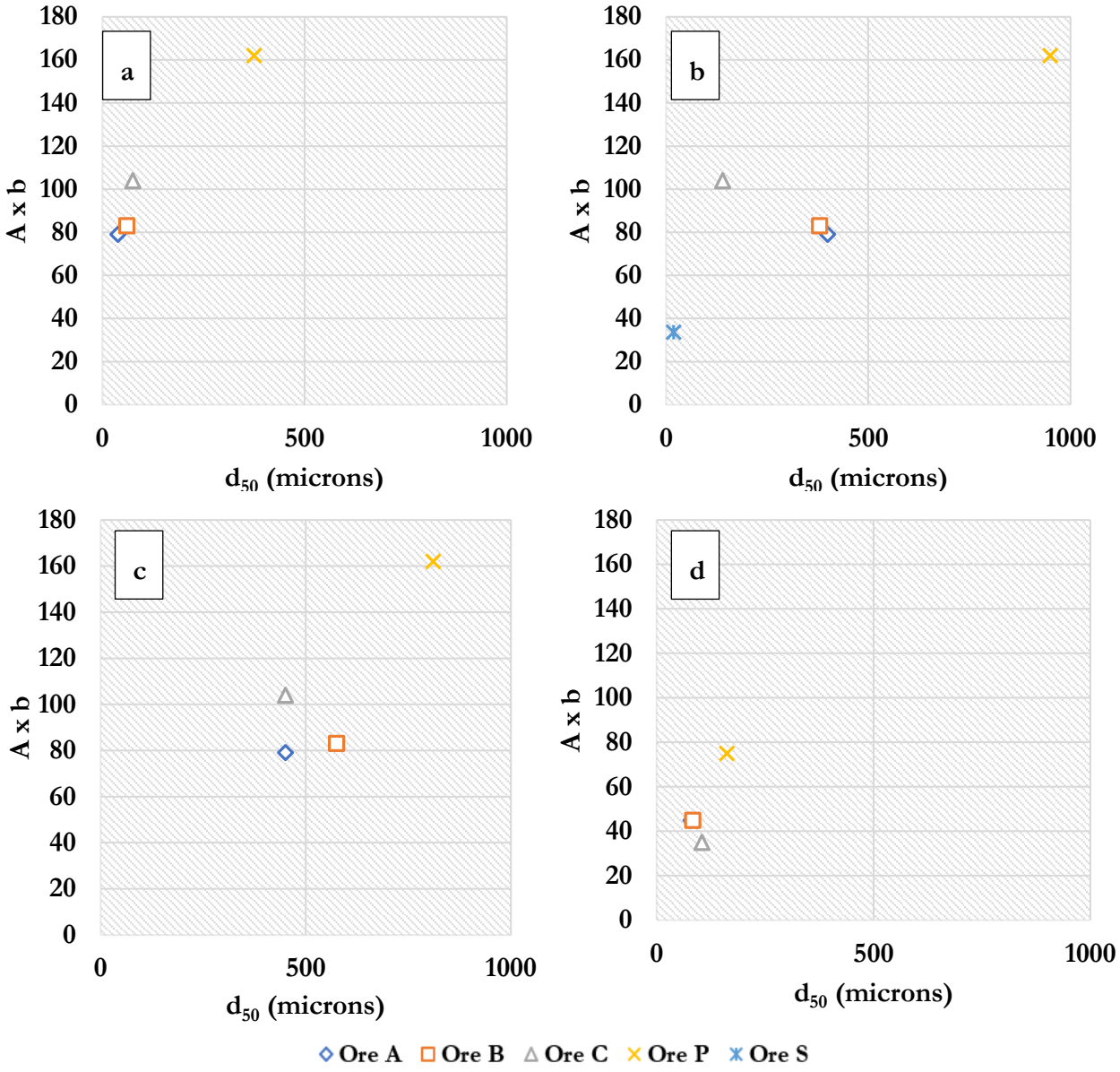

Figure 4-26: A comparison of the relationship between d_{50} and A x b for a) chalcopyrite, b) quartz, c) magnetite and d) pyrrhotite.

Figure 4-26 illustrates the relationship between grain size (d_{50}) and the ore competence parameter (Axb). From Figure 4-26a, it was observed that as the chalcopyrite mineral grain size increases, so does the ore competence parameters i.e. the ore becomes softer. A similar trend is observed in Figure 4-26b with the exception of ore C, which has a smaller quartz grain size than ores A and B and a higher Axb values than ores A and B. A similar anomaly with regards to ore C is also

observed in the graphs for magnetite and pyrrhotite. The differences observed in ore C are also a clear indication that grain size is not the only control on the hardness of an ore. However generally speaking, an overall trend can be established from the graphs shown in Figure 4-26 i.e. as the d_{50} or the mineral increases, so does the Axb parameter which means the ore is softer. This trend is consistent with the other results presented in previous sections.

The work of Eberhardt et al (1999) showed that increasing the grain size led to larger intergranular cracks and larger grain boundaries which promoted crack propagation and extension by providing continuous paths of weakness. This means that an increase in grain size leads to a decrease in rock strength and therefore an increase in the ore competence parameters. The findings were attributed to an increase in the surface area available for contact due to the decrease in grain size. An increase in contact area results in less stress per unit area due to distribution of the stress across the increased contact area. Smaller grains lead to a decrease in porosity and therefore more tightly held particles which are harder to break. Therefore, ore P is the least competent because it is composed of the largest grains of the constituent dominant minerals. The combination of larger grains means that the grains are less tightly bonded to each other allowing them to break easily. Ores A and B have similar d_{50}s for the minerals investigated and therefore shows similar breakage characteristics.

The same reasoning can be applied to ore S which was fine grained and homogenous as shown by the grain size distributions in Figure 4-6 (quartz only) and Figure 4-7. The d_{50} of all the minerals found in ore S is on the order of 10-25 microns therefore they can be classified as fine grained according to the grain size classification scale used for this study. As explained above, fine grains are more tightly held together and therefore more resistant to breakage which is consistent with the ore breakage characteristics observed for ore S.

Looking back at the hypothesis set out in chapter 2, it was hypothesized that an ore with a coarse grained texture will break to form a finer progeny than an ore with a fine grained texture. Observations made in this studied showed that ores consisting of finer grains size distribution had a high resistance to breakage with the opposite being true for coarser grained ore types investigated. The results obtained therefore proved hypothesis 1 presented in section 2.8.

The influence of the grain size is consistent with the relative mineralogy on the ore breakage properties. It is an accepted fact that an ore is only as hard as its constituent minerals and their associated relative abundance within the ore. Mohs hardness scale is an accepted qualitative scale that ranks various minerals according to their scratch resistance. Table 4-6 provides a summary of the relative abundance and the Mohs hardness of the most abundant minerals in all the ore samples.

Table 4-6: Relative abundance and Mohs hardness of most dominant minerals in each ore type (adapted from Webminerals).

Mineral	Mineral Mass %					Mohs Hardness
	Ore A	Ore B	Ore C	Ore P	Ore S	
Chalcopyrite	1.6	2.0	0.6	15.2	-	3.5
Galena	0.5	0.5	6.4	0.1	-	2.5
Pyrrhotite	2.0	2.0	0.8	12.0	-	4.0
Magnetite	57.1	53.8	58.8	55.9	-	6.0
Quartz	6.8	6.8	2.5	9.8	31.4	7.0
Pyroxmangite	21.0	26.2	27.7	0.3	-	5.5
Mica	-	-	-	-	44.3	2.5

The hardness of an ore can therefore be considered to be a function of the mineral hardness and its relative abundance. Quartz – the hardest mineral – is present in larger amounts in ore S than in the polymetallic sulfide ores. Though ore S contains mica (hardness 2.5), it should be noted that the mica is contained in a matrix of quartz and is fine grained which renders ore S more resistant to breakage. Three most dominant minerals in ore P are magnetite (hardness 7), pyrrhotite (hardness of 4) and chalcopyrite (hardness of 3.5). It is also worth noting that ore P contains only trace amount of pyroxmangite (hardness 5.5) compared to ores A-C. This would make Ore P the least resistant to breakage as it contains substantial amounts of the softer minerals (chalcopyrite and pyrrhotite) when compared to the other polymetallic ores.

Ore C, on the other hand, with a 6.40% Galena content as compared to the other ores at <1% is considered to be softer than ores A, B and S. This is also in addition to the fact that it contains the least amount of quartz (hardness 7). This renders or C, softer than ores A, B and S but harder than ore P. Ores A and B have similar breakage properties, and this is a result of the two ores having similar mineral content for the dominant minerals. Both ores are rich in magnetite, quartz and pyroxmangite which are the hardest of the minerals present in both ores. It is therefore clear that the more abundant the harder minerals, the more competent the ore type. Relating these two properties results in the conclusion that ore S is the hardest ore and ore P the softest.

5. THE LEAST PARTICLES PROTOCOL

Overview

This chapter seeks to investigate whether an abridged test protocol can be established to obtain the relevant ore competence parameters from minimal particles. The results obtained from the standard JKRBT ore breakage procedure is compared to the results obtained for the proposed least particles protocol. Deductions are then drawn based on the presented results as to whether the proposed protocol is fit to be used in situations where sample availability is a problem. The results of a case study using the proposed least particles protocol is then presented.

5.1 Introduction

The JKRBT is a rapid characterisation device however the sample preparation and progeny screening is still time and energy consuming. A matrix of 12 RBT tests requires 360 particles grouped in small particle size fractions which can prove to be difficult to achieve in situations of limited sample availability. Reducing the amount of sample required for RBT tests would help address these challenges. The Least Particles Protocol (LPP) aims to address the challenges associated with RBT testing by reducing the number of particles required in each test while still obtaining representative ore breakage indices. As such, the LPP is similar to the standard RBT procedure except for the number of particles used in each test as outlined in section 3.4.1.

5.2 Data Validation

Validation of the LPP comprised four RBT test matrices i.e. two tests on drill core particles and two tests on crushed ore particles. Shale was selected for investigation because of its homogeneity and fine grained texture which are likely to give consistent breakage results. Both drill core particles and crushed ore particles were subjected to RBT tests using the standard test protocol (30 particles) to provide reference ore breakage parameters. The remaining tests were conducted according to the least particles protocol described in section 3.4.1 i.e. six groups of five particles were tested at each condition for both drill core and crushed particles. The whole validation process consisted of 147 RBT tests using 1260 particles (both drill core and crushed). The number of tests and particles was high in order to obtained statistically valid and representative results.

To validate the LPP, ore breakage parameters obtained from tests using 30 particles are compared to the ore breakage parameters obtained using less than 30 particles. As the RBT tests were carried out in groups of 5 particles, only 25, 20, 15 and 10 particles were considered as options. 10 particles were the minimum number considered as it was low enough to minimize the number of particles while still maintaining the statistical validity of the RBT tests in terms of number of particles used in each test. Sieving data from groups of five were combined to obtain the desired number of particles for example, 25 particles comprised of five randomly chosen sieving data sets condensed together. 20 particles comprised of condensed sieving data from four randomly chosen sieving data sets out of the six available data sets at each testing condition. The same methodology was used for the 15 particles and 10 particles.

The goal of the validation process is to choose the minimum number of particles that can be used to obtain ore breakage parameters that are within a 2% tolerance level to those obtained using the standard test procedure. The data validation process is summarized in Figure 5-1. Breakage parameters were obtained from the condensed PSDs from which the experimental t_{10} value could be extracted. Breakage models (t_{10} model and the Size Dependent Model) were used to predict t_{10} values based on estimated model parameters. Microsoft Excel Solver was used to compare experimental t_{10} to the model predicted t_{10} and minimize the sum of squares by iterating the process while changing the model parameters. When the sum of squares is at its minimum, the model parameters are accepted. Ore competence indicators were then calculated and took the form Axb (t_{10} model) and $3600.M.f_{mat}.x$ (Size Dependent Model).

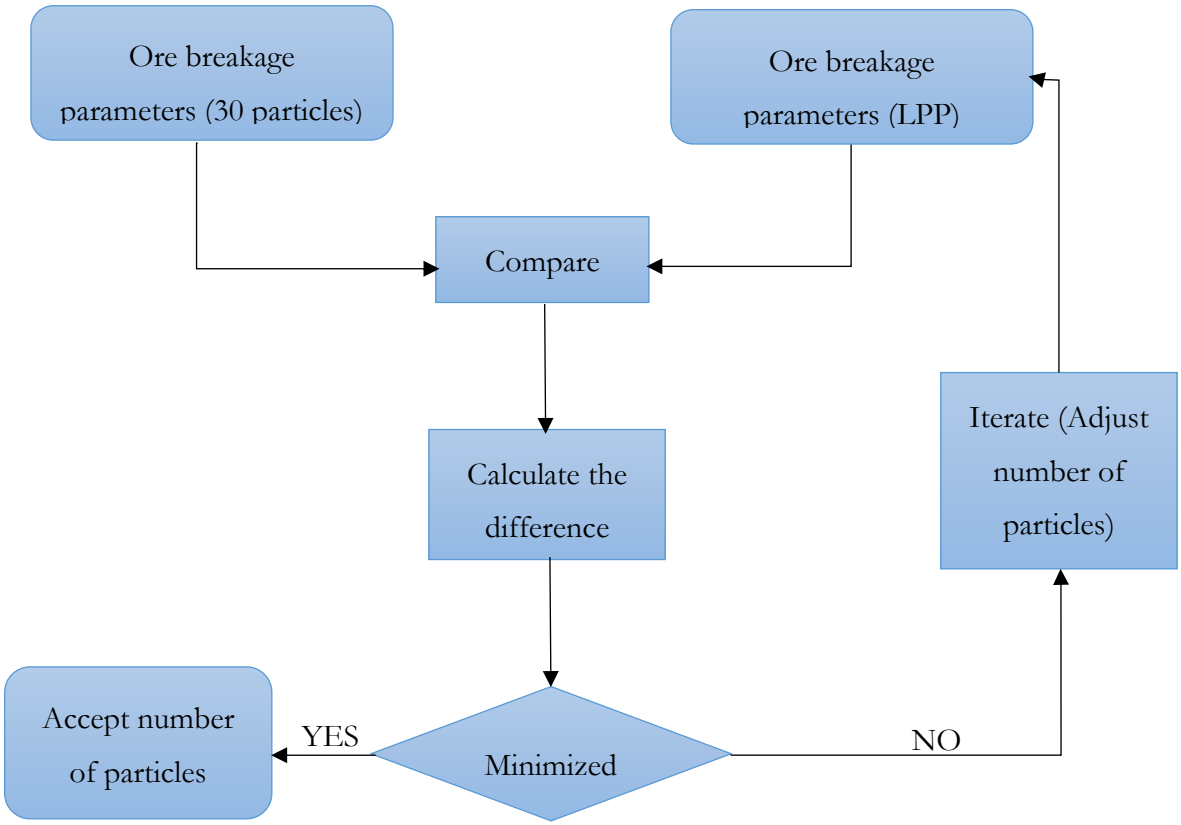

Figure 5-1: Flowchart illustrating the process used for the LPP.

The ore breakage parameters used to compare the standard test procedure to the LPP included the t_{10} value and the ore competence indicators (Axb and $3600.M.F_{mat}.x$). Higher priority was given to the ore competence indicators as they show the overall competence of the ore and allow for comparison between ores. Additionally, in the case of the Axb values, they can be compared to the typical ore indicator ranges shown in Table 2-3.

5.3 Particle size distributions

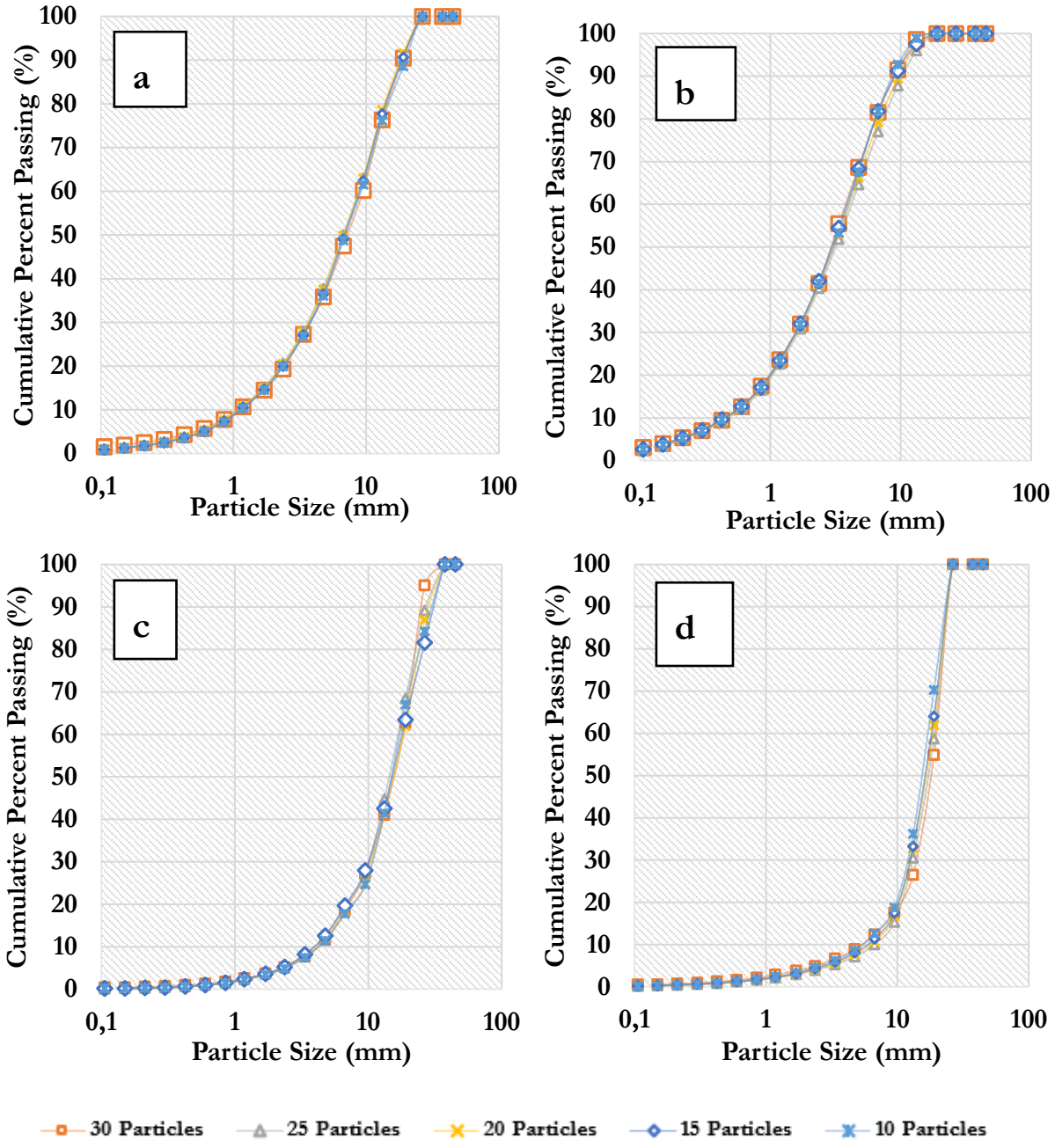

Figure 5-2: Progeny particle size distributions for a) very large at 1kWh/t (Crushed), b) large at 2.5kWh/t (crushed) c) large at 0.25kWh/t (crushed) and d) large at 0.25kWh/t (drill core).

Progeny particle size distributions (PSD) were used to evaluate the extent of damage exhibited for the different number of particles compared to the standard 30 particle test. PSDs were plotted as the cumulative percentage of material passing a sieve size as illustrated by Figure 5-2. The comparison was performed for all test conditions however only the PSDs shown in Figure 5-2 are used for discussion purposes.

As illustrated in Figure 5-2a, as the number of particles per test decreases, the PSD produced is closely related to the PSD resembling the standard test at the same conditions. A similar relationship is observed at all energy-size combinations tested. A comparison of Figure 5-2a and Figure 5-2b shows that a decrease in input energy leads to a coarse progeny size distribution. Additionally, Figure 5-2d shows that this relationship also holds for drill core particles. This implies that in terms of the PSD produced, all number of particles produce very similar PSDs and therefore the 30-particle test can be replaced by any of the potential protocols. However, this deduction cannot be made based solely on the PSD and therefore additional comparisons of the ore breakage parameters is required.

5.4 Degree of Breakage

A comparison of the extent of breakage for each number of particles was performed for both crushed ore and drill core particles using the t_{10}. Figure 5-3 illustrates the comparison of the degree of breakage for all size fractions tested at 0.25 kWh/t and 1 kWh/t for both crushed and drill core particles. The error bars presented represent the standard error which measures the accuracy of the average t_{10} in representing the t_{10}s used to obtain the average. No error bars are shown for the 30-particle test as no repeats were performed for the standard test.

A comparison of Figure 5-3a and Figure 5-3b shows that crushed ore particles consistently produced higher t_{10} values than drill core particles at the same conditions. An increase in the t_{10} indicates that the progeny particles contain more fine particles. This trend is consistent for all the energy-size combinations tested. The observed behavior is similar to that discussed in chapter 4.4.

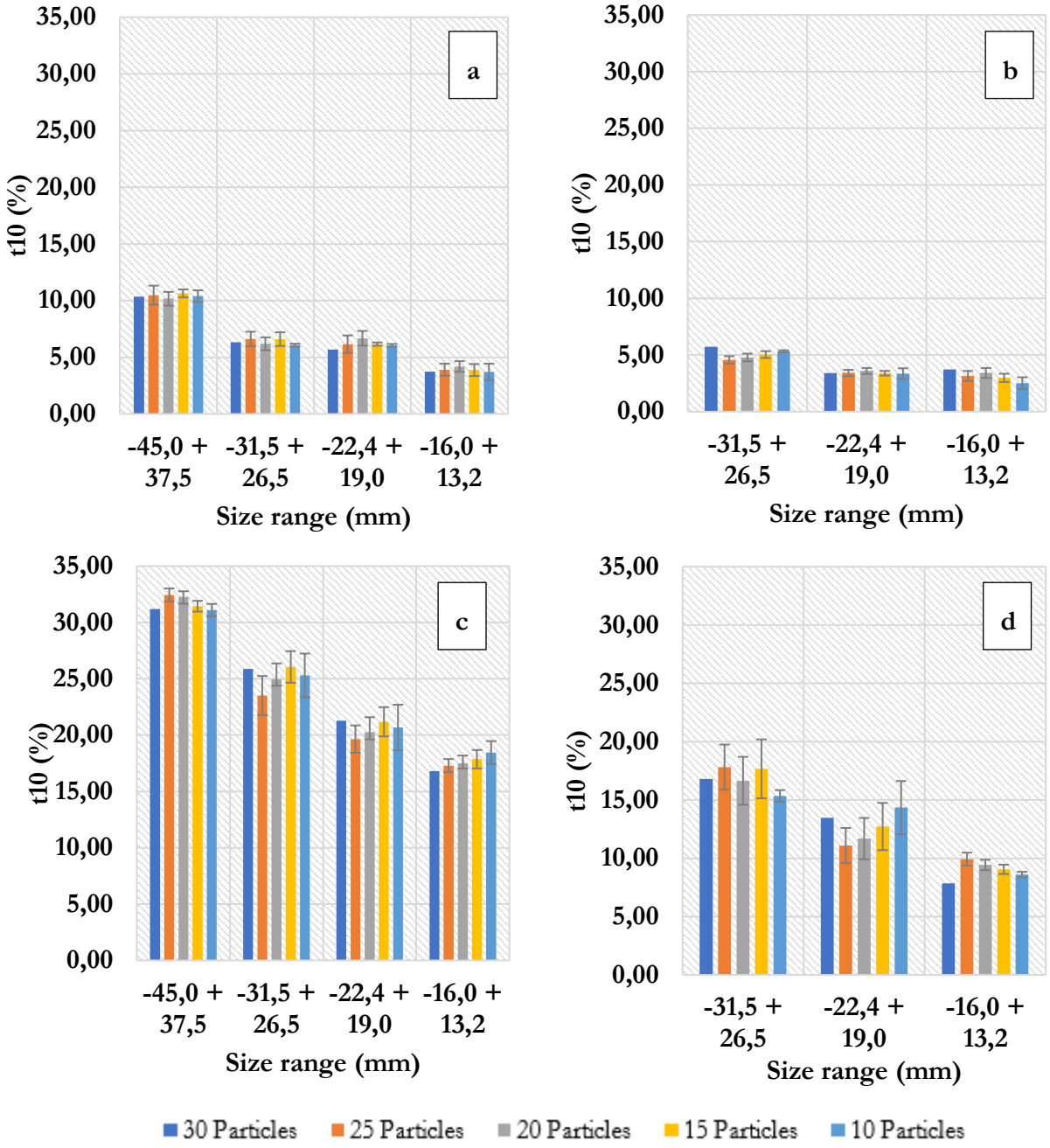

Figure 5-3: Comparison of the degree of breakage for different particle numbers at a) 0.25kWh/t (Crushed) b) 0.25kWh/t (drill core) c) 1kWh/t (crushed) and d) 1 kWh/t (drill core).

Figure 5-3c shows that the t_{10} values obtained for the different number of particles fell within the same range for all conditions tested. For example, crushed ore particles in the very large size fraction tested at 1 kWh/t energy resulted in the following t_{10} values: 31.19%, 31.54%, 31.13%, 31.50% and 31.14% for the 30, 25, 20, 15 and 10 particle tests respectively. These t_{10} values are within 0.5% of each other. This trend is observed for drill core particles as well.

Looking at Figure 5-3, though the t_{10} values for the different number of particles, it can be seen that they are all closely related to the t_{10} for the standard test. This implies that in terms of the degree of fineness achieved by each of the tests, any one of them could be used to substitute the

standard test as a similar degree of fineness can be achieved using less particles than 30 depending on the sample availability. The t_{10} values combined with the PSDs however are not adequate enough to draw an informed conclusion as they do not give an indication of the ore competence. Additionally, the t_{10} has a direct impact on the ore competence indicator (Axb and $3600.M.f_{mat}x$) which is the most useful ore breakage parameter. The experimental data therefore needs to be fitted to ore breakage models to observe the sensitivity of the ore breakage indicator to changes in t_{10} values.

5.5 Energy-Size relationships

The RBT data for each number of particles was fitted to the t_{10} breakage model and the size dependant breakage model in order to obtain the overall ore competence parameters. The results of the fitting of the data to the t_{10} model are summarised in Table 5-1 and Table 5-2. A comparison of the ore competence parameters shown in Table 5-1 shows the closeness of the A, b and Axb parameters obtained for the different numbers of particles. It can be seen that there is a negligible difference in the Axb parameter obtained as they are within the 2% tolerance limit. However, the difference in the A values obtained is above the tolerance limit. The A value represents the maximum degree of breakage achieved while the Axb parameter refers to the overall ore competence. Between these two parameters, Axb is more useful in the geometallurgy context as it gives an overall view of the ore in terms of breakage and hardness. The Axb parameter therefore outweighs the importance of the minor differences in the A value.

The same is true for the drill core parameters shown in Table 5-2. The results show that abridged tests with minimal number of particles can be used to substitute the standard test and still obtain similar ore competence parameters.

Table 5-1: Summary of the ore competence parameters for each number of particles using the t_{10} model for crushed ore S.

Number of particles	A (%)	b	A*b
30	42,54	0,79	33,57
25	44,42	0,73	32,36
20	45,28	0,73	32,95
15	45,44	0,74	33,53
10	44,65	0,74	33,18

Table 5-2: Summary of the ore competence parameters for each number of particles using the t_{10} model for drill core.

Number of particles	A (%)	b	A*b
30	56,17	0,26	14,80
25	47,38	0,32	15,17
20	55,89	0,26	14,50
15	44,79	0,35	15,61
10	61,48	0,23	14,44

Table 5-3: Summary of the ore competence parameters for each number of particles using the size-dependent model for crushed ore.

		Mean particle size (mm)			
		41,1	28,9	20,6	14,5
Number of particles	M (%)	$3600.M.F_{mat}.x$			
30	42,54	190,5	164,3	109,7	60,4
25	44,42	196,9	143,4	110,3	63,5
20	45,28	190,7	149,8	108,4	68,3
15	45,44	185,6	158,4	105,4	72,6
10	44,65	185,4	153,3	106,4	70,8

Table 5-4: Summary of the ore competence parameters for each number of particles using the size-dependent model for drill core.

		Mean particle size (mm)		
		28,9	20,6	14,5
Number of particles	M (%)	$3600.M.F_{mat}.x$		
30	56,3	81,3	69,6	67,5
25	47,4	90,3	51,9	40,9
20	55,9	102,5	63,0	40,0
15	44,8	75,5	54,4	40,1

The results of the fitting of the RBT data to the size-dependant model are summarised in Table 5-3 and Table 5-4. Comparing the parameters shown in Table 5-3, it is evident that there is no significant difference in the overall competence parameters obtained. Difference can be seen on the M parametrs which represents the highest degree of breakage achieved. The M parameter is similar to the A parameter in the previous model. However, in the geomet context, the overall ore

competence parameter is of more importance than the M value. Therefore, though there were noticeable differences in the M parameter, the overall ore competence parameters were closely related and gave the same understanding. This is also true for the parameters shown in Table 5-4 for drill cores. All the results presented in this chapter show that the proposed abridged ore breakage characterisation test that uses the minimal number of particles to extract ore breakage indices can be applied. The number of particles can be reduced to as little as 10 particles per test while still obtaining the similar ore breakage indices as those obtained from the standard procedure.

5.6 Case study: Application of the Least Particles Protocol

This section presents the results obtained from the application of the least particles protocol on an ore type (ore P) that is not homogenous and consistent (variable ore type). Ore P was selected for this case study as it has the most significant differences in terms of mineralogy and texture when compared to ore S which was used to develop the protocol. This was done in order to test the viability of using the least particle method even with ores that tend to not show consistent breakage results due to ore variability. From previous sections, it was shown that 10 particles are the least number of particles that can be used in order to obtain breakage results that are within 2% of the breakage results obtained using the standard 30 particle test. Test work on ore P was conducted using the least particles protocol for 10 particles which is compared to the standard method which uses 30 particles.

5.6.1 Particle size distributions

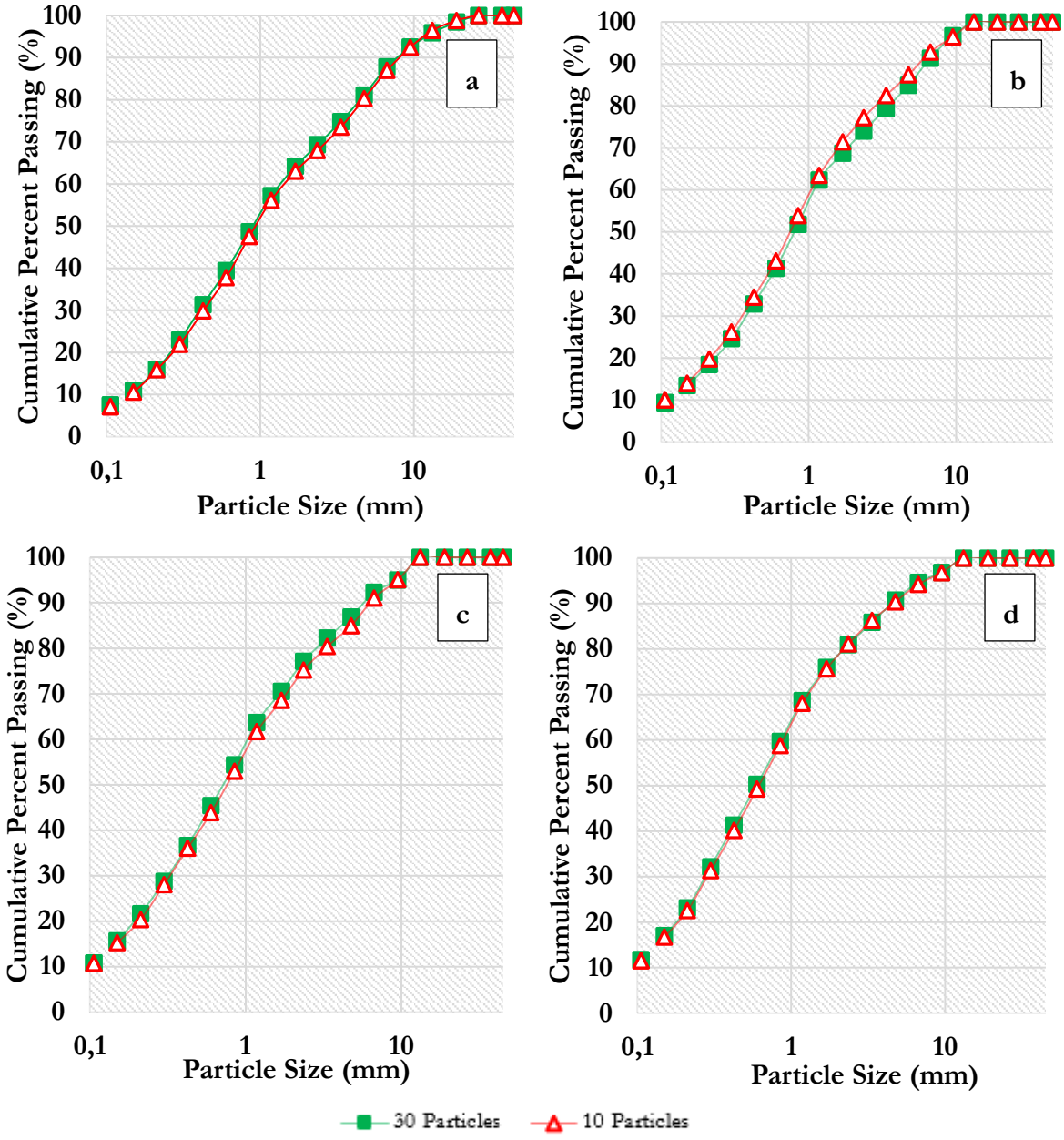

Figure 5-4: Ore P particle size distributions at 1 kWh/t for a) very large, b) large, c) medium and d) small size fractions.

The particle size distributions illustrated in Figure 5-4 show a comparison between the PSD obtained for the standard 30 particle tests and the PSD obtained using the proposed least particles protocol. In all cases, it can be seen that the differences in the PSDs obtained for both test procedures are minimal as illustrated by the green and red lines almost always overlapping with each other. This is a positive result for the least particles protocol as it shows that the same particle

size distribution obtained using numerous particles is the same as that obtained by using fewer particles with 10 particles per test being the minimum.

5.6.2 Degree of Breakage

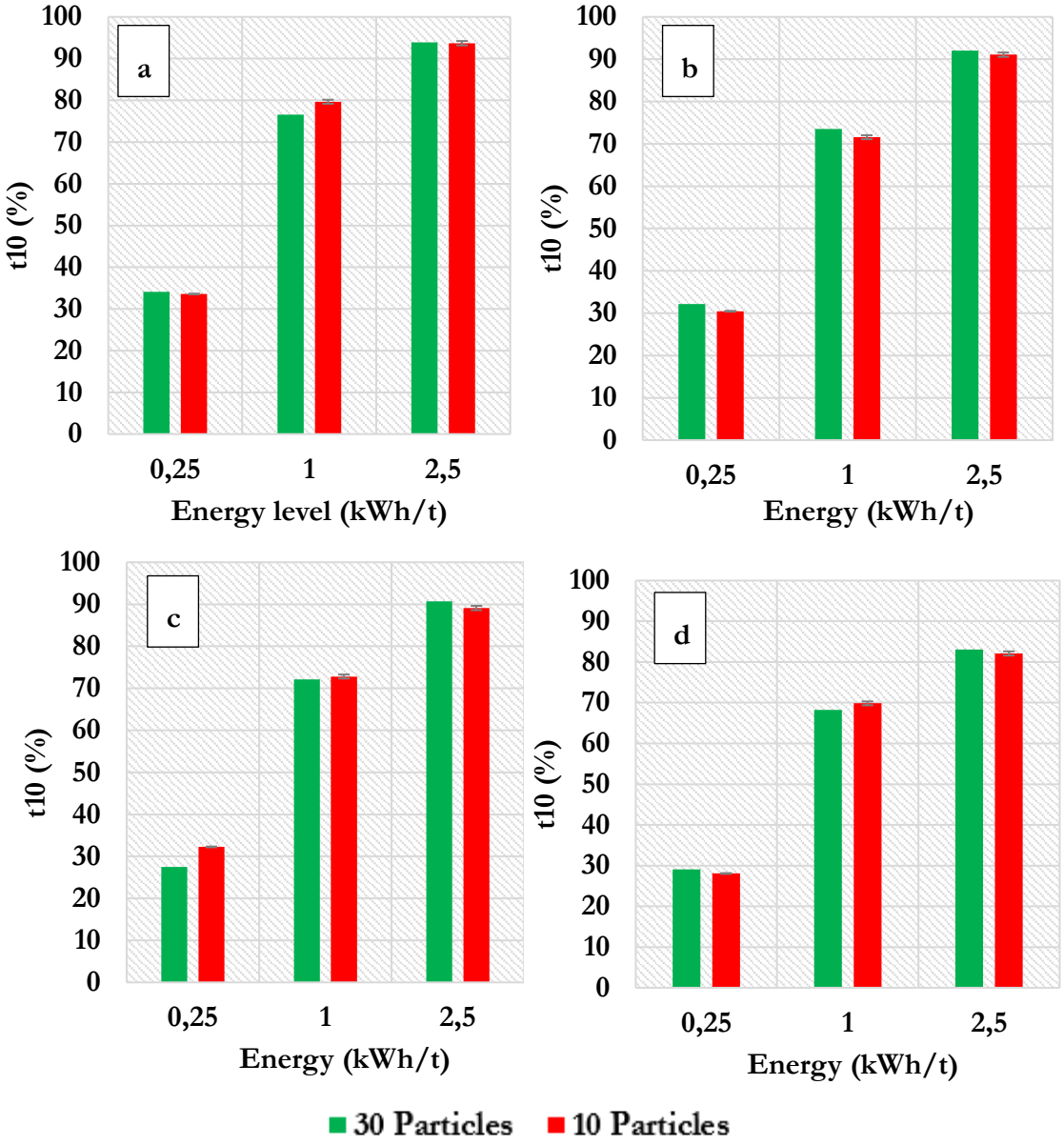

Figure 5-5: Comparison of the degree of breakage between the standard test and the least particles protocol for a) large (crushed) b) medium (crushed), c) large (drill core) and d) medium (drill core) at all energy levels tested.

The comparison of the degree of breakage achieved by the standard test and the least particles protocol at different conditions is shown in Figure 5-5. As before, the error bars on the red bars (least particles protocol) represent the standard error which measures the accuracy of the average t10 in representing the t_{10}s used to obtain the average. It can be seen that the least particles protocol achieves a t_{10} value that is similar to the t_{10} value obtained using the standard test. The results obtained show that the least particles protocol can be used as an abridged test when samples are

scarce to still achieve the same degree of breakage as the standard test. These results also show that the least particles protocol can be used for both fine grained and coarse grained ore types and therefore should be valid for other ore. The t_{10} values have a direct impact on the overall ore competence parameters which are discussed in the following section.

5.6.3 Energy-size Relationship

The RBT data obtained for ore P was fitted to the t_{10} breakage model and the size dependant breakage model in order to obtain the overall ore competence parameters. The results of the fitting of the data to the t_{10} model are summarised in Table 5-5. A comparison of these ore competence parameters shows the closeness of the A, b and Axb parameters obtained for the standard test and the least particles protocol. The overall ore competence parameter for crushed ore was 162.1 and 161.6 for the standard and least particles protocol respectively. These two parameters are within 0.5 units of each other which is within the 2% tolerance limits and can therefore be considered to be a negligible difference. The same trend is observed with drill core particles.

Table 5-5: Comparison of the ore competence parameters between the standard test and the least particles protocol using the t_{10} model for Ore P crushed ore and drill core.

Crushed Ore			
Number of particles	A (%)	b	A*b
30	92,37	1,755	162,1
10	91,65	1,763	161,6
Drill Core			
Number of particles	A (%)	b	A*b
30	86,14	1,577	135,8
10	86,53	1,618	140,0

Fitting the RBT data obtained for ore P to the size dependent model produces the ore parameters summarized in Table 5-6 and Table 5-7 for crushed ore and drill core respectively. Comparing the overall ore competence parameters ($3600Mf_{mat}x$) obtained for the standard test and least particles protocol, it is evident that there is no significant difference between the two. The ore competence parameters from the fitting of the full particle range recommended for ore characterisation and the least particle method are similar for crushed ore particles. A similar observation was made for the tests performed using drill core particles. The implication of this observation is that the results show that for global process indicators such as those used and required in geometallurgy, 10 particles can be used to obtain sufficiently reliable ore competence parameters.

Table 5-6: Comparison of the ore competence parameters between the standard test and the least particles protocol using the SDM for Ore P crushed ore.

	M (%)	f_{mat}	x (m)	3600M.f_{mat}.x
30 Particles	92,4	0,0524	0,0411	716
		0,0629	0,0289	604
		0,0799	0,0206	548
		0,1021	0,0145	493
10 Particles	91,7	0,0510	0,0411	691
		0,0669	0,0289	638
		0,0759	0,0206	517
		0,1044	0,0145	501

Table 5-7: Comparison of the ore competence parameters between the standard test and the least particles protocol using the SDM for Ore P drill core.

Ore	M (%)	f_{mat}	x (m)	3600M.f_{mat}t.x
30 Particles	86,1	0,0624	0,0289	559
		0,0770	0,0206	493
		0,0928	0,0145	418
10 Particles	86,5	0,0648	0,0288	583
		0,0771	0,0206	496
		0,0977	0,0145	443

5.7 Discussion

Overall, the results obtained using ore P help build a strong case for the use of an abridged breakage protocol. The results showed that the least particles protocol can be used to obtain very similar and closely related results to those obtained using the standard test for both crushed ore and drill core. Where differences occur, they are all within the tolerance limit. In the geometallurgy context, difference of up to 4% are acceptable based on the results presented. This is also supported by the fact that difference smaller than 4% have minimal impact on the overall ore competence parameters which are the main concern of geometallurgy tests. The work of (Stark, Perkins & Napier-Munn, 2011) showed every good measurement of Axb has a standard deviation of 4% as a result of experimental error when one breakage characterisation device operator is used. This therefore means that variations in ore competence parameters within a tolerance limit of 4% are acceptable when using the LPP.

It is also worth noting the complete difference in the mineralogy (Table 4-1) and texture (Figure 4-6 and Figure 4-7) of the two ores used to develop and test the LPP. Ore S is a fine grained Malmesbury shale that is homogenous with mineral grain sizes of the order 10-25 microns while ore P is a medium grained polymetallic sulfide ore that is heterogenous with mineral grains of the order 20-1700 microns. This therefore means that the LPP can safely be used when working with ores that contain minerals between 10-1700 microns.

The impact of these findings is far reaching. If used, the least particles protocol has the potential to greatly reduce the sample mass required to conduct ore breakage characterisation tests. This abridged protocol will be especially useful in situations where the amount of ore available for metallurgical testing is limited. Additionally, the time and manpower normally required to prepare samples for ore breakage characterisation will be reduced due to less sample being required. This will be especially useful in situations of sample scarcity or when the ore breakage characterisation tests need to be conducted in a short space of time. It is also worth noting that the LPP was proved to work for fine grained ore type and a coarse grained ore type and therefore should be valid for other ore types even ore with different mineralogical compositions. To top it all off, this protocol works for both crushed ore and drill core which will be useful during exploration and mine planning where drill cores play a pivotal role.

6. CONCLUSIONS AND RECOMMENDATIONS

Overview

In this chapter, conclusions are drawn based on the results presented. The objectives, hypotheses and key questions set out at the beginning of the thesis are also assessed. In conclusion, recommendations for future work are proposed.

6.1 Conclusions

The scope of this thesis was guided by the objectives and hypotheses that were postulated. The first objective of this thesis was to "determine the relationship between crushed ore and drill core particles". The second objective was to "determine the relationship between ore mineral texture and the ore breakage characteristics in geometallurgy". The third and final objective was to "develop an abridged ore breakage characterisation test protocol that can be applied to both crushed ore and drill core particles and considers the effects of textural variability".

6.1.1 Comparison of the ore breakage characteristics of drill core and crushed ore

A comparison of the ore breakage characteristics of drill core and crushed ore was presented in chapter 4 in fulfillment of the first objective. Drill core and crushed ore samples of five different ore types were compared. The ore breakage results showed that drill core particles consistently produced a lower t_{10} value than crushed particles at the same conditions. The same trend was also observed across all size classes and ore types tested. The differences in t_{10}'s for crushed and drill core particles were attributed to the relationship between contact area and energy absorption.

Hypothesis 1 given in section 2.8 was that "drill core particles will produce a coarser product than crushed particles. This is because crushed particles are angular in shape whereas drill core particles are cylindrical thus offer less contact surface for energy absorption". The work presented in chapter 4 supports this hypothesis. The key question posed to assess this hypothesis was "Is there a difference in the ore breakage characteristics and liberation profiles of drill core and crushed ore?". Results obtained showed that there was a significant difference in the ore breakage characteristics and liberation profiles of drill core and crushed ore with drill core being more resistant to breakage and therefore having less liberated minerals. These differences were attributed to differences in the particle shape between the crushed particles (angular) and drill core particles

(cylindrical). Energy absorption occurs at the point of contact between the stress and the particle surface therefore angular particles have a larger surface area exposed for contact than cylindrical particles. This means crushed ore absorbs more energy and therefore breaks more easily than drill cores.

6.1.2 The effect of mineralogy and texture on ore breakage characteristics

The effect of mineralogy and texture on ore breakage characteristics was assessed in line with the second objective. Ore breakage characterisation tests were performed on five mineralogically and texturally different ore types (Ores A-C, P and S). The results presented in chapter 4 clearly showed the effect of mineralogy and texture on the ore types tested. It was observed that ore S was the most resistant to breakage while ore P proved to be the least resistant to breakage. Ore A was found to be more competent than ore B and ore C but less competent that ore S.

Hypothesis 2 presented in section 2.8 was that "that an ore with a coarse grained texture will break to form a finer progeny than an ore with a fine grained texture". The results reported in chapter 4 support this hypothesis. The key question posed to assess this hypothesis was "What is the effect of mineral texture variability on the ore breakage characteristics?". Differences in the ore competences indicators of the ores tested were attributed to the combined control of mineralogy and texture. In terms of texture, the differences in the ore breakage characteristics were attributed to the grain size distribution of the dominant constituent minerals for each sample. It was observed that ore P had the largest grains and least resistance to breakage while ore S had the smallest d_{50}s and therefore smallest grains and was the most resistant to breakage. Smaller grains lead to a decrease in porosity and therefore more tightly held particles which are harder to break. Therefore, ore P is the least competent because it is composed of the largest grains of the constituent dominant minerals. The combination of larger grains means that the grains are less tightly bonded to each other allowing them to break easily. Ores A and B have similar d_{50}s for the minerals investigated and therefore shows similar breakage characteristics. The d_{50} of all the minerals found in ore S is on the order of 10-25 microns therefore they can be classified as fine grained which are more tightly held together and therefore more resistant to breakage.

In terms of mineralogy, the differences observed in the ore breakage characteristics were attributed to the relative mineral abundance and individual mineral hardness. Quartz – the hardest mineral – is present in larger amounts in ore S than in the polymetallic sulfide ores. Though ore S contains mica (hardness 2.5), it should be noted that the mica is contained in a matrix of quartz and is fine

grained which renders ore S more resistant to breakage. Three most dominant minerals in ore P are magnetite (hardness 7), pyrrhotite (hardness of 4) and chalcopyrite (hardness of 3.5). It is also worth noting that ore P contains only trace amount of pyroxmangite (hardness 5.5) compared to ores A-C. This would make Ore P the least resistant to breakage as it contains substantial amounts of the softer minerals (chalcopyrite and pyrrhotite) when compared to the other polymetallic ores. It is therefore clear that the more abundant the harder minerals, the more competent the ore type. Relating these two properties results in the conclusion that ore S is the hardest ore and ore P the softest.

6.1.3 The least particles protocol

In line with the third objective of this thesis, the least particles protocol was developed in chapter 5 as an abridged ore breakage characterisation test protocol that can be applied to both crushed ore and drill core particles and considers the effects of textural variability. The LPP was based on the standard ore breakage characterisation procedure but the number of particles required per test was reduced from 30 particles to 10 particles while still obtaining consistent breakage results. The LPP was developed using an ore S which was homogenous and fine grained. The application of the LPP to a variable and coarser grained ore was performed in a case study using ore P.

Hypothesis 3 presented in section 2.8 was that "an abridged test can be performed using a fewer number of particles to obtain similar ore competence parameters to the standard procedure while using minimal samples. Additionally, this abridged test can be applied on a different ore type despite its mineralogical and textural composition". The results presented in chapter 5 support this hypothesis. The key question posed to address this hypothesis was "Is there a relationship between the mineral texture, number of particles per test and the relative hardness indices for crushed ore and drill core?". Results presented in chapter 5 show that the proposed abridged ore breakage characterisation test that uses the minimal number of particles to extract ore breakage indices can be applied for both homogenous and heterogenous ore types with mineral grains between 10-1700 microns. In terms of mineral texture, as exhibited by the two mineralogically and texturally different ores used in chapter 5, differences in mineralogy and texture do not affect the ability of the LPP to act as an abridged protocol in times of sample shortage. The results also show that the proposed least particles protocol can be used for ore breakage characterisation tests using both crushed ore and drill core particles. The number of particles can be reduced to as little as 10 particles per test while still obtaining the similar ore breakage indices as those obtained from the

standard procedure. The abridged protocol will be especially useful in situations where the amount of ore available for metallurgical testing is limited.

6.2 Recommendations

Based on the outcome of this thesis, the following recommendations for future work are proposed:

- **A quantitative measure of texture should be investigated**: This will make it possible to comprehensively link a textural description of ore variability to an ore competence indicator (Axb). Ultimately, this information can prove to be vital and serve as proxy data for process engineers to monitor processing behaviour and better manage ore variability.
- **Establish the robustness of the Least Particles Protocol**: In this study, only two ore types were used on the LPP. More case studies on the least particles protocol with various ore types that are mineralogically and textural different should be carried out to access the ultimate robustness of the LPP. Focus should be on ores which exhibit ore variability and as well as different grain sized ores.

7. REFERENCES

Akram, M. & Bakar, M.Z.A. 2007. Correlation between Uniaxial Compressive Strength and Point Load Index for Salt-Range Rocks. *Pakistan Journal of Engineering and Applied Sciences*. 1(50):1–8. DOI: 10.3208/jgssp.IRN-08.

Bailie, R., Armstrong, R. & Reid, D. 2007. Composition and single zircon U-Pb emplacement and metamorphic ages of the Aggeneys Granite Suite, Bushmanland, South Africa. *South African Journal of Geology*. 110(1):87–110. DOI: 10.2113/gssajg.110.1.87.

Ballantyne, G.R. & Powell, M.S. 2014. Benchmarking comminution energy consumption for the processing of copper and gold ores. *Minerals Engineering*. 65:109–114. DOI: 10.1016/J.MINENG.2014.05.017.

Ballantyne, G.R., Peukert, W. & Powell, M.S. 2015. Size specific energy (SSE) - Energy required to generate minus 75 micron material. *International Journal of Mineral Processing*. 136:2–6.

Bbosa, L.S. 2006. Measurement Of Impact Breakage Properties Of Ore Particles Using A Series Of Devices (MSc. Thesis). University of Cape Town.

Bbosa, L.S., Powell, M.S. & Cloete, T.J. 2006. An investigation of impact breakage of rocks using the split Hopkinson pressure bar. *Journal of The South African Institute of Mining and Metallurgy*. 106(4):291–296.

Becker, M., Jardine, M.A., Miller, J.A. & Harris, M. 2016. X-ray Computed Tomography: A geometallurgical tool for 3D textural analysis of drill core? In *Proceedings of the 3rd AusIMM International Geometallurgy Conference, Perth, Western Australia. 15-17 June 2016*. 15–16.

Bérubé, M.A. & Marchand, J.C. 1984. Evolution of the mineral liberation characteristics of an iron ore undergoing grinding. *International Journal of Mineral Processing*. 13(3):223–237. DOI: 10.1016/0301-7516(84)90005-X.

Bond, F.C. 1952. The third theory of comminution. *Trans. American Institute of Mining,*. 193:484–494.

Bourgeois, F.S. & Banini, G.A. 2002. A portable load cell for in-situ ore impact breakage testing. *International Journal of Mineral Processing*. 65(1):31–54. DOI: 10.1016/S0301-7516(01)00057-6.

Bradshaw, D., Wilkie, G., Becker, M., Evans, C.L. & Lotter, N.O. 2019. Ore Liberation analysis. In *Dunne, R., Komar Kawatra, S., Young, C. (Eds.), SME Mineral Processing and Extractive Metallurgy Handbook. Society for Mining, Metallurgy, and Exploration, Inc.* 69–88.

Broch, E. & Franklin, J.A. 1972. The point-load strength test. *International Journal of Rock Mechanics and Mining Sciences and*. 9(6):669–676. DOI: 10.1016/0148-9062(72)90030-7.

Bueno, M.P., Kojovic, T., Powell, M.S. & Shi, F. 2013. Multi-component AG/SAG mill model. *Minerals Engineering*. 43–44:12–21. DOI: 10.1016/j.mineng.2012.06.011.

Chandramohan, R., Holtham, P. & Powell, M. 2010. the Influence of Particle Shape in Rock Fracture. In *XXV International Mineral Processing Congress, Brisbane, Australia, 6-10 September 2010*. 3163–3171.

Chaponda, B. 2011. Effect of operating variables on IsaMill™ performance using platinum bearing ores (MSc. Thesis). University of Cape Town.

Chikochi, C. 2017. Ore breakage characterisation of UG2 deposits using the JK RBT (MSc. Thesis). University of Cape Town.

Cleary, P.W. 1998. Predicting charge motion, power draw, segregation and wear in ball mills using discrete element methods. *Minerals Engineering*. 11(11):1061–1080. DOI: 10.1016/S0892-6875(98)00093-4.

Cloete, L.M., Slabbert, W. & Siguiri, A. 2018. Current Geometallurgical initiatives at the Siguiri Gold Mine , Guinea. In *SAIMM Geometallurgy Conference, Cape Town, South Africa, 6–8 August 2018*. 6–8.

Cole, D.I., Ngcofe, L., Halenyane, K. & Clay, B. 2014. *Mineral Commodities In The Western Cape Province, South Africa*.

Cropp, A. & Goodall, W. 2013. *The influence of rock texture on mineral processing*. Carlton VIC 3053 Australi.

Eberhardt, E., Stimpson, B. & Stead, D. 1999. Effects of Grain Size on the Initiation and Propagation Thresholds of Stress-induced Brittle Fractures. *Rock Mechanics and Rock Engineering*. 32(2):81–99. DOI: 10.1007/s006030050026.

Francioli, D., Yahyaei, M., Tavares, L.M., Powell, M. & Federal, U. 2014. Characterizing attrition of rock under incremental low- energy impacts. *XXVII International Mineral Processing Congress, Santiago, Chile, 20-24 OCtober 2014*. (October):1–9.

Genç, Ö., Ergün, L. & Benzer, H. 2004. Single particle impact breakage characterization of materials by drop weight testing. *Physicochem. Prob. Miner. Process*. 38:241–255.

Gordon, H. 2019. Mineralogical and textural characterisation of Cu-Pb ores from the Swartberg deposit: A geometallurical approach to quantifying ore variability (MSc. Thesis). Stellenbosch University.

Harbort, GJ; Lam, K. and S.C. 2013. The use of Geometallurgy to Estimate Comminution Parameters within Porphyry Deposits. In *Proceedings The Second AusIMM International Geometallurgy Conference (GeoMet) 2013, Melbourne, Australia, 30September-2October 2013*. V. 1. 229.

Hukki, R. 1961. Proposal for a solomonic settlement between the theories of von Rittinger, Kick, and Bond. *Transactions of the Society of Mining Engineers of American Institute of Mining*. 223:403–408.

Jankovic, A., Dundar, H. & Mehta, R. 2010. Relationships between comminution energy and product size for a magnetite ore. *Journal of the Southern African Institute of Mining and Metallurgy*. 110(3):141–146.

Jardine, M. 2016. Three dimensional quantitative textural analysis of nickel sulphide ore using X-ray computed tomography and grey level co-occurrence matrices on drill core (MSC. Thesis). University of Cape Town.

JKTech. 2012. *JKTech Rotary Breakage Tester User Manual*.

Kawatra, S.K. 2006. *Advances in comminution*. Society for Mining, Metallurgy, and Exploration.

Kesler, B.S.E. 2007. *Mineral Supply and Demand into the 21st Century*. J. Briskey & K.. Schulz, Eds.

Ketcham, R.A. & Carlson, W.D. 2001. Acquisition, optimization and interpretation of X-ray computed tomographic imagery: applications to the geosciences. *Computers & Geosciences*. 27(4):381–400. DOI: 10.1016/S0098-3004(00)00116-3.

Kick, F. 1883. *Das Gesetz der proportionalen Widerstande und seine anwendung felix*. Leipzig, Germany.

King, R.P. 1994. Comminution and liberation of minerals. *Minerals Engineering*. 7(2–3):129–140. DOI: 10.1016/0892-6875(94)90059-0.

King, R.P. 2001a. Modeling and Simulation of Mineral Processing Systems. *Modeling and Simulation of Mineral Processing Systems*. 403. DOI: 10.1016/B978-0-08-051184-9.50004-3.

King, R.P. (Ronald P. 2001b. *Modeling and simulation of mineral processing systems*. Butterworth-Heinemann.

King, R.P. & Schneider, C.L. 1998. Mineral liberation and the batch communition equation. *Minerals Engineering*. 11(12):1143–1160. DOI: 10.1016/S0892-6875(98)00102-2.

Kojovic, T. & Shi, F. 2002. *Update on the JKRBT (JKMRC Rotary Breakage Tester)*.

Leung, K. 1987. An energy based, ore specific model for autogenous and semi-autogenous grinding mills (PhD Thesis). University of Queensland.

Little, L., Wiese, J., Becker, M., Mainza, A. & Ross, V. 2016. Investigating the effects of particle shape on chromite entrainment at a platinum concentrator. *Minerals Engineering*. 96–97:46–52. DOI: 10.1016/J.MINENG.2016.06.003.

De Magalhães, F.N. & Tavares, L.M. 2014. Rapid ore breakage parameter estimation from a laboratory crushing test. *International Journal of Mineral Processing*. 126:49–54. DOI: 10.1016/j.minpro.2013.11.007.

Mainza, A. 2017. The role of classification in the mineral processing circuit. In *The 15th European Symposium on Comminution and Classification Proceedings, Izmir, Turkey, 11-14September 2017*. 2.

Mariano, R. & Annieli, R. 2016. Measurement and modelling of the liberation and distribution of minerals in comminuted ores. The University of Queensland. DOI: 10.14264/uql.2016.1081.

Mariano, R.A., Evans, C.L. & Manlapig, E. 2016. Definition of random and non-random breakage in mineral liberation - A review. *Minerals Engineering*. 94:51–60. DOI: 10.1016/j.mineng.2016.05.005.

McClung, C.R. & Viljoen, F. 2011. Mineralogical Assessment of the Metamorphosed Broken Hill Sulfide Deposit, South Africa Implications for Processing Complex Orebodies. In *Proceedings of the 10th International Congress for Applied Mineralogy (ICAM), Trondheim, Norway, 1-5August 2011*. 427–434.

Mudd, G. 2004. Sustainable Mining : An Evaluation of Changing Ore Grades and Waste Volumes. In *International Conference on Sustainability Engineering & Science, Auckland, New Zealand - 6-9 July 2004*. 1–13.

Murr, D., Workman, L. & Jack, E. 2015. Blasting Influence On Comminution. In *SAG Conference, Vancouveur, Canada, 20-24september 2015*. 1–21.

Mwanga, A., Lamberg, P. & Rosenkranz, J. 2015. Comminution test method using small drill core samples. *Minerals Engineering*. 72:129–139. DOI: 10.1016/j.mineng.2014.12.009.

Mwanga, A., Rosenkranz, J. & Lamberg, P. 2015. Testing of Ore Comminution Behavior in the Geometallurgical Context—A Review. *Minerals*. 5(2):276–297. DOI: 10.3390/min5020276.

Napier-Munn, T. 2015. Is progress in energy-efficient comminution doomed? *Minerals Engineering*. 73:1–6. DOI: 10.1016/j.mineng.2014.06.009.

Napier-Munn, T.J., Morrell, S., Morrison, R.D. & Kojovic, T. 1996. *Mineral comminution circuits : their operation and optimisation*. Julius Kruttschnitt Mineral Research Centre.

Narayanan, S.S. 1987. Modelling the performance of industrial ball mills using single particle breakage data. *International Journal of Mineral Processing*. 20(3–4):211–228. DOI: 10.1016/0301-7516(87)90067-6.

Norazirah, A., Fuad, S.H.S. & Hazizan, M.H.M. 2016. The Effect of Size and Shape on Breakage Characteristic of Mineral. *Procedia Chemistry*. 19:702–708. DOI: 10.1016/j.proche.2016.03.073.

OECD. 2018. *Steel Market Developments: Q2 2018*.

Petruk, W. 2000. *Applied mineralogy in the mining industry*. Elsevier Science BV.

Rittinger, R.. 1867. Lehrbuch der Aufbereitungskunde. *Ernst and Korn*. 2(10):12–19.

Roy, M.P., Paswan, R.K., Sarim, M.D., Kumar, S., Jha, R.R. & Singh, P.K. 2016. Rock fragmentation by blasting -A review. *Journal of Mines, Metals and Fuels*. 64(9):424–431.

Schroe, K. 2016. *Production, Handling and Characterization of Particulate Materials*. V. 25. DOI: 10.1007/978-3-319-20949-4.

Shi, F. 2011. *Efficiency Improvements In Coal Fired Utilities*.

Shi, F. & Kojovic, T. 2007. Validation of a model for impact breakage incorporating particle size effect. *International Journal of Mineral Processing*. 82(3):156–163. DOI: 10.1016/j.minpro.2006.09.006.

Shi, F., Kojovic, T., Larbi-Bram, S. & Manlapig, E. 2009. Development of a rapid particle breakage characterisation device - The JKRBT. *Minerals Engineering*. 22(7–8):602–612. DOI: 10.1016/j.mineng.2009.05.001.

Sinnott, M., Cleary, P.W. & Morrison, R. 2006. Analysis of stirred mill performance using DEM simulation: Part 1– Media motion, energy consumption and collisional environment. *Minerals Engineering*. 19(15):1537–1550. DOI: 10.1016/J.MINENG.2006.08.012.

Song, B. & Chen, W. 2005. Split Hopkinson pressure bar techniques for characterizing soft materials. *Latin American Journal of Solids and Structures*. 2(June):113–152.

Stark, S., Perkins, T. & Napier-Munn, T. 2011. JK drop weight parameters: A statistical analysis of their accuracy and precision and the effect on SAG mill comminution circuit simulation. .

Australasian Institute of Mining and Metallurgy Publication Series. 121–145.

Tanaka, T. 1966. Comminution laws: Several Probabilities. *Industrial and Engineering Chemistry Process Design and Development*. 5(4):353–358. DOI: 10.1021/i260020a001.

Tavares, L.M. 2007. *Chapter 1 Breakage of Single Particles: Quasi-Static*. V. 12. DOI: 10.1016/S0167-3785(07)12004-2.

Tavares, L.. & King, R.. 1998. Single-particle fracture under impact loading. *International Journal of Mineral Processing*. 54(1):1–28. DOI: 10.1016/S0301-7516(98)00005-2.

Tungpalan, K., Wightman, E. & Manlapig, E. 2015. Relating mineralogical and textural characteristics to flotation behaviour. *Minerals Engineering*. 82:136–140. DOI: 10.1016/j.mineng.2015.02.005.

Vassiliev, P. V, Ledoux, H. & Gold, C. 2008. Modeling Ore Textures and Mineral Liberation Using 3D Voronoi Diagrams. *International conference on Numerical geometry, grid generation and scientific computing (NUMGRID2008)*. (v):220–225.

Vogel, L. & Peukert, W. 2003. Breakage behaviour of different materials—construction of a mastercurve for the breakage probability. *Powder Technology*. 129(1–3):101–110. DOI: 10.1016/S0032-5910(02)00217-6.

Voigt, M. 2017. Using X-ray computed tomography for the 3D textural analysis of drill core in geometallurgy (MSc Thesis). University of Cape Town.

Walker, W., Lewis, K., McAdams, W. 1937. Principles of Chemical Engineering. *The Journal of Physical Chemistry*. 41(9):1231–1231. DOI: 10.1021/j150387a017.

Wills, B.A. & Napier-Munn, T. 2006. *Wills' mineral processing technology : an introduction to the practical aspects of ore treatment and mineral recovery*. Butterworth-Heinemann.

Xia, K. & Yao, W. 2015. Dynamic rock tests using split Hopkinson (Kolsky) bar system - A review. *Journal of Rock Mechanics and Geotechnical Engineering*. 7(1):27–59. DOI: 10.1016/j.jrmge.2014.07.008.

Ye, X., Gredelj, S., Skinner, W. & Grano, S.R. 2010. Regrinding sulphide minerals — Breakage mechanisms in milling and their influence on surface properties and flotation behaviour. *Powder Technology*. 203(2):133–147. DOI: 10.1016/J.POWTEC.2010.05.002.

Yildirim, B.G., Bradshaw, D., Powell, M., Evans, C. & Clark, A. 2014. Development of an effective and practical Process Alteration Index (PAI) for predicting metallurgical responses of Cu

porphyries. *Minerals Engineering*. 69:91–96. DOI: 10.1016/j.mineng.2014.07.009.

Zuo, W. & Shi, F. 2016. Ore impact breakage characterisation using mixed particles in wide size range. *Minerals Engineering*. 86:96–103. DOI: 10.1016/j.mineng.2015.12.007.

8. APPENDIX A

1. Raw data

Raw Data for all the tests conducted can be found online on the following link:

https://docs.google.com/spreadsheets/d/1mLxydcwkR5hgw7mfujQoWIQ8h89rL0pWJwbx5IAcZPM/edit?usp=sharing

	Relative abundance of crystalline phases (mass %)	
Mineral	**Ore P**	**Ore S**
Quartz	15	33
Plagioclase	-	16
K-feldspar	-	8
Mica	-	37
Amphibole	-	3
Chlorite	-	4
Magnetite	49	-
Chalcopyrite	18	-
Pyrrhotite	14	-
Sphalerite	3	-

9. APPENDIX B

Table 9-1: XRD results obtained for ore P and S.

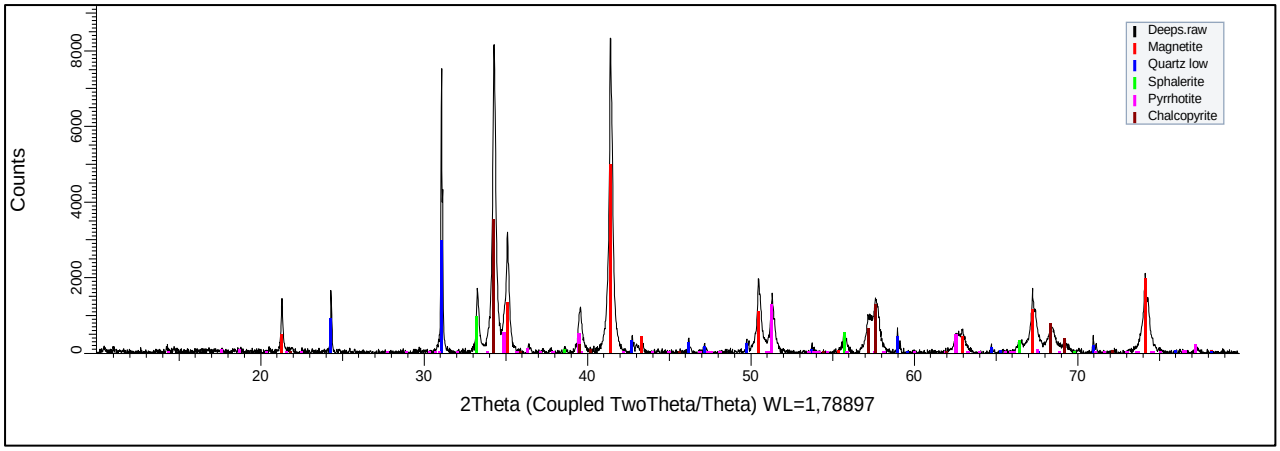

Figure 9-1: Diffractogram of ore P.

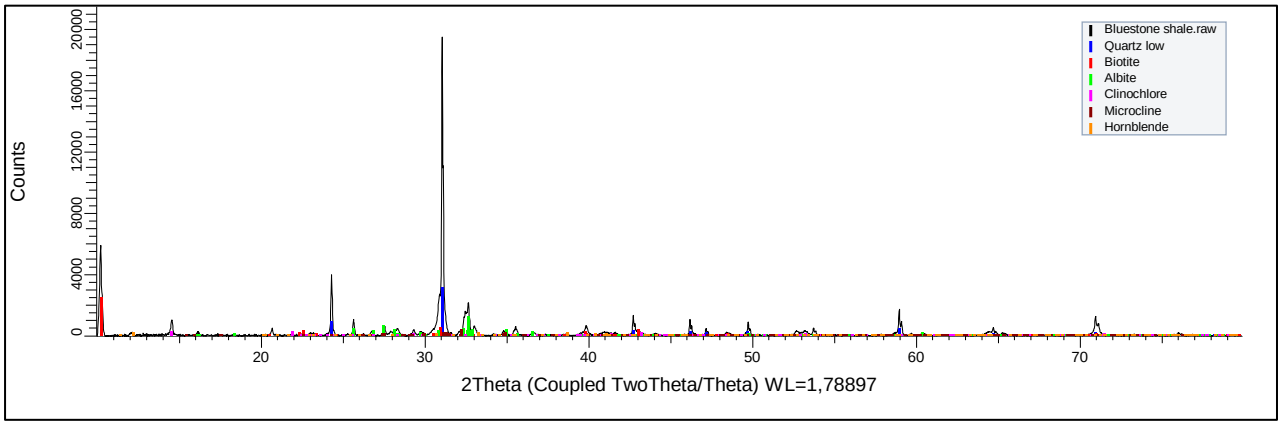

Figure 9-2: Diffractogram of ore S.

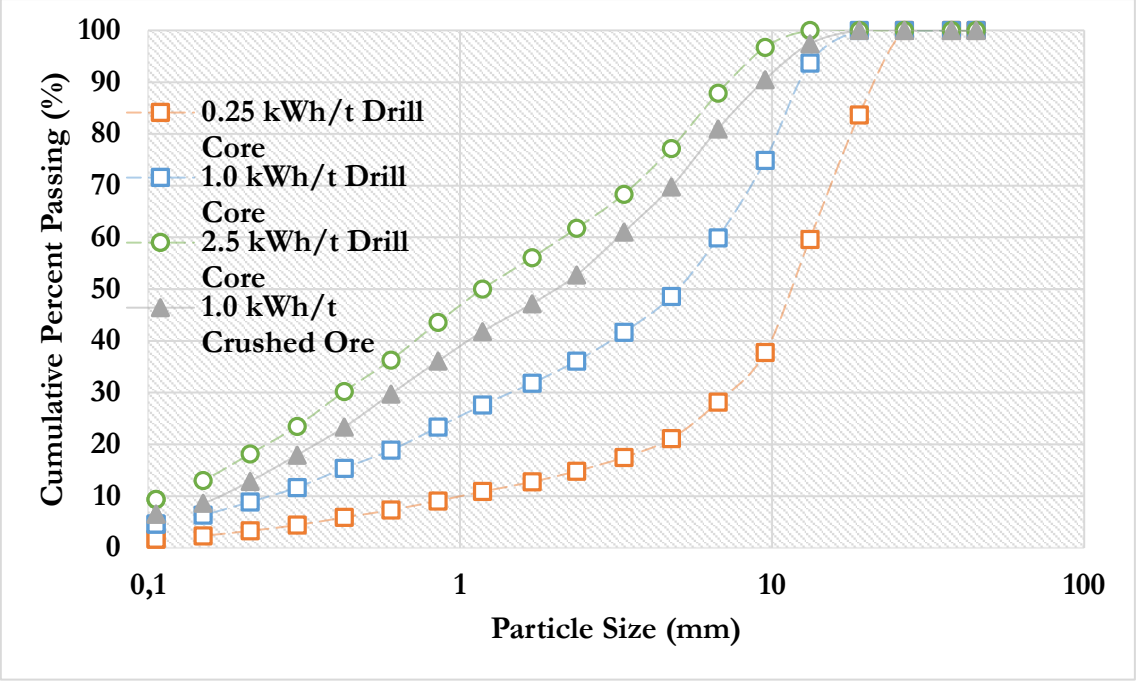

Figure 9-3: A comparison of the particle size distributions at all energy levels for medium size class drill core and crushed ore particles of ore A.

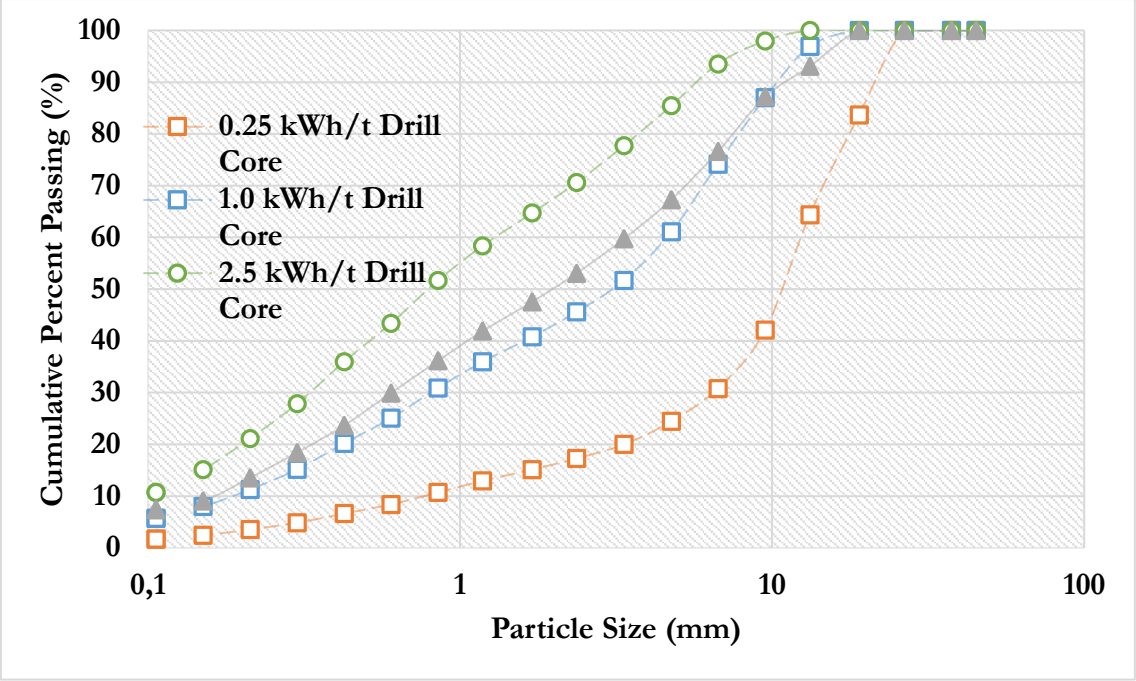

Figure 9-4: A comparison of the particle size distributions at all energy levels for medium size class drill core and crushed ore particles of ore B.

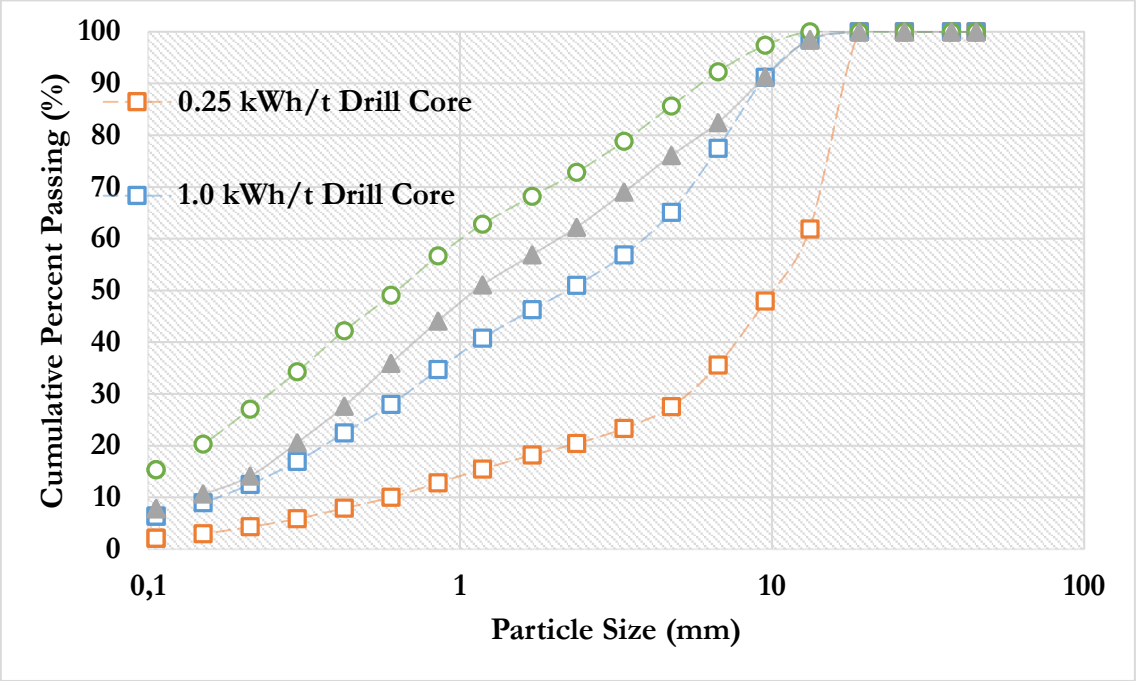

Figure 9-5: A comparison of the particle size distributions at all energy levels for medium size class drill core and crushed ore particles of ore C.

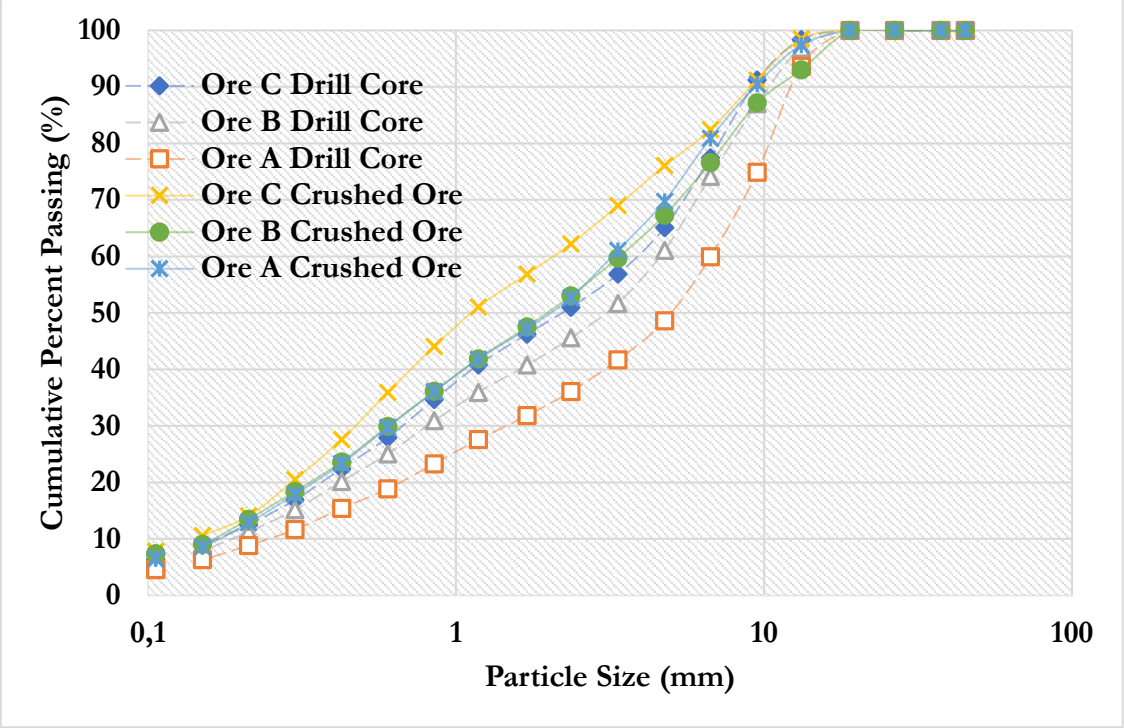

Figure 9-6: Comparison of the particle size distributions for the medium size class of ore A, ore B and ore C at 1kWh/t for both crushed ore and drill core.

Table 9-2: Summary of t_{10} obtained for standard tests (crushed ore).

		Ore S	Ore A	Ore B	Ore C	Ore P
Size Class	Specific Input Energy (Ecs)	t10				
mm	kWh/t	%				
Very Large	0,1	4,08				22,22
	0,25	10,35				39,18
	1	31,19				77,70
Large	0,25	6,32				34,13
	1	25,86				76,54
	2,5	48,01				93,88
Medium	0,25	5,68				32,17
	1	21,28	49,67	50,01	59,28	73,53
	2,5	36,64				92,06
Small	0,25	3,73				27,49
	1	16,80				72,13
	2,5	24,63				90,70

Table 9-3: Summary of t_{10} obtained for standard tests (drill core).

		Ore S	Ore A	Ore B	Ore C	Ore P
Size Class	Specific Input Energy (Ecs)	t10				
mm	kWh/t	%				
Large	0,25	5,73	14,31	15,74	22,56	30,88
	1	16,81	44,14	45,20	44,93	71,41
	2,5	36,87	67,96	62,97	71,97	90,31
Medium	0,25	3,40	13,69	16,08	19,18	29,04
	1	13,46	33,75	42,94	48,38	68,21
	2,5	25,09	58,64	67,35	70,27	83,06
Small	0,25	3,74	20,45	16,29	20,94	27,58
	1	7,85	50,69	41,60	50,79	62,35
	2,5	19,49	67,55	55,86	65,21	81,38